Rad5 Recruitment and Function in the *Saccharomyces cerevisiae* Replication Stress Response

by

David William Michael Gallo

A thesis submitted in conformity with the requirements
for the degree of Doctor of Philosophy

Department of Biochemistry
University of Toronto

Rad5 Recruitment and Function in the *Saccharomyces cerevisiae* Replication Stress Response

David William Michael Gallo

Doctor of Philosophy

Department of Biochemistry
University of Toronto

2018

Abstract

DNA replication stress poses a significant threat to the genome integrity of actively dividing cells and is observed in many pathological human disorders. Replication stress is caused by endogenous or exogenous events that slow or block the DNA replication machinery. All cells have an evolutionarily conserved DNA replication stress response that slows down cell division until DNA replication is complete and DNA can be segregated. The Post-Replication Repair (PRR) pathway allows tolerance of chemical- and UV-induced DNA lesions in both an error-free and an error-prone manner. In classical PRR, PCNA monoubiquitination recruits translesion synthesis (TLS) DNA polymerases that can replicate through lesions in a mutagenic manner. Polyubiquitination of PCNA by the ubiquitin ligase Rad5 initiates error-free PRR, using the sister chromatid as a template for DNA synthesis in lieu of the lesion-containing strand. I find that Rad5 forms nuclear foci after exposure to types of replication stress where DNA base lesions are likely absent. In this study I characterize how Rad5 is recruited to nuclear foci and how Rad5 functions in lesion-less replication stress. Using a genome-wide high-throughput screen I identified 23 genes that are required for robust Rad5 recruitment to nuclear foci. I revealed that the HSP40 chaperone Ydj1 in conjunction with the HSP70s Ssa1 and Ssb1 promote

Rad5 relocalization and replication stress resistance. To characterize Rad5 function in lesion-less replication stress I monitored the genome-wide association of Rad5 using ChIP-seq and found it binds to sites near stressed DNA replication forks. In addition to template switching activity at stressed replication forks, Rad5 also recruits TLS polymerases to repair ssDNA gaps, preventing mitotic defects and chromosome breaks. My data indicates that Rad5 is the central effector of PRR at stressed replication forks, where it promotes template switching and mutagenic repair of undamaged ssDNA that arises during physiological and exogenous replication stress.

Acknowledgments

First off, I would like to thank my PhD supervisor Dr. Grant Brown. In addition to being a fantastic scientific mentor he has provided ample opportunities to attend conferences, give talks, and network with leaders in our field. I would also like to thank my committee members for their comments and support throughout my PhD. Next I would like to thank the Brown lab members past and present. It has been a pleasure to work with such inspiring and outgoing people who made my PhD experience fulfilling and entertaining. Finally, I would like to thank my friends and loved ones. Thank you for putting up with late nights and weekend experiments, I could not have done this without them.

Table of Contents

List of Tables

List of Figures

List of Appendices

Chapter 1
Introduction

1 Introduction

1.1 DNA replication stress

DNA replication is a fundamental process in every cell. DNA replication in eukaryotic cells is initiated at replication origins by melting dsDNA into a replication bubble with two dsDNA-ssDNA junctions called replication forks, a process called origin firing (Bell and Dutta, 2002; Burgers and Kunkel, 2017; Waga and Stillman, 1998). DNA replication is initiated by Pol α/primase which synthesizes a short RNA primer that is extended in the 5'-3' direction using each parent strand as a template. Due to the 5'-3' nature of DNA polymerization the leading strand replicates in a continuous fashion and is catalyzed by Pol ε. Lagging strand synthesis is catalyzed by Pol ∂ and requires repriming during DNA replication to make short polynucleotides called Okazaki fragments that are ultimately ligated together. In addition to the polymerases DNA replication requires the DNA helicase Cdc45-GINS-MCM_{2-7} (CMG) and the sliding clamp and processivity factor PCNA among others. DNA replication proceeds bi-directionally away from each origin until the genome is duplicated and cells can progress through mitosis and divide to form a mother and a daughter.

There are a variety of endogenous and exogenous circumstances that impair replication fork progression which are collectively referred to as replication stress (Zeman and Cimprich, 2014). In my thesis I will refer to all impaired fork structures as stressed replication forks, keeping in mind that different triggers of replication stress likely lead to different fork structures. Stressed replication forks pose two significant problems for genome integrity: First, completing DNA replication is threatened which could lead to loss of genetic information. Second, there is increased ssDNA at stressed replication forks making it vulnerable to breaks and inappropriate transactions. To protect genome integrity cells mount a replication stress response controlled by the DNA replication checkpoint, a kinase signalling cascade that rewires the cellular program to cope with stress. The response favours bulk DNA replication completion and intact chromosome segregation at the expense of smaller and less harmful mutations. Failure to activate the DNA replication stress response or exposure to chronic replication stress leads to a broad range of defects in humans including developmental disorders, premature aging, neurological disorders and cancer (Gaillard et al., 2015; López-Otín et al., 2013; Macheret and Halazonetis, 2015; Zeman and Cimprich, 2014). Understanding how the replication stress response is orchestrated,

how it impacts genome integrity and how its failure results in pathological outcomes is the overarching goal of my research.

1.2 Sources of DNA replication stress

Replication stress results from a variety of endogenous and exogenous situations that include: DNA secondary structures, repetitive DNA, protein-DNA complexes, transcription-replication conflicts, DNA base damage, DNA lesions, imbalanced dNTPs or histones, mutated DNA replication machinery and expression of oncogenes (Figure 1.1) (Muñoz and Méndez, 2017; Zeman and Cimprich, 2014). In the next section I will explain how they arise in eukaryotic cells.

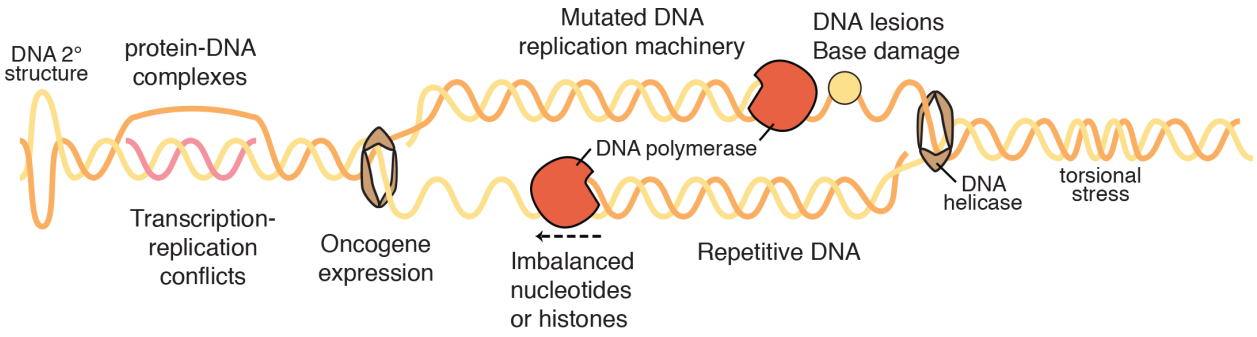

Figure 1.1 Sources of replication stress. Replication stress results from scenarios that block replication forks and result in unscheduled ssDNA. Types of endogenous and exogenous replication include: DNA secondary structures, repetitive DNA, protein-DNA complexes, transcription-replication conflicts, DNA base damage, DNA lesions, imbalanced dNTPs or histones, mutated DNA replication machinery and expression of oncogenes.

1.2.1 DNA secondary structures and repetitive DNA

Eukaryotic genomes have regions that are prone to form structures other than B-form DNA that pose a problem for DNA replication. These structures include cruciforms, hairpins, G-quadraplexes, H-DNA or Z-DNA (Figure 1.1). They are commonly composed of repetitive DNA sequences and they impede replication fork progression resulting in replication stress (Mirkin and Mirkin, 2007). A common class of repeats are called trinucleotide repeat sequences (TNRs) (Kim and Mirkin, 2013; McMurray, 2010). TNRs undergo replication-dependent expansion and contraction under physiological conditions and are therefore intrinsically unstable. TNR instability is accelerated by mutations in the DNA replication machinery or induction of replication slippage. Another repetitive sequence prone to form secondary structures is quartets of guanines in GC-rich regions of the genome called G4 structures (Bochman et al., 2012). The guanines form planar structures that are stabilized by non-canonical hydrogen bonds. G4

structures are actively unwound by the Pif1 DNA helicase and failure to unwind them, by abrogating Pif1 or addition of chemical stabilizers, results in genome instability (Duan et al., 2015; Paeschke et al., 2013). Inverted repeats also pose a significant problem for replication forks to overcome and are prone to gross chromosomal rearrangements if there are stressed replication forks in the vicinity (Mizuno et al., 2009, 2013). Therefore, repetitive genomic sequences are a significant contributor to endogenous replication stress.

1.2.2 Protein-DNA complexes

Many DNA transactions are mediated by high affinity protein-DNA complexes, which pose a physical barrier for replication forks (Figure 1.1). The most abundant protein-DNA complexes in cells are nucleosomes, as most of the DNA in the nucleus is tightly wrapped around histones and organized into nucleosome complexes and higher-order chromatin. The average compactness of chromatin falls somewhere between open euchromatin and compact heterochromatin. An intricate network of chaperones shuttles histones around replication forks and deposits new histones on nascent DNA (Hammond et al., 2017; Venkatesh and Workman, 2015). Nonetheless, even with functional histone chaperones heterochromatic regions of the genome are more prone to replication stress (Jiang et al., 2009; Rozenzhak et al., 2010; Szilard et al., 2010). In addition to histones, other protein-DNA obstacles also form at unused origins (Wang et al., 2001), mating type locus (Ivessa et al., 2003), telomeres (Ivessa et al., 2002), centromeres (Greenfeder and Newlon, 1992) and actively transcribed regions (Section 1.2.3). Replication fork progression through these complexes is mediated by the Rrm3 DNA helicase (Ivessa et al., 2003). Interestingly, artificial targeting of protein-DNA complexes to non-native loci like the Tus-Ter replication fork barrier from *E.coli* (Larsen et al., 2014; Willis et al., 2014) or the Fob1 replication fork barrier from yeast (Calzada et al., 2005) results in DNA replication stress. Thus, it is important to clear protein-DNA complexes to avoid triggering replication stress.

1.2.3 Transcription-Replication conflicts (TRC)

Transcription-replication conflicts arise when replication and transcription try to occupy the same DNA template and result in replication stress (Figure 1.1) (Bermejo et al., 2012; García-Muse and Aguilera, 2016; Helmrich et al., 2013). To avoid such conflicts DNA replication and transcription must be carefully choreographed. DNA unwinding during transcription initiation induces topological stress that results in replication stress (Bermejo et al., 2009; Tuduri et al.,

2009). To combat topological stress, the DNA replication checkpoint (Section 1.3) signals for release of transcribed genes from the nuclear pore alleviating the topological stress (Bermejo et al., 2011). Transcription-replication conflicts also occur when transcription complexes and replication complexes approach each other from different directions (head-on) or are travelling in the same direction (co-directional). Both head-on (Prado and Aguilera, 2005; Srivatsan et al., 2010; Vilette et al., 1996) and co-directional (Azvolinsky et al., 2009; Merrikh et al., 2011) collisions cause replication stress although head-on appear to be more problematic (Hamperl et al., 2017). To minimize head-on collisions, transcription and replication in bacteria are oriented co-directionally (Rocha, 2004). Furthermore, head-on collisions at the highly-transcribed ribosomal DNA (rDNA) locus in yeast are actively blocked by the DNA binding protein Fob1 (Brewer et al., 1992; Takeuchi et al., 2003). Yet another transcription-replication conflict occurs when transcribed RNA re-anneals to a complimentary DNA template and displaces a ssDNA strand, forming a DNA:RNA hybrid or R-loop (Santos-Pereira and Aguilera, 2015). Replication fork collisions with R-loops result in stressed replication forks, and R-loops accumulate at transcription termination regions, rDNA, pericentric regions and telomeres. Multiple mRNA processing proteins that affect R-loop formation were identified in genome-wide screens (Paulsen et al., 2009; Stirling et al., 2012; Wahba et al., 2011). These proteins work by either actively preventing R-loop formation or by removing R-loops once they have formed. R-loop formation is prevented by the THO/TREX transcription elongation complex (Huertas and Aguilera, 2003), the SR RNA splicing proteins (Li and Manley, 2005), the FACT transcriptional chromatin remodeling complex (Herrera-Moyano et al., 2014) and topoisomerases (Bermejo et al., 2009; Tuduri et al., 2009). R-loops are unwound by RNA-DNA helicases (Alzu et al., 2012; Sollier et al., 2014; Yuce and West, 2013) and the RNA is degraded by RNase H (Huertas and Aguilera, 2003; Wahba et al., 2011). Finally, in mammalian cells BRCA2 helps process R-loops at stressed replication forks (Bhatia et al., 2014). This overwhelming body of evidence clearly implicate transcription-replication conflicts as a major source of endogenous DNA replication stress.

1.2.4 Base damage and lesions

DNA base damage and lesions pose a significant problem for the replication forks to overcome and result in DNA replication stress (Figure 1.1) (Ciccia and Elledge, 2010). Damage from natural decay of purines leads to abasic sites that halt DNA replication (Haracska et al., 2001).

Another form of base damage is DNA deamination caused by hydrolysis or reactive oxygen species (ROS) (Yonekura et al., 2009). Deamination of cytosine produces uracil that base pairs with adenosine resulting in G:C to A:T mutations. In addition to cytosine deamination, rNTPs are incorporated by DNA polymerases at a substantial rate (Dalgaard, 2012). Ribonucleotides in the template strand distort the DNA helix from B- to A-form DNA (Wahl and Sundaralingam, 2000) resulting in replication stress (Lazzaro et al., 2012; McElhinny et al., 2010). Replication stress is further amplified due to inappropriate rNTPs processing by topoisomerase I leading to non-ligatable ssDNA nicks (Kim et al., 2011; Williams et al., 2013). As is the case with R-loops, RNaseH also removes rNTPs from DNA (Sparks et al., 2012).

Bulkier DNA lesions from UV-induced intra-strand crosslinks include cyclobutane pyrimidine dimers and 6-4 pyrimidine pyrimidones. Bases can also be alkylated by the methyl donor S-adenosyl methionine (Rydberg and Lindahl, 1982). Methyl methanesulfonate (MMS) is used experimentally to induce similar DNA alkylation products as S-adenosyl methionine. Bulky DNA lesions cannot fit in the replicative polymerases active sites but can be replicated by specialized translesion synthesis (TLS) polymerases (Section 1.4.2).

Base damage that covalently links the two strands of DNA together, or interstrand crosslinks, cannot be unwound by the helicase and represent a very toxic type of lesion. Interstrand crosslinks are catalyzed endogenously by acetaldehydes (Brendel et al., 2010; Brooks and Theruvathu, 2005; Garaycoechea et al., 2018; Lorenti Garcia et al., 2009). Induction of interstrand crosslinks by platinum based drugs are used as cancer therapeutics because they induce replication stress in rapidly dividing cancer cells (Johnstone et al., 2016). Interstrand crosslinks are repaired by the genes in the Fanconi Anemia pathway and the extreme toxicity of interstrand crosslinks is evident in the severe developmental defects and cancer predisposition in patients with mutations in these genes (Kottemann and Smogorzewska, 2013). Together, DNA base damage and lesions, whether endogenous or exogenous in nature, are a constant source of replication stress in cells.

1.2.5 Imbalanced dNTP, histones and DNA replication machinery

Imbalanced dNTP or histone pools and mutated DNA replication components lead to replication stress. Cells with decreased dNTP pools (Singh and Xu, 2016), elevated dNTP pools (Davidson et al., 2012; Poli et al., 2012) or imbalanced dNTP pools (Watt et al., 2015) all experience

replication stress (Figure 1.1). The rate limiting step of dNTP production is catalyzed by the ribonucleotide reductase complex (Chabes et al., 2003) and the ribonucleotide reductase inhibitor hydroxyurea (HU) is experimentally used to inhibit dNTP production in cells (Singh and Xu, 2016). Pools of dNTPs are also exhausted when too many origins fire and the cell cannot keep up with dNTP demand (Beck et al., 2012). The dNTP pools are tightly controlled by the DNA replication checkpoint (see section 1.3.5) during replication stress. After DNA is synthesized it must be coated with histones and assembled into chromatin. As is the case with dNTPs, increases in histone abundance (Groth et al., 2007; Herrero and Moreno, 2011) or histone depletion (Mejlvang et al., 2014) results in replication stress. Mutation of the DNA replication machinery and histone chaperones also leads to replication stress due improper replisome function (Aguilera and García-Muse, 2013). Thus, the substrates and proteins required for DNA replication must be tightly controlled to avoid replication stress.

1.2.6 Oncogene-induced replication stress

Mutated or over-expressed oncogenes lead to increased cell cycle progression and cell proliferation (Figure 1.1). Mechanistically, oncogene expression deregulates replication origin firing ultimately leading to replication stress (Gaillard et al., 2015; Hills and Diffley, 2014). For example, over-expression of c-Myc increases origin firing and impairs fork progression because c-Myc positively regulates expression of DNA replication and cell cycle progression genes (Dominguez-Sola et al., 2007; Srinivasan et al., 2013). Early G1/S-phase entry is common theme amongst oncogenes and is promoted by expression and localization of cyclin proteins. Cyclin D1 nuclear accumulation leads to origins initiating DNA replication twice in the same cell cycle, or DNA re-replication (Aggarwal et al., 2009). Mdm2 overexpression induces cyclin D2 expression and induces early G1/S transition (Frum et al., 2014). Cyclin E overexpression interferes with pre-RC assembly (Ekholm-Reed et al., 2004) leading to replication stress (Bartkova et al., 2005). Deregulated origin firing and fork progression is another common theme in cancer cells and results in dNTP exhaustion which further drives cancer development (Bester et al., 2011; Burrell et al., 2013; Saldivar et al., 2012). Indeed, the Bcl2 oncogene inhibits RNR activity decreasing dNTP levels (Xie et al., 2014), and supplementing cancer cells with exogenous nucleosides relieves replication stress (Bester et al., 2011; Burrell et al., 2013). In addition to dNTP depletion oncogenes also cause replication stress by increasing transcription-replication conflicts. Oncogenic $HRAS^{V12}$ overexpression up-regulates transcription and induces R-loops (Kotsantis et

al., 2016) while replication stress caused by Cyclin E overexpression is rescued by transcription inhibition (Jones et al., 2013). While increased replication stress is an important driver of cancer development, it also differentiates cancer cells from normal cells and can be exploited as a therapeutic target.

1.3 The DNA replication checkpoint in yeast

The DNA replication checkpoint senses DNA replication stress and promotes DNA replication completion while maintaining genome integrity. In yeast, it is largely redundant with the DNA damage checkpoint and shares many of the same components. The DNA replication checkpoint activates a kinase signaling cascade resulting in repression of late origin firing, inhibition of cell cycle progression, activation of DNA damage response genes and dNTP synthesis and replication fork protection (Figure 1.2). The DNA replication checkpoint is well conserved from yeast to humans owing in part to the essential functions during replication stress. Failure to activate the DNA replication checkpoint during replication stress results in severe genome instability and growth defects. Here, I will explain how the DNA replication checkpoint senses replication stress and activates the replication stress response in budding yeast.

1.3.1 Activation

The DNA replication checkpoint is activated by ssDNA at stressed replication forks (Figure 1.2) (Katou et al., 2003; Sogo et al., 2002). Accumulation of ssDNA at stressed replication forks is thought to occur by helicase-polymerase uncoupling (Byun et al., 2005) with nucleolytic degradation of nascent DNA strands contributing in certain circumstances (Sogo et al., 2002). Exposed ssDNA is coated by the heterotrimeric replication protein A (RPA) complex (Brill and Stillman, 1991; Wold, 1997) which recruits the apical DNA replication checkpoint kinase Mec1-Ddc2 (Rouse and Jackson, 2002; Zou and Elledge, 2003). In addition to Mec1, Tel1 can also act as the apical kinase in the S-phase checkpoint although its role is more important for checkpoint signaling at double strand breaks (DSB). RPA also recruits the alternative clap loader Rad24 to 5’ ssDNA-dsDNA junctions (Majka and Burgers, 2003; Majka et al., 2006a). Rad24 loads the 911 complex composed of Ddc1-Rad17-Mec3 (Majka et al., 2006b) where Ddc1 further activates Mec1 (Majka et al., 2006b; Navadgi-Patil and Burgers, 2009). In turn, Mec1 phosphorylates Ddc1 which recruits Dpb11, an essential protein required for DNA replication initiation (Puddu et al., 2008) that is also required for DNA replication checkpoint activation.

Another essential DNA replication factor, Dna2, is important for checkpoint activation (Kumar and Burgers, 2013). Together, Ddc1, Dpb11 and Dna2 act in a somewhat redundant manner to fully activate Mec1 (Wanrooij et al., 2016). Once Mec1 is fully activated it phosphorylates downstream effectors to kick-off the replication stress response.

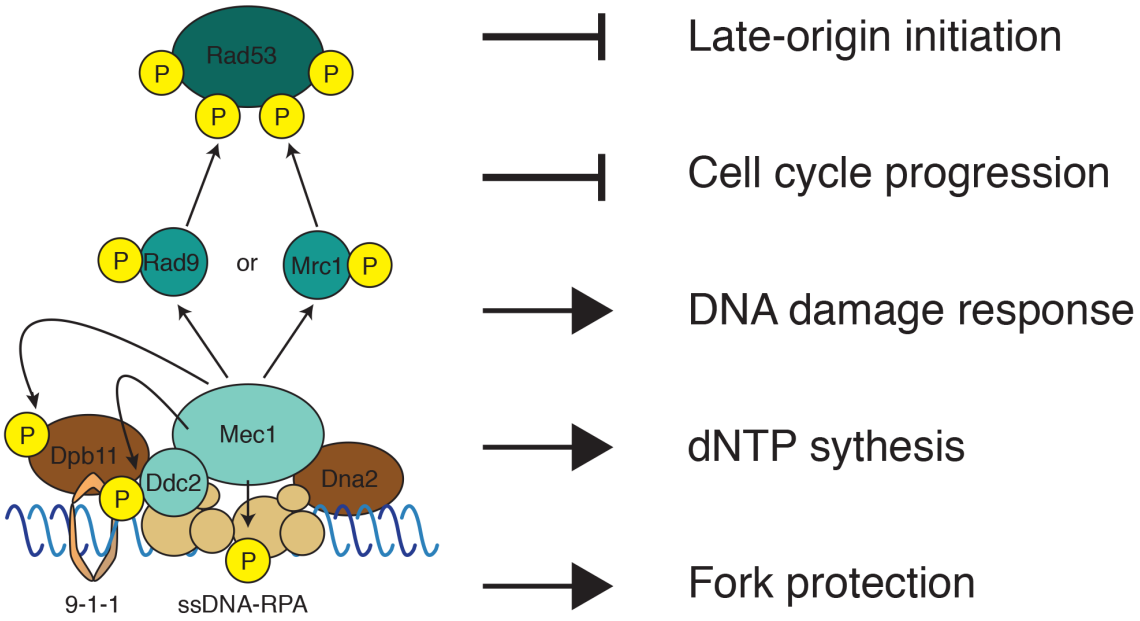

Figure 1.2 DNA replication checkpoint activation. At stressed replication forks ssDNA-RPA recruits Ddc2 in complex with Mec1, the apical DNA replication checkpoint kinase. Mec1 phosphorylates RPA, Ddc1 (in the 9-1-1 complex), and Dpb11 which, along with Dna2, fully activate Mec1 signaling at stressed replication forks. Mec1 phosphorylates the Mrc1 or Rad9 adaptors, which allow Mec1 to phosphorylate and activate Rad53, the central effector kinase in the DNA replication checkpoint. Mec1 and Rad53 together phosphorylate a suite of proteins leading to late origin and cell cycle repression, expression of DNA damage response genes, expansion of dNTP pools and replication fork protection.

DNA replication checkpoint activation at stressed replication forks is transduced from Mec1 to another important signaling kinase Rad53. Mec1 phosphorylates Mrc1 which is both a constitutive member of the replication fork and a checkpoint adapter protein (Chen and Zhou, 2009; Osborn and Elledge, 2003). Phosphorylated Mrc1 physically interacts with and activates Rad53 (Smolka et al., 2006; Tanaka and Russell, 2004). In the DNA damage checkpoint Mrc1 is replaced by the checkpoint adapter protein Rad9. Together, Mec1 and Rad53 phosphorylate a suite of proteins that orchestrate the DNA replication response to promote DNA replication completion and cell survival.

1.3.2 Repression of late origin firing and cell cycle progression

Activation of the DNA replication checkpoint inhibits cells from completing DNA replication (Figure 1.2) (Santocanale and Diffley, 1998; Shirahige et al., 1998; Tercero and Diffley, 2001). One way to inhibit DNA replication progression is to slow down replication fork progression. However, DNA replication fork rate does not change between wild type and checkpoint defective mutants experiencing MMS -induced replication stress (Tercero and Diffley, 2001). An alternative way to inhibit DNA replication completion is to inhibit replication origin firing. Origins follow a temporal firing pattern during S-phase and broadly fall into either early- or late-firing categories (Raghuraman et al., 2001; Yabuki et al., 2002). Rad53 inhibits late origins from firing by phosphorylating and inhibiting the essential DNA initiation proteins Sld3 and Dbf4 (Lopez-Mosqueda et al., 2010; Zegerman and Diffley, 2010). This preserves late origins for use once the stress is relieved. Repression of late-origin firing is not an essential function of the checkpoint during replication stress because a separation of function *MEC1* allele that is incapable of origin repression but retains other checkpoint functions does not have growth defects in replication stress (Tercero et al., 2003).

In budding yeast, the DNA replication checkpoint also inhibits mitosis to avoid transmission of under-replicated or damaged DNA to daughter cells. To inhibit chromosome segregation Mec1 promotes sister-chromatid cohesion and inhibits spindle elongation by stabilizing the securin Pds1 (Clarke et al., 2001; Zhou et al., 2016). Furthermore, Rad53 directly inhibits the mitotic exit network signaling pathway required for mitotic exit and cell division (Hu et al., 2001; Zhou et al., 2016). Delaying mitosis does not suppress the growth defects of *MEC1* or *RAD53* mutants in replication stress (Tercero et al., 2003; Zegerman and Diffley, 2010), suggesting that mitotic delay is not an essential function of the DNA replication checkpoint.

1.3.3 Activation of DNA damage response genes and dNTP synthesis

The DNA replication checkpoint induces expression of DNA repair and DNA replication genes (Figure 1.2) (Allen et al., 1994; Gasch et al., 2001). To achieve this Rad53 phosphorylates Nrm1 which relieves transcriptional repression of these genes (De Bruin and Wittenberg, 2009; De Oliveira et al., 2012; Travesa et al., 2012). Activation of DNA repair genes effectively couples the DNA replication and damage response allowing DNA repair of DNA damage that results in replication stress.

The DNA replication checkpoint also upregulates dNTP production during the replication stress response. Regulating dNTP levels is extremely important in cells (Elledge et al., 1993) and the rate limiting step in dNTP production is catalyzed by the ribonucleotide reductase complex (RNR) (Chabes et al., 2003). To regulate dNTP levels Mec1 and Rad53 phosphorylate and activate Dun1, another DNA replication checkpoint signaling kinase (Bashkirov et al., 2003; Chen et al., 2007; Lee et al., 2008a). Upon S-phase entry activated Dun1 inhibits Rfx1 resulting in RNR gene transcription (Huang et al., 1998). Dun1 also phosphorylates Sml1, an allosteric inhibitor of RNR, which is degraded leaving activated RNR complexes (Zhao and Rothstein, 2002; Zhao et al., 2001). Finally, Dun1 phosphorylates Dif1 targeting it for degradation to allow RNR complex assembly and robust dNTP sythesis (Lee et al., 2008b; Wu and Huang, 2008).

MEC1 and *RAD53* are essential genes and deletion of Sml1 rescues lethality in *MEC1* and *RAD53* mutants indicating an essential function for the DNA replication checkpoint is in normal DNA replication (Desany et al., 1998; Zhao et al., 1998). However, deletion of Sml1 does not rescue the replication stress sensitivity of *MEC1* and *RAD53* mutants. During DNA damage RNR gene expression is induced (Chabes et al., 2003), and over expression of RNR genes rescues *RAD53* sensitivity to HU (Morafraile et al., 2015). Therefore, relieving RNR inhibition during DNA replication stress is not enough for survival; RNR expression must be induced. However, RNR expression must be tightly regulated because deregulated dNTP pools affect fork rate, mutagenesis and chromosome stability (Chabes et al., 2003; Davidson et al., 2012; Poli et al., 2012; Watt et al., 2015). The fine tuning of dNTP levels is evidenced by the multiple layers at which the DNA replication checkpoint regulates dNTP production during both normal and stressed DNA replication.

1.3.4 Replication fork protection

The DNA replication checkpoint protects stressed replication forks from degradation and promotes DNA replication restart after stress is relieved (Figure 1.2) (Morafraile et al., 2015; Tercero and Diffley, 2001). *RAD53* mutants treated with HU accumulate fork structures that have ssDNA and look like reversed forks by electron microscopy, indicating arrested forks are damaged in checkpoint mutants (Lopes et al., 2001; Sogo et al., 2002). The ssDNA in *RAD53* mutants results from Exo1-dependant resection (Cotta-Ramusino et al., 2005) which is usually inhibited by Rad53 (Morin et al., 2008). Interestingly, *EXO1* mutation rescues the replication

restart defect of *RAD53* cells after MMS (Segurado and Diffley, 2008) or HU treatment (Morafraile et al., 2015). Furthermore, the DNA replication checkpoint also limits stressed replication fork reversal by phosphorylating Dna2 (Hu et al., 2012). Thus, the DNA replication checkpoint prevents pathological fork structures by preventing unscheduled fork reversal and resection.

The DNA replication checkpoint also protects stressed replication forks by retaining the DNA replication machinery in a replication-competent state. HU treated *MEC1* and *RAD53* mutant cells do not retain components of the DNA replication machinery at stressed replication forks (Cobb et al., 2003, 2005; Katou et al., 2003; Rossi et al., 2015). To protect replication forks Mec1 phosphorylates the DNA helicase Sgs1 which leads to retention of the components (Bjergbaek et al., 2005; Cobb et al., 2003, 2005). However, it is not clear if the DNA replication machinery fully dissociates from chromatin or if it only slides away from the fork (De Piccoli et al., 2012) Interestingly, multiple DNA replication components are phosphorylated by either Mec1 or Rad53; however, the functional significance of many targets is poorly understood (BastosdeOliveira et al., 2015; Chen et al., 2010; Smolka et al., 2007; Zhou et al., 2016). Regardless, an essential function of the DNA replication checkpoint at stressed replication forks is to keep the replication fork poised for DNA synthesis following recovery from replication stress.

1.4 The Post-Replication Repair pathway

The eukaryotic Post-Replication Repair (PRR) pathway acts as a line of defense against base lesions encountered by DNA replication forks (Prakash, 1981). It functions by allowing the replisome to bypass sites of fork blockages to complete bulk DNA replication, leaving repair of the blockage and/or DNA synthesis in the vicinity for a later time. Because of its extensive study during bypass of MMS- or UV- induced DNA lesions it is sometimes referred to as the DNA Damage Tolerance pathway (Branzei and Szakal, 2016; Garcia-Rodriguez et al., 2016). The PRR pathway is activated primarily by ssDNA at stressed-replication forks and signals for lesion bypass via PCNA ubiquitination in either an error-prone or error-free manner (Figure 1.3). To bypass lesions the error-prone branch employs mutagenic Translesion Synthesis (TLS) DNA polymerases that replicate through blockages while the error-free branch borrows DNA homologous recombination repair proteins to utilize the sister chromatid as a template for

bypass. In the classical PRR pathway model monoubiquitination of PCNA on the conserved lysine 164 ($PCNA_{K164}$) signals for error-prone by-pass while polyubiquitination of the same residue signals for error-free bypass. PRR pathway activation and branch choice is regulated by multiple pathways and is not fully understood. Failure to activate PRR at the right time results in activation of an alternative homologous recombination (HR) pathway and genome instability. Importantly, deregulation of the PRR pathway in humans leads to both initiation and progression of cancer. Understanding how the PRR pathway is regulated is crucial to understand how it impacts human health. In the following section I will explain how the PRR pathway is activated and regulated in budding yeast and humans, drawing insight from other organisms when it is available.

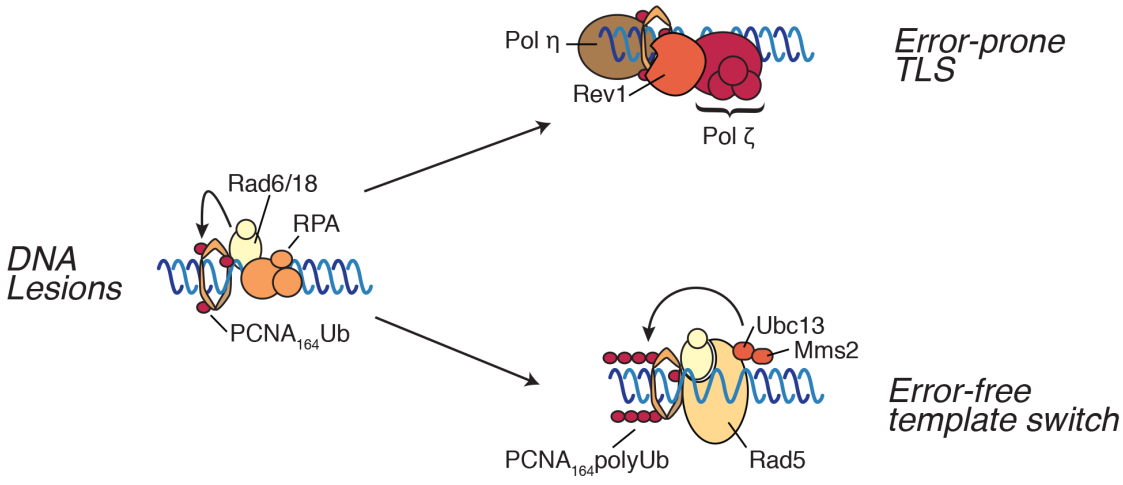

Figure 1.3 Post-Replication Repair (PRR) pathway activation in budding yeast. Lesions on DNA cause replicative polymerase stalling. Exposed ssDNA is coated by RPA and signals for ubiquitination of $PPCNA_{K164}$ by Rad6/Rad18. $PCNA_{K164}Ub$ recruits TLS polymerases (Rev1, Pol ζ and Pol η in budding yeast) that can replicate through lesions in a mutagenic and error-prone manner. Alternatively Rad5/Ubc13/Mms2 catalyzes $PCNA_{K164}$PolyUb chains that signal for error-free lesion bypass by a template switching recombination based mechanism.

1.4.1 Activation of $PCNA_{K164}Ub$

The primary signal for PRR activation is RPA coated ssDNA at stressed replication forks (Figure 1.3) (Hedglin and Benkovic, 2015). In budding yeast, both ssDNA (Bailly et al., 1997) and RPA (Davies et al., 2008) at replication forks recruit the E3 ubiquitin ligase Rad18, which has binding domains for ssDNA, RPA and PCNA. In complex with the E2 ubiquitin conjugase Rad6, Rad18 transfers a ubiquitin to $PCNA_{K164}$ (Bailly et al., 1997; Hoege et al., 2002). In mammalian cells ssDNA at stressed replication forks also induces PCNA monoubiquitination (Chang et al., 2006; Niimi et al., 2008). Human Rad18 binds ssDNA and fork structures through its SAP domain

(Tsuji et al., 2008) and acts with Rad6B catalyze $PCNA_{K164}Ub$. The high conservation of $PCNA_{K164}$, Rad18 and Rad6 underpins how important the PRR pathway is at stressed replication forks.

The complexity of higher eukaryotic genomes appears to require more sophisticated PRR regulation than their single-celled ancestors. Regulation of replication fork accessibility by the chromatin remodelers ZBTB1 and KAP-1 creates local areas of relaxed chromatin allowing access for PCNA ubiquitination (Kim et al., 2014). Additional physical interactions between Rad18 and chromatin are mediated by ubiquitinated histone H2A (Inagaki et al., 2011). Rad18 is subject to cell cycle regulation by DDK phosphorylation (Masai and Vaziri, 2010) and checkpoint regulation by ATR-dependent c-Jun phosphorylation in response to DNA damage (Barkley et al., 2012). In addition to regulation by phosphorylation, other proteins that interact with Rad18 and promote PCNA ubiquitination include BRCA1 (Vincent et al., 2013), SIVA1 (Han et al., 2014), NBS1 (Yanagihara et al., 2011) CRL4A/4B (Sertic et al., 2013), PTIP (Thomas et al., 2008) and Claspin (Yang et al., 2008). Inhibition of $PCNA_{K164}$ deubiquitination by spartan (Juhasz et al., 2018) is also important for Rad18 recruitment and PRR function (Centore et al., 2012). Finally, there may be additional E3 ligases responsible for PCNA ubiquitination because Rad18 null DT40 (Simpson et al., 2006) or mouse (Shimizu et al., 2017) cells are still able to ubiquitinate PCNA.

In the majority of PRR studies UV- or MMS-lesions are the primary source of replication stress. However, it is clear that PCNA is ubiquitinated in replication stress arising from other types of exogenous sources such as dNTP depletion (HU), oxidative stress (H_2O_2) and even DSBs (IR) (Davies et al., 2008). Replication stress from mutation of DNA replication machinery components, such as the non-essential pol ∂ subunit Pol32 (Karras and Jentsch, 2010) or replication initiation factor Mcm10 (Becker et al., 2014) also leads to PCNA ubiquitiniation. In addition to replication stress, PCNA ubiquitination is important during unperturbed DNA replication. The genetic interaction profile of *PCNA-K164R* has very high correlation with mutants that are defective in lagging-strand DNA synthesis indicating they perform similar functions in cells (Becker et al., 2015). In fission yeast, loss of PCNA ubiquitination results in slow S-phase progression, defects in late-replicating regions and increased frequency of replication gaps (Daigaku et al., 2017). Furthermore, PCNA is ubiquitinated in Xenopus egg

extracts in unperturbed S-phase (Leach and Michael, 2005). Taken together, the data indicate that PRR responds to a wide range of endogenous and exogenous types of replication stress.

1.4.2 Error-prone TLS polymerases

In the classical PRR model, the $PCNA_{K164}Ub$ signal recruits TLS polymerases to insert bases opposite lesions in a mutagenic fashion, a process termed error-prone bypass (Figure 1.3) (Vaisman and Woodgate, 2017). Most TLS polymerases are Y-family polymerases, in contrast to the B-family replicative polymerases (Table 1.1). In yeast there are 3 TLS polymerases: the UV lesion tolerance polymerase Pol η, the deoxycytidyl transferase Rev1 and the B-family member Pol ζ, which is recruited to DNA by Rev1 and shares subunits with Pol ∂. There are two additional Y-family polymerases in humans: the extender polymerase Pol κ, and Pol ι which has lyase activity required for excision repair of damaged bases. All TLS polymerases have low catalytic activity, fidelity and processivity compared to the replicative polymerases. They have more flexible active sites to accommodate lesions but this also means they dissociate from DNA easily and misincorporate bases. Misincorporation is problematic considering TLS polymerases lack 3'-5' proof reading activity (Khare and Eckert, 2002). Therefore, tight regulation of TLS recruitment and activity is important to limit the mutagenic synthesis of TLS polymerases to the appropriate time and place.

Pol ζ is the only B-family TLS polymerase and made up from the catalytic subunit Rev3 and the non-catalytic subunits Rev7, Pol31 and Pol32, with the latter two being shared with Pol ∂ (Johnson et al., 2012; Lee et al., 2014; Makarova et al., 2012). Pol ζ can insert bases opposite lesions but is more efficient at extending primer termini even though it is ~100x more error-prone than the other B-family polymerases (Zhong et al., 2018). The remaining TLS polymerases belong to the Y-family and are all single polypeptides. Pol η is very important for UV tolerance because it inserts bases opposite CPD and 6-4 photoproduct lesions with high accuracy (Masutani et al., 1999a; Zhang et al., 2000). Pol ι can also bypass UV-induced lesions if Pol η is not functional (Vaisman et al., 2006). Pol κ bypasss benzo-a-pyrene lesions accurately (Huang et al., 2003b) and could be important for bypass of similar lesions induced by environmental pollutants (Ogi et al., 2002). Thus, while there is redundancy amongst the TLS polymerases they each have specialized functions for specific types of lesions or non-lesion stress (see below).

$PCNA_{K164}Ub$ serves as a recruitment signal and attachment point for TLS polymerases at stressed replication forks. The Y-family polymerases have either ubiquitin-binding zinc domains (UBZ) and ubiquitin -binding motif domains (UBM) that facilitate interaction with $PCNA_{K164}Ub$ at stressed replication forks (Bienko et al., 2005). Additionally, Pol κ, Pol ι and Pol η each have PCNA interacting peptide (PIP) boxes (Hishiki et al., 2009) which increase their activity when bound to PCNA (Masuda et al., 2015). Rev1 has no PIP box but still binds to both PCNA (Murakumo et al., 2006) and $PCNA_{K164}Ub$. Interestingly, Rev1 serves as a scaffold for recruitment and regulation of the other TLS polymerases (Boehm et al., 2016). It physically interacts with Rev7 of Pol ζ which is required for Pol ζ mutagenesis (Murakumo et al., 2001). TLS polymerases are also subject to phosphorylation (Pages et al., 2009; Sabbioneda et al., 2006) and ubiquitination (Mcintyre and Woodgate, 2015) further modifying their function. In addition to PCNA, Rad18 physically interacts with both Pol κ (Bi et al., 2006) and Pol η (Watanabe et al., 2004) and spartan recruits p97 to regulate TLS activity (Davis et al., 2012; Mosbech et al., 2012). Together the multiple levels of regulation ensure proper usage of TLS polymerases and limit their mutagenic potential.

In addition to lesion tolerance, TLS polymerases are needed for robust tolerance of lesion-less replication stress and can replicate DNA from undamaged templates (Bournique et al., 2017). Cells activate Rev1 and Pol ζ to bypass non-B hairpin structures (Northam et al., 2014) and Pol ζ is needed for TNR stability when the replicative polymerases are compromised (Shah et al., 2012). Interestingly, Rev1 binds and disrupts G4 structures (Eddy et al., 2014) and Pol η and Pol κ promote DNA replication through them (Betous et al., 2009). In addition to difficult to replicate sequences, Pol ζ-dependent mutagenesis increases upon HU exposure (Northam et al., 2010) and in DNA replication machinery mutants (Northam et al., 2006). Pol ζ is essential for proliferation in mammalian cells and prevents mitotic defects and chromosome breaks during replication stress (Bhat et al., 2013; Lange et al., 2012). Pol η also relocalizes to nuclear foci after HU treatment (Buisson et al., 2014) and is required for genome stability (Bergoglio et al., 2013; Rey et al., 2009). Interestingly, SUMOylated Pol η travels with unperturbed replication forks which is required for robust resistance to replication stress (Despras et al., 2016). Thus, the utilization of TLS polymerases on undamaged templates is emerging as a common mechanism to cope with lesion-less replication stress.

Table1.1 TLS polymerase characteristics

Pol	*S. cerevisiae*	*H. sapiens*	Family	Characteristics
Rev1	REV1	REV1	Y	• Specifically incorporates dCMP opposite abasic sites and undamaged template dG • Acts as scaffold protein that interacts with TLS polymerases ζ, η, ι and κ • Generates mutations at G-C base pairs during immunoglobulin gene somatic hypermutation
Pol ζ	REV3 REV7 POL31 POL32	REV3L REV7L POLD2 POLD3	B	• Bypasses lesions unassisted • Works with other TLS polymerases to facilitate the extension step of TLS • Stimulated by an interaction with Rev1 • Murine homozygous knockout is embryonic lethal
Pol η	RAD30	POLH	Y	• Bypasses a thymine–thymine CPD relatively efficiently and accurately • Defects lead to the sunlight-sensitive and cancer-prone xeroderma pigmentosum variant (XP-V) phenotype • Regulated by ubiquitination and phosphorylation • Generates mutations at A-T base pairs during immunoglobulin gene somatic hypermutation
Pol κ	……	POLK	Y	• Prone to making -1 frameshift mutations • Accurately and efficiently bypasses a number of N^2-dG lesions • Plays additional roles in repair synthesis steps of nucleotide excision repair
Pol ι	……	POLI	Y	• Incorporates opposite template dA reasonably accurately, but opposite template dT in a highly error-prone manner

1.4.3 Error-free template-switching and $PCNA_{K164}PolyUb$ by Rad5/HLTF/SHPRH

In an alternate PRR branch, $PCNA_{K164}Ub$ can be extended to K63-linked polyubiquitin chains signaling for template-switching bypass of DNA lesions in an error-free fashion (Figure 1.3). The RING finger E3 ligase Rad5 (Johnson et al., 1992; Johnsons et al., 1994) together with the E2 complex Ubc13 and Mms2 catalyzes the formation of $PCNA_{K164}PolyUb$ chains (Eddins et al.,

2006; Moraes et al., 2001; VanDemark et al., 2001). Rad5 physically interacts with PCNA (Choi et al., 2015) and with Ubc13 to guide Ubc13-Mms2 polyubiquitination of PCNA (Hoege et al., 2002; Parker and Ulrich, 2009; Ulrich, 2000). The conserved human homologs of Ubc13-Mms2 are Ubc13-Uev1 while Rad5 function appears to be split between two homologs, HLTF and SHPRH (Unk et al., 2010). HLTF and SHPRH each mediate PCNA polyubiquitination depending on the type of replication stress. $PCNA_{K164}$polyUb signals for lesion bypass using the sister chromatid as the synthesis template instead of the lesion-containing strand (Papouli et al., 2005; Pfander et al., 2005; Zhang and Lawrence, 2005). To accomplish template-switching the error-free branch borrows parts from the homologous recombination (HR) DSB repair pathway. In addition to ubiquitin ligase activity, Rad5 and HLTF have conserved HIRAN and helicase domains (Unk et al., 2010). The relative complexity of template-switching repair and overlap with other DNA damage repair pathways has made unravelling the mechanism of template-switching an active area of research.

Extensive studies of template-switching in budding yeast revealed important contributions from DNA replication and HR components (Branzei and Szakal, 2016). The proposed template-switching model posits that ssDNA gaps left behind replication forks are filled using the newly synthesized sister chromatid as a template instead of the blockage containing strand (Figure 1.4). Blockages on the lagging strand can result in ssDNA gaps behind DNA replication forks because of discontinuous lagging strand synthesis. However, blockages on the leading strand pose a more significant barrier and would require a repriming event past the lesion for bulk DNA synthesis to proceed. In line with this the DNA initiating complex Pol α/primase/Ctf4 in budding yeast (Fumasoni et al., 2015), and human PrimPol (Mourón et al., 2013) are required for template-switching activity.

A mechanism similar to HR repair of DSBs is proposed to fill the ssDNA gaps left behind the fork (Figure 1.4). HR is initiated when Rad52 and a Rad55-Rad57 heterodimer loads Rad51 on ssDNA, replacing RPA. Rad51-ssDNA filaments perform a homology search assisted by Rad54 where the 3' end of ssDNA invades the sister chromatid duplex DNA displacing the non-complementary strand to form a displacement loop (D-loop). In budding yeast, Rad51, Rad52 (Branzei et al., 2008), RPA, Rad55, Rad57, pol∂ and Exo1 are all required for D-loop formation during template-switching (Vanoli et al., 2010). Rad51-ssDNA filament formation during template-switching is also facilitated by the Shu complex (*SHU1, SHU2, PSY3 and CSM1*) (Ball

et al., 2009; Godin et al., 2018; Xu et al., 2013). Template-switching appears to be conserved in human cells (Izhar et al., 2013) and HLTF promotes D-loop formation (Burkovics et al., 2014). The D-loop is processed into a pseudo-double Holliday-Junction (Giannattasio et al., 2014) as DNA is polymerized. When gap filling nears completion the DNA intermediates form sister chromatid junctions that are resolved by a Sgs1-Top3 complex to produce non-crossover products (Branzei et al., 2008; Liberi et al., 2005). SUMOylation of Smc5/6 by Ubc9-Mms2 promotes resolution of sister chromatid junctions (Branzei et al., 2006; Sollier and Branzei, 2009). Interestingly, Smc5/6 and Sgs1 are also needed to resolve sister chromatid junctions that form in late replicating regions providing further evidence that PRR responds to endogenous replication stress (Menolfi et al., 2015). If template-switching intermediates persist until mitosis Mus81-Mms4 and Slx1-Slx4 nucleases are upregulated by mitotic kinases and promote cross-over prone resolution (Gritenaite et al., 2014; Szakal and Branzei, 2013; West et al., 2015). The DNA replication checkpoint actually safeguards template-switching intermediates from inappropriate processing to cross-overs by Mus81-Mms4 during S phase (Szakal and Branzei, 2013). Importantly, if the template-switching branch is fully functional the outcome is error-free ssDNA gap repair.

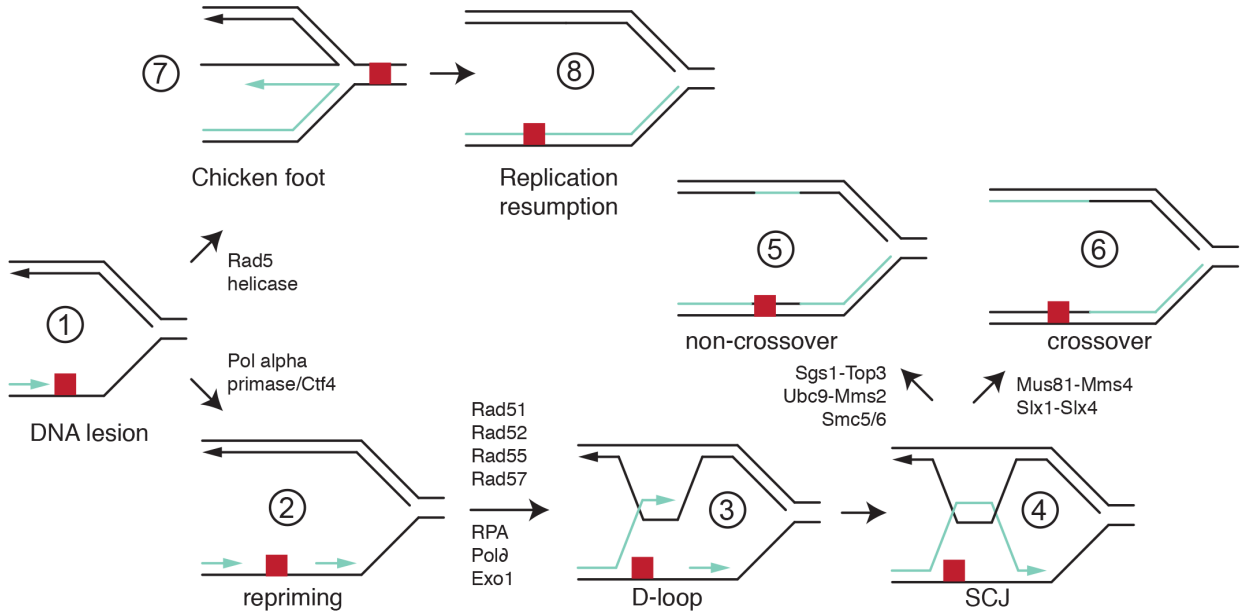

Figure 1.4 Proposed mechanism of Template-Switching and fork reversal, the error-free branch of PRR. 1) DNA lesions lead to polymerase stalling and PRR activation. 2) Blocks on the leading or the lagging strand are re-primed downstream of the lesion (leading strand is shown). 3) Analogous to canonical homologus recombination the 3' end of ssDNA invades the sister chromatid duplex DNA displacing the non-complementary strand to form a displacement loop (D-loop). 4) After gap filling is complete the DNA intermediates form sister chromatid junctions. 5) Sister chromatid junctions are normally resolved by a Sgs1-Top3 complex that is dependent on SUMOylation of Smc5/6 by Ubc9-Mms2, and which produces non-crossover products. 6) Sister chromatid junctions can be processed by Mus81-Mms4 or Slx1-Slx4 to produce crossover products and genome rearrangements. 7) In the error-free PRR branch, Rad5 helicase activity is proposed to reverse stalled replication forks to a chicken foot structure where the two nascent DNA strands anneal to allow for replication that bypasses the template strand lesion. 8) The chicken foot is unwound and normal DNA replication resumes

In addition to the RING finger ubiquitin ligase domain, Rad5 and HLTF have conserved SNF2 helicase and HIRAN domains (Figure 1.5). Rad5 has ssDNA dependent ATPase activity (Johnsons et al., 1994) and *in vitro* replication fork reversal activity (Blastyák et al., 2007; Minca and Kowalski, 2010). HLTF also has *in vitro* replication fork reversal activity (Achar et al., 2011; Blastyák et al., 2010; Kile et al., 2015). Additional PRR mediated fork reversal in mammalian cells occurs from $PCNA_{K164}$PolyUb recruitment of the fork reversal helicase ZRANB3 (Ciccia et al., 2012; Vujanovic et al., 2017; Weston et al., 2012; Yuan et al., 2012). Fork reversal is proposed to result in a structure termed a chicken-foot where the two complimentary nascent DNA strands base pair (Figure 1.4). A chicken foot structure in theory is suitable for template-switching but little evidence of this structure exists in wild type cells. Studies of Rad5 helicase function in cells were complicated by lack of a true ligase and helicase separation of function mutant. The ATPase mutant $Rad5_{DE682,682AA}$ has been extensively characterized as the helicase dead allele. However, recent studies demonstrated that

$Rad5_{DE682,682AA}$ also affects PCNA polyubiquitination by disrupting physical interactions between Rad5 and both PCNA and Ubc13 (Ball et al., 2014; Choi et al., 2015). A true separation of function allele was isolated, Rad5-Q1106D (Choi et al., 2015), which should help clear up the contribution of Rad5 helicase activity to PRR in budding yeast.

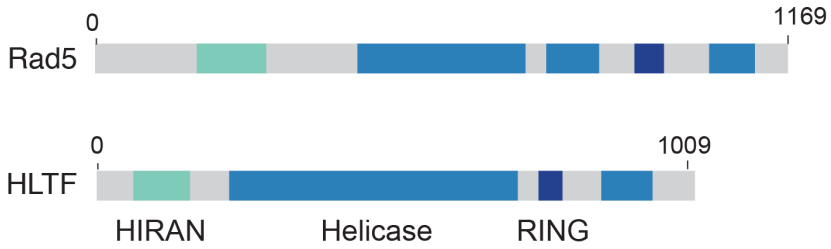

Figure 1.5 Domain drawings of Rad5 and HLTF. Rad5 and HLTF have an N-terminal HIRAN domain important for localization and DNA binding, a RING finger E3 ubiquitin ligase domain required for polyubiquitination of PCNA and a SNF2 helicase domain required for in vitro replication fork reversal activity.

Structural studies conducted on the HIRAN domain of higher eukaryotes have identified key features that facilitate physical interaction with DNA (Hishiki et al., 2015; Kile et al., 2015; Kobbe et al., 2016; Korzhnev et al., 2016). The HIRAN domain forms a pocket that binds the free 3'OH of a ssDNA overhang. This provides a mechanism to protect the 3' end of nascent DNA and promote D-loop formation or other DNA metabolic transactions (Burkovics et al., 2014). Protein-DNA or protein-protein interactions mediated by the HIRAN domain of Rad5 and HLTF likely regulate their subcellular localization and function during the replication stress response.

1.4.4 Regulation of PRR and pathway choice

Pathway choice between TLS and template-switching in cells appears to be regulated during the cell cycle by protein expression and physical interactions. The general theme appears to be that template-switching is preferred in S-phase while TLS is preferred in G2-phase. Expression of Rad6 and Rad18 remains relatively constant throughout out the cell cycle but is upregulated in response to DNA damage (Lyakhovich and Shekhar, 2004; Madura et al., 1990; Masuyama et al., 2005). However, Rad5 expression peaks in S-phase (Ortiz-Bazán et al., 2014) and sister chromatid junctions resulting from template-switching form predominantly in early S-phase (Branzei et al., 2008; Gonzalez-Huici et al., 2014; Karras et al., 2013; Minca and Kowalski, 2010). This is partially due to action of the DNA bending enzyme Hmo1 that funnels repair down the error-free branch (Gonzalez-Huici et al., 2014). Conversely, Rev1 expression peaks in

G2-phase (Waters and Walker, 2006) and TLS function appears to be more important for repair of UV-induced ssDNA gaps if PRR function is restricted to G2/M-phase of the cell cycle (Daigaku et al., 2010), although both template-switching and TLS branches are active in repair of MMS-induced gaps in G2-phase (Karras and Jentsch, 2010). Interestingly, mutation rate is correlated with replication timing in yeast (Lang and Murray, 2011) and humans (Stamatoyannopoulos et al., 2009) with earlier replicating regions having lower mutation rates. Why TLS is preferred in G2 when there is a homologous chromosome available for template-switching remains a mystery.

The order of recruitment in the classical PRR pathway is challenged by observations that place Rad5 upstream of TLS function. At the *CAN1* locus, widely used to measure mutation frequency, *rad5*Δ cells have an increased mutation rate compared to wild type cells, favouring the classical PRR model where loss of the error-free branch funnels bypass to the error-prone branch (Huang et al., 2003a). Yet, historically *RAD5* was named *REV2* because *rad5*Δ supresses UV-induced mutations at other genomic loci (Lemontt, 1971). Furthermore, Rad5 physically interacts with Rev1 (Fan et al., 2018; Kuang et al., 2013; Pagès et al., 2008; Xu et al., 2016) and the Rad5-Rev1 interaction is important for UV-induced Rev1-dependent mutagenesis (Xu et al., 2016). HLTF also supports increased UV-induced mutagenesis by enhancing PCNA monoubiquitination and subsequent Pol η recruitment (Lin et al., 2011). Therefore, it appears that Rad5 may sit upstream of TLS recruitment in the PRR pathway and possibly orchestrate pathway choice.

1.4.5 Alternative HR at stressed replication forks

In lieu of PRR eukaryotic cells utilize an alternative and parallel HR-mediated pathway in response to replication stress. The alternative HR pathway is globally suppressed during S-phase and appears to only function in G2-phase in the absence of PRR. Suppression of HR at replication forks is mediated by SUMOylation of $PCNA_{K164}$ by Ubc9-Siz1 (Figure 1.6) (Hoege et al., 2002). PCNA is SUMOylated during unperturbed S-phase (Parker et al., 2008) to prevent unscheduled HR at physiological replication forks. $PCNA_{K164}$SUMO recruits the anti-recombinase protein Srs2 which disrupts Rad51 filaments (Krejci et al., 2003; Papouli et al., 2005; Pfander et al., 2005; Veaute et al., 2003). In mammals PARI inhibits HR at replication forks which is also dependent on PCNA SUMOylation (Burkovics et al., 2016; Gali et al., 2018;

Moldovan et al., 2012). However, global inhibition of Rad51 filament formation at stressed replication forks is not compatible with the template-switching branch of PRR. Budding yeast upregulate Rad51 filament formation for template-switching by Esc2-mediated degradation of Srs2 and Elg1-mediated removal of SUMOylated PCNA from chromatin (Parnas et al., 2010; Urulangodi et al., 2015). In general, *SRS2* mutants suppress the replication stress sensitivity of *PRR* mutants by allowing the alternative HR pathway to operate earlier in the cell cycle (Lawrence and Christensen, 1979; Schiestl et al., 1990). Regardless, PRR is the preferred choice for replication stress tolerance in eukaryotic cells.

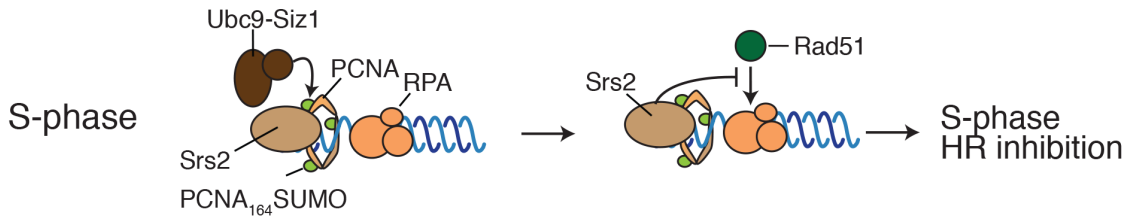

Figure 1.6 Inhibition of canonical HR during DNA replication. PCNA is SUMOylated on K164 by Ubc9-Siz1 in S-phase. $PCNA_{K164}SUMO$ recruits the anti-recombinase protein Srs2 which inhibits Rad51 filament formation on ssDNA.

1.4.6 Defects in the PRR pathway and cancer

The PRR pathway is emerging as an important regulator of genome stability and cancer progression. On one hand, the PRR pathway safeguards cells against replication stress and suppresses genome instability that leads to cancer initiation. On the other hand, upregulation of PRR during the progression of cancer allows cells to cope with oncogene-induced replication stress. Thus, the PRR pathway acts to both suppress and promote cancer progression depending on the context and timing.

In budding yeast defective PRR leads to genome instability. PRR mutants have increased recombination because the only pathway left for replication stress resistance is the alternative HR pathway (Liefshitz et al., 1998). Cells defective for PCNA ubiquitination such as *rad6*Δ, *rad18*Δ and *rad5*Δ also have increased gross chromosome rearrangements (GCRs) which could result from inappropriate HR events (Smith et al., 2004). Removal of HR components generally decreases GCR in PRR mutants (Motegi et al., 2006; Putnam et al., 2009, 2010). However, this is also accompanied by a dramatic sensitivity to replication stress, likely due to persistence of ssDNA or other genotoxic intermediates in mitosis.

In mammalian cells, germline loss of PRR expression or loss of function mutations result in cancer susceptibility, implicating PRR genes as tumor suppressors. Lack of TLS polymerases results in various forms of cancer susceptibility. The most famous example is Pol η deficiency that results in xeroderma pigmentosum (XPV) which is accompanied by extremely high sunlight-induced skin cancer (Masutani et al., 1999b). Pol $\iota^{-/-}$ mice are susceptible to induced lung cancer (Iguchi et al., 2014) and loss of Pol ζ increases spontaneous tumorigenesis (Wittschieben et al., 2010). Members of template-switching pathway have also been described as tumor suppressors. Loss of HLTF mRNA expression due to promoter methylation was observed in colon (Moinova et al., 2002) and digestive tract cancers (Leung et al., 2003) $HLTF^{-/-}$ mice do not form gut cancers but when crossed to a predisposed intestinal cancer genotype ($APC^{min/-}$) have increased tumor formation and genomic instability (Sandhu et al., 2012). In addition to gut cancers, low HLTF expression is observed in some melanoma and leukemia cell lines (Mackay et al., 2009) and expression of truncated and possibly dominant negative HLTF isoforms are observed in some cancers (Capouillez et al., 2008, 2009). Finally, the SHPRH genomic locus is a known hotspot for rearrangements during cancer progression (Sood et al., 2003). Together these findings indicate that the PRR pathway has tumor suppressing roles.

Recent evidence points to PRR pathway upregulation as mechanism to cope with oncogene-induced replication stress. Over-expression of the oncogene Cyclin E or promoting cell cycle progression by inhibiting geminin or Wee1 leads to ssDNA exposure, replication fork slowing, Rad18-dependent PCNA ubiquitination and TLS activity (Sekimoto et al., 2015; Yang et al., 2017). In agreement with PRR being important for oncogene survival, depletion of Rad18 sensitizes cells to Cyclin E over-expression and to treatment with the Wee1 inhibitor MK-177. Interestingly, some tumors specifically upregulate PRR by expressing MAGE-A4 which is normally restricted to germline cells (Simpson et al., 2005). MAGE-A4 upregulates PRR by stabilizing Rad18 and promoting TLS activity (Gao et al., 2016). In fact, increased expression of TLS polymerases is observed in many types of cancer (Hoffmann and Cazaux, 2010), and increased TLS mutagenesis is emerging as an important cause of tumor heterogeneity. Rev1 drives mutagenesis and development of lung cancer (Dumstorf et al., 2009), increased expression of Pol ι drives hyper mutation and progression of esophageal and bladder cancer cells (Sun et al., 2015; Yuan et al., 2013) and upregulation of Pol κ promotes tumor heterogeneity and tumorigenesis (Bavoux et al., 2005).

Similar to oncogene-induced stress, many cancer therapeutics induce replication stress and activate the PRR pathway. There is mounting evidence that TLS polymerases can replicate through lesions caused by frontline platinum-based cancer therapeutics in a mutagenic fashion leading to chemoresistance (Vaisman et al., 2000). Hyper-activation of PCNA monoubiquitination by RAD6B overexpression confers chemoresistance (Lyakhovich and Shekhar, 2004). Moreover, suppression of Rev1 (Xie et al., 2010) and Rev3 (Doles et al., 2010; Wu et al., 2004) inhibits drug-induced mutagenesis and subsequent chemoresistance in various cancer types. This makes TLS polymerases an attractive small molecule drug target to either inhibit DNA polymerization or inhibit PRR-mediated protein-protein interactions. A few inhibitors of each type are in development and it will be exciting see how these perform in the clinic (Korzhnev and Hadden, 2016).

1.5 Rationale for thesis

Rad5 re-localizes to nuclear foci when cells are treated with agents that promote lesion-less replication stress (Fan et al., 2018; Ortiz-Bazán et al., 2014; Tkach et al., 2012). Foci form under conditions that do not result in DNA base lesions, implicating PRR in the replication stress response in addition to lesion tolerance. Furthermore, PRR mutants have growth defects in the presence of lesion-less replication stress (Daee et al., 2012). How Rad5 re-localization is regulated and how this leads to resistance of lesion-less replication stress is unknown

The aim of my research is to define how Rad5 localization is regulated and what role Rad5 plays during lesion-less replication stress. In Chapter 2, I describe a high-throughput genome-wide screen to identify regulators of Rad5 focus formation. I reveal that heat shock proteins are required for Rad5 foci to form and are required for resistance to replication stress. In Chapter 3 I describe an approach to characterize Rad5 foci and refine the understanding of Rad5 functions during lesion-less and endogenous replication stress. I demonstrate that Rad5 foci form in S-phase and that Rad5 is recruited and retained at stressed replication forks, both of which depend on $PCNA_{K164}Ub$. At stressed replication forks Rad5 promotes Rev1 recruitment and TLS activity on undamaged templates. Absence of Rad5 at stressed replication forks results in accumulation of ssDNA, checkpoint activation, anaphase bridges and chromosome breakage. Importantly, I define a role for PRR in mutagenic repair of undamaged ssDNA caused by both physiological and exogenous sources of replication stress. I also establish that Rad5 is the main effector of

PRR signalling and reveal its role as a scaffold to facilitate TLS polymerase-facilitated repair of, and cell survival during, replication stress.

My results in budding yeast will lead way to studies of how PRR drives cancer progression and drug resistance. If cancer cells upregulate PRR to survive oncogene-induced replication stress then down regulating PRR could offer a selective means to inhibit cancer cell proliferation. Moreover, increased TLS mutagenesis leads to tumor heterogeneity and evolution. Many frontline cancer therapeutics result in DNA base damage that is replicated by TLS polymerases, further exacerbating mutagenesis and leading to chemoresistance. Future studies looking at the role of HLTF in cancer cell survival and TLS-induced mutagenesis will help resolve some of these issues.

Chapter 2
A genome-wide screen identified heat shock proteins as regulators of Rad5 focus formation

ACKNOWLEGMENTS

I would like to thank Bryan-Joseph San Luis (Boone lab) for providing strains used in follow-up analysis of screen hits.

2 A genome-wide screen identified heat shock proteins as regulators of Rad5 focus formation

2.1 Summary

Rad5 forms nuclear foci after treatment with HU. Previous studies indicate that Rad5-dependent polyubiquitination of PCNA is required for error-free bypass of MMS- or UV-induced DNA lesions but there is little insight into the role of Rad5 in response to HU-induced replication stress, where base lesions are likely absent. Additionally, how Rad5 is recruited and regulated during replication stress is unknown. To understand what mechanisms underpin Rad5 function I screened the yeast gene deletion collection by high-content confocal microscopy and identified 23 genes that are important for Rad5 focus formation during HU-induced replication stress. Of these genes *YDJ1*, a yeast heat-shock protein (HSP) 40 chaperone, is required for Rad5 focus formation. *YDJ1* and *RAD5* mutants are epistatic for HU sensitivity, suggesting they operate in the same resistance pathway. In addition to Ydj1, I found that the HSP70s Ssa1 and Ssb1 are Ydj1 co-chaperones mediating Rad5 relocalization and HU resistance. My results indicate that HSP chaperones regulate replication stress resistance and PRR function in budding yeast.

2.2 Results

2.2.1 A genome-wide screen identifies 23 non-essential gene deletions that reduce Rad5 focus formation.

To start, I wanted to confirm that Rad5 reproducibly forms sub-nuclear foci in HU treatment. I treated mid-logarithmic *RAD5-GFP NUP49-RFP* cells with 200 mM HU for 60 min followed by imaging in the GFP, RFP and DIC channels. Nup49 is a component of the nuclear pore and is used as a nuclear periphery marker. I observed that Rad5-GFP forms nuclear foci in these conditions (Figure 2.1A). I also tested the parent Rad5-GFP strain from the GFP collection (Huh et al., 2003) and further confirmed that Rad5-GFP reproducibly forms nuclear foci in HU-induced replication stress (Figure 2.1B).

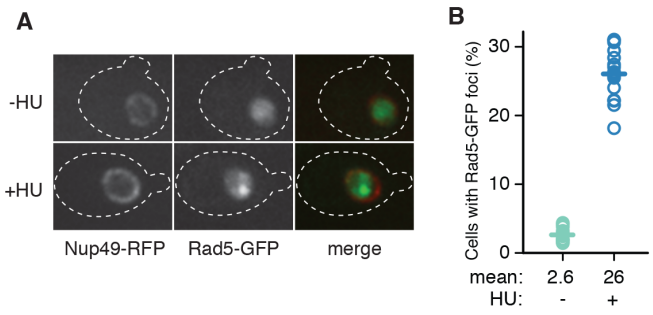

Figure 2-1 Rad5 forms nuclear foci in response to HU treatment. Logarithmic phase *RAD5-GFP NUP49*-RFP cells with the indicated mutations were left unperturbed or treated with 200 mM HU for 60 minutes and imaged by confocal microscopy in the RFP, GFP and DIC channels. The RFP, GFP or merged channels are shown, with the cell outline represented by a dashed line. (B) Mid-logarithmic phase *RAD5-GFP* cells were treated as in A. The percent of cells with at least one focus is plotted for each replicate and the means are shown as solid bars. At least 100 cells of each type were scored for each replicate.

Having established that Rad5 foci form in HU treatment, I set out to identify regulators of Rad5 by conducting a genome-wide high-throughput confocal microscopy screen (Torres and Brown, 2015). Using synthetic genetic array technology Rad5-GFP and the fluorescent cytoplasmic marker RPL39pr-TdTomato were crossed into the complete *S. cerevisiae* haploid non-essential gene deletion collection, consisting of ~4500 strains. The resulting strains were imaged on a high-throughput confocal microscope in the absence or presence of 200 mM HU. I visually inspected images for a decrease in foci relative to wild type controls to identify regulators. From the initial the screen I identified 133 deletion mutants that had a decrease in Rad5 foci. I validated each of these 133 strains individually in duplicate by manual confocal microscopy and arrived at 23 single gene deletions that showed at least a 25% decrease in the number of cells with Rad5-GFP foci during HU-treatment (Figure 2.2A). Examples of individual deletion strains are shown in Figure 2.2B and a summary of the results are in Table 2.1. To identify common functions, processes or components among the Rad5 regulators I performed GO term enrichment analysis (Figure 2.2C). Although there were no molecular function GO terms enriched, there were two biological processes enriched, protein ubiquitination (*SLX8, MMS2, ASF1, MUB1, YDJ1* and *BRE5*) and iron assimilation by reduction and transport (*FTR1* and *FET3*). Interestingly, Ftr1 and Fet3 together form the high-affinity iron permease complex which is the only enriched cellular component GO term retrieved (Figure 2.2C).

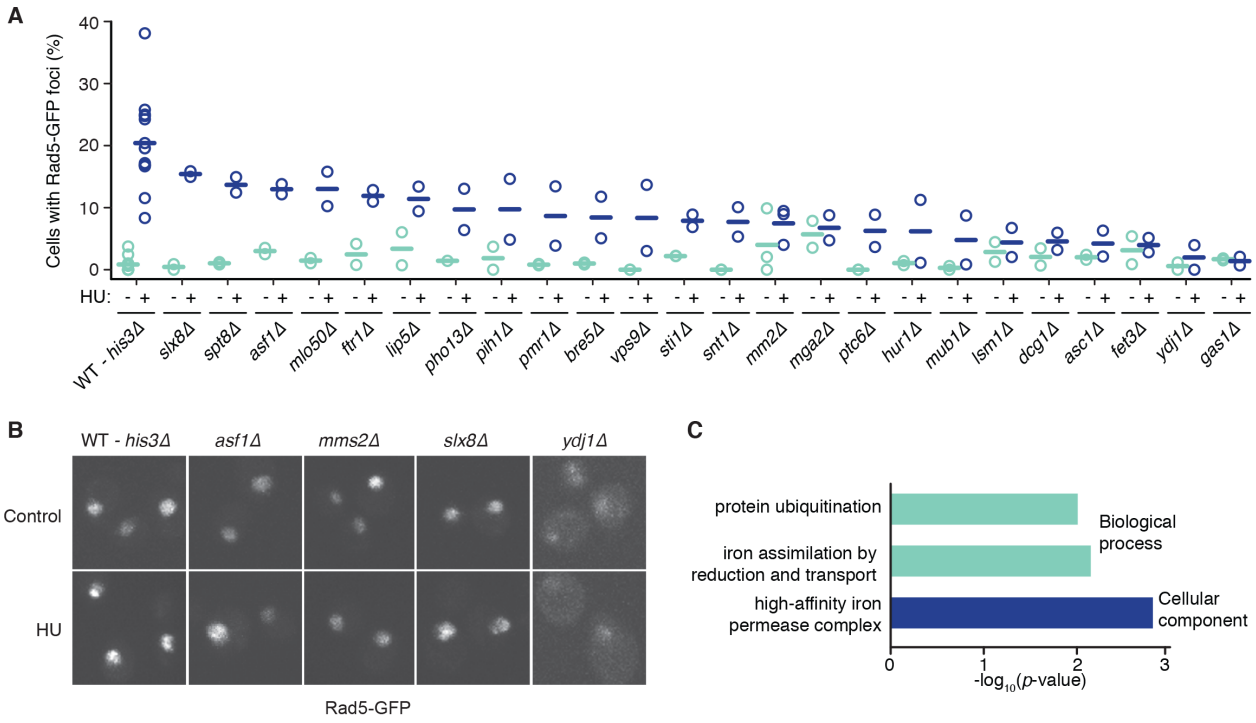

Figure 2.2 Genome-wide high-throughput screen reveals 23 non-essential gene deletions that reduce Rad5 focus formation. (A) Mid-logarithmic phase *RAD5-GFP RPL39pr-TdTomato* with the indicated deletion were treated with 200 mM HU for 60 minutes, harvested and imaged. his3Δ is used as a wild type control during SGA. The percent of cells with at least one focus is plotted for each replicate and the means are shown as solid bars. At least 100 cells of each type were scored for each replicate. (B) Representative micrographs in the GFP channel of the indicated strains. (C) GO-term enrichment analysis was performed on the validated list of genes identified in the screen.

I was interested in following up hits that directly interact with Rad5 to facilitate recruitment and function during HU-induced replication stress. First, I tested Rad5 protein abundance in the deletion mutants to see if the recruitment defect was indirectly caused by lower Rad5 levels. *RAD5-FLAG* was introduced into each of the deletions and the resulting strains were grown to mid-log phase and either treated with 200 mM HU for 60 min or left unperturbed. The cells were TCA fixed and subjected to SDS-PAGE western analysis with antibodies against FLAG to detect Rad5, and PGK as a loading control (Figure 2.3A). Densitometry was used calculate and plot the Log_2 wild type to Rad5 abundance ratio (Figure 2.3B). The order of increasing severity on Rad5 focus formation from Figure 2.2A was maintained to visualize any trends in abundance related to focus formation. The majority of gene deletions do not have a major effect on Rad5 abundance, although *ydj1*Δ, *mub1*Δ, *asc1*Δ and *asf1*Δ had decreases of approximately 2-fold in either unperturbed or HU-treated conditions, and *lsm1*Δ had a >4-fold decrease in both conditions. Therefore, I conclude that decreases in protein abundance do not, for the most part, correlate with decreased Rad5 recruitment to nuclear foci.

Table 2.1 Summary of genome-wide screen hits

				Cells with Rad5 foci		Rad5 abundance change (Log2)			
ORF	Gene	Name	Description	no drug	HU	no drug	HU	HU sensitivity	GI
YCR033W	SNT1	SaNT domains	Subunit of the Set3C deacetylase complex that interacts directly with the Set3C subunit, Sif2p; putative DNA-binding protein; mutant has increased aneuploidy tolerance	0.0	7.7	0.1	0.0	-	-
YCR079W	PTC6	Phosphatase Two C	Mitochondrial type 2C protein phosphatase (PP2C) with similarity to mammalian PP1Ks; involved in mitophagy; null mutant is sensitive to rapamycin and has decreased phosphorylation of the Pda1 subunit of pyruvate dehydrogenase	0.0	6.3	0.1	-0.2	-	-
YDL236W	PHO13	PHOsphate metabolism	Alkaline phosphatase specific for p-nitrophenyl phosphate; also has protein phosphatase activity	0.0	9.7	0.7	0.1	-	-
YER116C	SLX8	Synthetic Lethal of unknown (X) function	Subunit of Slx5-Slx8 SUMO-targeted ubiquitin ligase (STUbL) complex; stimulated by prior attachment of SUMO to the substrate; contains a C-terminal RING domain; forms nuclear foci upon DNA replication stress	0.8	15.4	0.4	-0.5	+	Addative
YER145C	FTR1	Fe TRansporter	High affinity iron permease; involved in the transport of iron across the plasma membrane; forms complex with Fet3p; expression is regulated by iron; protein abundance increases in response to DNA replication stress	2.5	11.9	0.1	-0.5	+	Addative
YGL087C	MMS2	Methyl MethaneSulfonate sensitivity	Ubiquitin-conjugating enzyme variant; involved in error-free postreplication repair; forms a heteromeric complex with Ubc13p, an active ubiquitin-conjugating enzyme; cooperates with chromatin-associated RING finger proteins, Rad18p and Rad5p; protein abundance increases in response to DNA replication stress	4.0	7.5	0.2	0.7	+	Epistatic
YGL167C	PMR1	Plasma Membrane ATPase Related	High affinity Ca2+/Mn2+ P-type ATPase required for Ca2+ and Mn2+ transport into Golgi; involved in Ca2+ dependent protein sorting and processing; mutations in human homolog ATP2C1 cause acantholytic skin condition Hailey-Hailey disease	0.8	8.7	-0.5	-0.1	+	Addative
YGL168W	HUR1	HydroxyUrea Resistance	Protein of unknown function; reported null mutant phenotype of hydroxyurea sensitivity may be due to effects on overlapping PMR1 gene	1.1	6.2	-0.3	-0.4	+	Addative
YHR034C	PIH1	Protein Interacting with Hsp90	Component of the conserved R2TP complex (Rvb1-Rvb2-Tah1-Pih1); R2TP complex interacts with Hsp90 (Hsp82p and Hsc82p) to mediate assembly large protein complexes such as box C/D snoRNPs and RNA polymerase II	1.9	9.7	-0.2	-0.1	-	-
YIR030C	DCG1	Dal80p-Controlled Gene	Protein of unknown function, expression is sensitive to nitrogen catabolite repression and regulated by Dal80p; contains transmembrane domain. Chromosomal coordinates close to IRC21	2.1	4.6	-0.5	0.2	-	-
YIR033W	MGA2	Multicopy suppressor of GAm1 (snf2)	ER membrane protein involved in regulation of OLE1 transcription, acts with homolog Spt23p; inactive ER form dimerizes and one subunit is then activated by ubiquitin/proteasome-dependent processing followed by nuclear targeting. Chromosomal coordinates close to IRC21	5.7	6.7	-0.8	-0.5	-	-
YJL115W	ASF1	Anti-Silencing Function	Nucleosome assembly factor, involved in chromatin assembly and disassembly, anti-silencing protein that causes derepression of silent loci when overexpressed; plays a role in regulating Ty1 transposition	3.0	13.0	-0.9	-1.2	++	Addative
YJL124C	LSM1	Like SM	Lsm (Like Sm) protein; forms heteroheptameric complex (with Lsm2p, Lsm3p, Lsm4p, Lsm5p, Lsm6p, and Lsm7p) involved in degradation of cytoplasmic mRNAs; forms cytoplasmic foci upon DNA replication stress	2.9	4.4	-2.6	-2.1	++	Addative
YLR049C	MLO50	Mitochondrially LOcalized protein of 50 kDa	Putative protein of unknown function	1.5	13.0	0.3	-0.1	+	Epistatic
YLR055C	SPT8	SuPpressor of Ty	Subunit of the SAGA transcriptional regulatory complex but not present in SAGA-like complex SLIK/SALSA, required for SAGA-mediated inhibition at some promoters	1.0	13.7	-0.1	-0.1	+	Addative
YML097C	VPS9	Vacuolar Protein Sorting	A guanine nucleotide exchange factor involved in vesicle-mediated vacuolar protein transport; specifically stimulates the intrinsic guanine nucleotide exchange activity of Vps21p/Rab5: similar to mammalian ras inhibitors; binds ubiquitin	0.0	8.3	0.0	0.2	++	Addative
YMR058W	FET3	FErrous Transport	Ferro-O2-oxidoreductase; required for high-affinity iron uptake and involved in mediating resistance to copper ion toxicity, belongs to class of integral membrane multicopper oxidases; protein abundance increases in response to DNA replication stress	3.1	4.0	-0.3	-0.5	+	Epistatic
YMR100W	MUB1	MUlti Budding	MYND domain-containing protein required for ubiquitination and turnover of Rpn4p; interacts with Ubr2p (E3) and indirectly with Rad6p (E2); short-lived protein degraded in a Ubr2p/Rad6p dependent manner (PMID:18070918); similar to the A. nidulans samB gene	0.3	4.8	-1.0	-0.2	-	-
YMR116C	ASC1	Absence of growth Suppressor of Cyp1	G-protein beta subunit and guanine nucleotide dissociation inhibitor for Gpa2p; ortholog of RACK1 that inhibits translation; core component of the small (40S) ribosomal subunit; regulates P-body formation induced by replication stress; represses Gcn4p in the absence of amino acid starvation	2.0	4.2	-0.3	-1.2	+++	Epistatic
YMR307W	GAS1	Glycophospholipid-Anchored Surface protein	Beta-1,3-glucanosyltransferase, required for cell wall assembly and also has a role in transcriptional silencing; localizes to the cell surface via a glycosylphosphatidylinositol (GPI) anchor; also found at the nuclear periphery	1.7	1.4	-0.4	-0.6	+	Addative
YNL064C	YDJ1	Yeast dnaJ	Type I HSP40 co-chaperone; involved in regulation of HSP90 and HSP70 functions; critical for determining cell size at Start as a function of growth rate; involved in protein translocation across membranes; member of the DnaJ family	0.6	2.0	-1.4	-1.3	++	Addative
YNR051C	BRE5	BREfeldin A sensitivity	Ubiquitin protease cofactor, forms deubiquitination complex with Ubp3p that coregulates anterograde and retrograde transport between the endoplasmic reticulum and Golgi compartments; null is sensitive to brefeldin A	1.0	8.4	-0.2	-0.6	+	Epistatic
YOR027W	STI1	STress Inducible	Hsp90 cochaperone, interacts with the Ssa group of the cytosolic Hsp70 chaperones and activates Ssa1p ATPase activity; interacts with Hsp90 chaperones and inhibits their ATPase activity; homolog of mammalian Hop	2.2	7.9	-0.1	0.2	-	-
YOR196C	LIP5	LIPoic acid	Protein involved in biosynthesis of the coenzyme lipoic acid, has similarity to E. coli lipoic acid synthase	3.4	11.4	ND	ND	-	-

To identify genes that are likely to function in the same genetic pathway as Rad5 I assessed HU-induced genetic interactions between *rad5*Δ and each of the gene deletions that decrease foci (Figure 2.4A). I was specifically looking for gene deletions that are both sensitive to HU and epistatic to *rad5*Δ for HU sensitivity. Epistasis for HU-induced fitness defects indicates the genes could operate in the same pathway or complex promoting HU resistance. From the 23 genes that decrease Rad5 foci, I was able to identify 11 additive genetic interactions (*YDJ1, SLX8, FET3, FTR1, PMR1, ASF1, LSM1, SPT8, VPS9 GAS1* and *MGA1*) and 4 epistatic genetic interactions (*MMS2, MLO50, ASC1, BRE5*) (Figure 2.4B). Mms2 forms part of the PCNA polyubiquitination machinery and was epistatic to *rad5*Δ confirming previous reports (Ulrich, 2001). These results indicate that many genes which are important for Rad5 focus formation are also important for HU resistance, yet, many appear to also operate in parallel HU-resistance pathways.

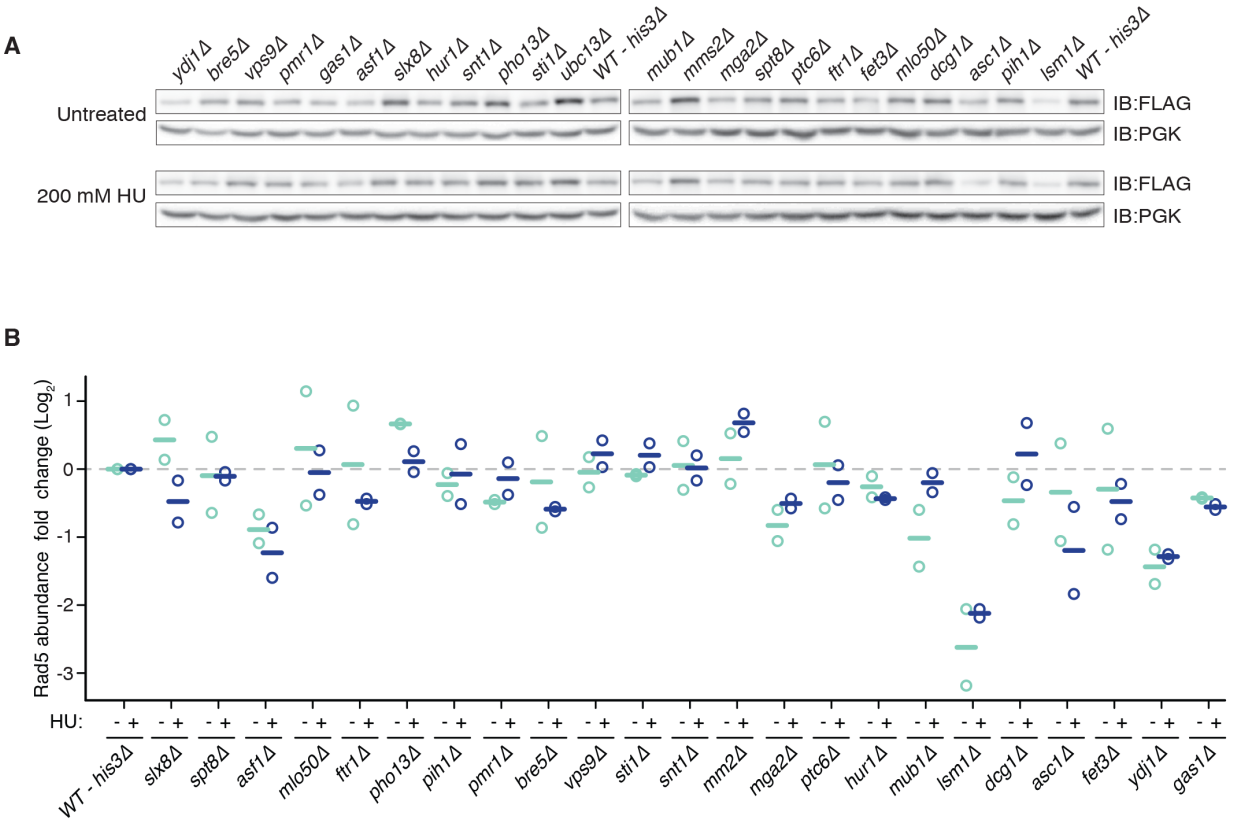

Figure 2.3 Decrease in Rad5 abundance is uncommon in mutants that fail to form Rad5 foci (A) Mid-logarithmic phase *RAD5-FLAG* cells with the indicated genetic backgrounds were treated with 200 mM HU and TCA fixed prior SDS-PAGE western blotting probed using FLAG- or PGK-specific antibodies. *his3*Δ is used as a wild type control. (B) The $\log_2$-fold change in abundance between wild type and the indicated gene deletion mutant was calculated following densitometry of the western blots in A. Each replicate is plotted as an open circle and the mean value is shown as a solid bar

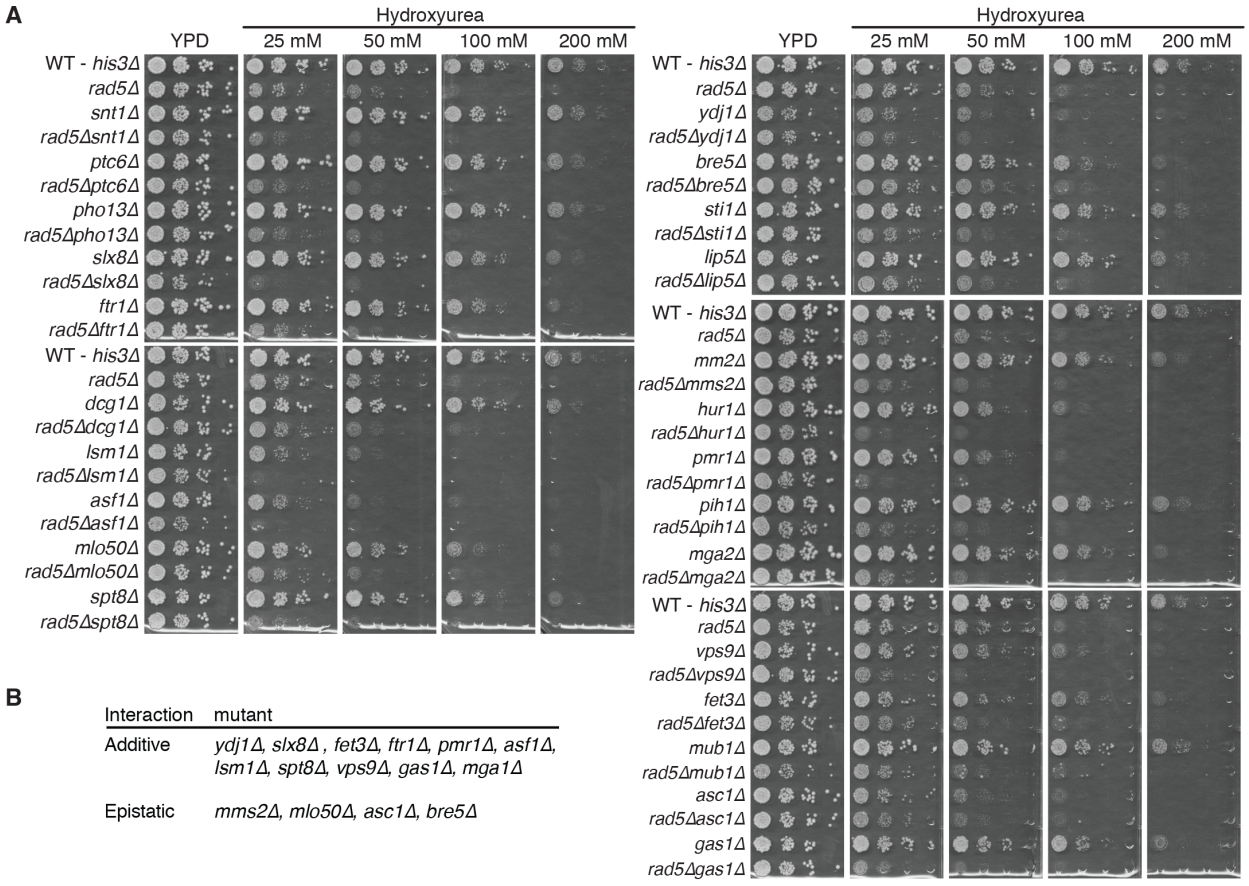

Figure 2.4 *RAD5* genetic interactions with gene deletion mutants that decrease Rad5 focus formation. (A) WT, *rad5*Δ and cells with the indicated gene deletions were grown to saturation, serially diluted, spotted on YPD and HU agar plates, and grown for 3 days at 30 ˚C. *his3*Δ is shown as a wild type control. (B) Additive and epistatic HU-induced genetic interactions were scored by visual inspection.

2.2.2 The HSP molecular chaperones Ydj1, Ssa1 and Ssb1 are required for Rad5 focus formation and resistance to HU-induced replication stress

For detailed follow-up studies I chose Ydj1, or Yeast DNAJ1, which is a type I HSP40 co-chaperone that functions during cellular stress (Cyr and Douglas, 1994). I chose Ydj1 because *ydj1*Δ is sensitive to HU (Figure 2.4A), has a severe Rad5 focus recruitment defect (Figure 2.2A-B) and only a modest decrease in abundance (Figure 2.3). Furthermore, the role of HSP chaperones in the DNA damage and replication stress response have not been thoroughly investigated. A search of the Rad5 protein sequence for a Ydj1 consensus binding motif revealed a conserved G{P}[LMQ]{P}X{P}{CIPMVW} binding site (Figure 2.5) (Kota et al., 2009). Furthermore, work from Walid Houry's lab in our department indicated that Rad5 and Ydj1

physically interact using TAP-tag AP-MS (Gong et al., 2009). The connections between Rad5 and Ydj1 in my data and the literature convinced me dig deeper into the role of HSPs in Rad5 function and replication stress.

```
Rad5 516 LAKPILKTMIKGGILSDEMGLGKTVAAYSLVLSCPHDS
           +P     + GGIL+D+MGLGKT+ A +++L+  HD
HLTF 281 KDRP---ENVHGGILADDMGLGKTLTAIAVILTNFHDG
```

Figure 2.5 Alignment of Rad5 and HLTF highlighting the conserved Ydj1 consensus peptide binding sequence

The HSP family of chaperones and co-chaperones work in a highly connected network to maintain protein homeostasis during cellular stress. Their roles in protein homeostasis are wide ranging, impacting disaggregation, refolding, degradation, remodeling and activation to name a few (Esser et al., 2004). The HSP family is further sub-classified based on their molecular weight into small HSP, HSP40, HSP70, HSP90 and HSP100 (Verghese et al., 2012). All HSP40s work by activating the ATPase activity of HSP70s through a conserved J domain and passing client proteins to them (Qiu et al., 2006). HSP90 functions as a homodimer and, along with many co-chaperones and HSP70s, remodel or activate client proteins. Small HSPs, HSP100s and HSP co-chaperones provide substrate specificity and other functions (Verghese et al., 2012).

Interestingly, my screen revealed that deletion of the HSP90 co-chaperones Pih1 and Sti1 also reduced Rad5 focus formation (Figure 2.2A). Pih1 is a component of the conserved Hsp90 co-chaperone complex Rvb1-Rvb2-Tah1-Pih1 (R2TP) that mediates large complex assembly (Nano and Houry, 2013; Zhao et al., 2005). Sti1 is a tetratrico-peptide repeat (TPR) Hsp90 co-chaperone that promotes Hsp70-Hsp90 interaction (Röhl et al., 2015). The connectivity of the HSP network and identification of HSP co-chaperones in the screen lead me to believe there are other HSPs involved in Rad5 focus formation and in the HU-induced replication stress response.

To test if other HSP family members were impacting Rad5 recruitment to nuclear foci and/or their role in HU resistance I deleted the HSP90 members *HSC82* and *HSP82* and the HSP100 family member *HSP104* in Rad5-GFP cells and looked at focus formation after HU treatment (Figure 2.6A). Only the deletion of *HSC82* caused a decrease in the number of cells with Rad5 foci compared to wild type, but the decrease was much less than was observed in *ydj1*Δ (Figure 2.2A). Deletion of *HSP82* or *HSP104* had no effect. I shifted my attention to the HSP70s that Ydj1 is presumably activating and cooperating with in Rad5 focus formation. Yeast have 9

nuclear/cytosolic HSP70s, and these are often functionally redundant (Gong et al., 2009). To narrow down the list I looked at HSP70s that physically interact with Rad5 and identified Ssa1, Ssa2 and Ssb1 as candidates (Gong et al., 2009). To test their role in the replication stress response I made single and double deletion combinations of *SSA1, SSA2* and *SSB1* and looked for decreased fitness in HU (Figure 2.6B). While none of the single mutants had an effect, *ssa1*Δ*ssb1*Δ double mutant cells were sensitive to HU. I tested if *ssa1*Δ*ssb1*Δ cells were able to form Rad5 foci. Strikingly, *ssa1*Δ*ssb1*Δ cells fail to form Rad5 foci during HU-induced replication stress (Figure 2.6C-D). These results suggest that Ssa1 and Ssb1 act redundantly in HU resistance and likely act with Ydj1 in promoting Rad5 focus formation.

2.3 Discussion

2.3.1 Protein ubiquitination and iron import are required for Rad5 focus formation

My screen revealed protein ubiquitination as an enriched biological processes required for Rad5 focus formation (Figure 2.2C). This is not surprising considering that ubiquitin signaling is common in the DNA replication stress response (Jackson and Durocher, 2013) and PRR pathway signaling is mediated by PCNA ubiquitination. What is surprising is the only PRR pathway member that I identified in the screen for reduced Rad5 focus formation was *MMS2*. Although I did not see an effect of *RAD6, RAD18* or *UBC13* mutation in the high-throughput screen, I subsequently took a candidate approach to look at how PRR pathway members affect Rad5 focus formation (Chapter 3). I revealed that *RAD6* and *RAD18* are fully required for Rad5 focus formation while *MMS2* and *UBC13* are only partially required (Figure 3.1E). Failure to retrieve *RAD6, RAD18* and *UBC13* mutants in the screen could result from slow growth phenotypes in these mutant or contamination from other strains on the plates

While *SLX8, BRE5* and *YDJ1* have no obvious link to PCNA monoubiquitination there is evidence that *ASF1* and *MUB1* might contribute to this reaction. The primary role of Asf1 is to deposit histones H3 and H4 on nascent DNA (Tyler et al., 1999) but Asf1 also promotes low levels of PCNA monoubiquitination in *rad6*Δ cells (Kats et al., 2009). Mub1 forms an E2/E3 complex with Rad6-Ubr2 required for N-end rule degradation of target proteins (Ju et al., 2008). I speculate that *asf1*Δ cells directly and *mub1*Δ cells indirectly reduce PCNA monoubiquitination leading to Rad5 recruitment defects.

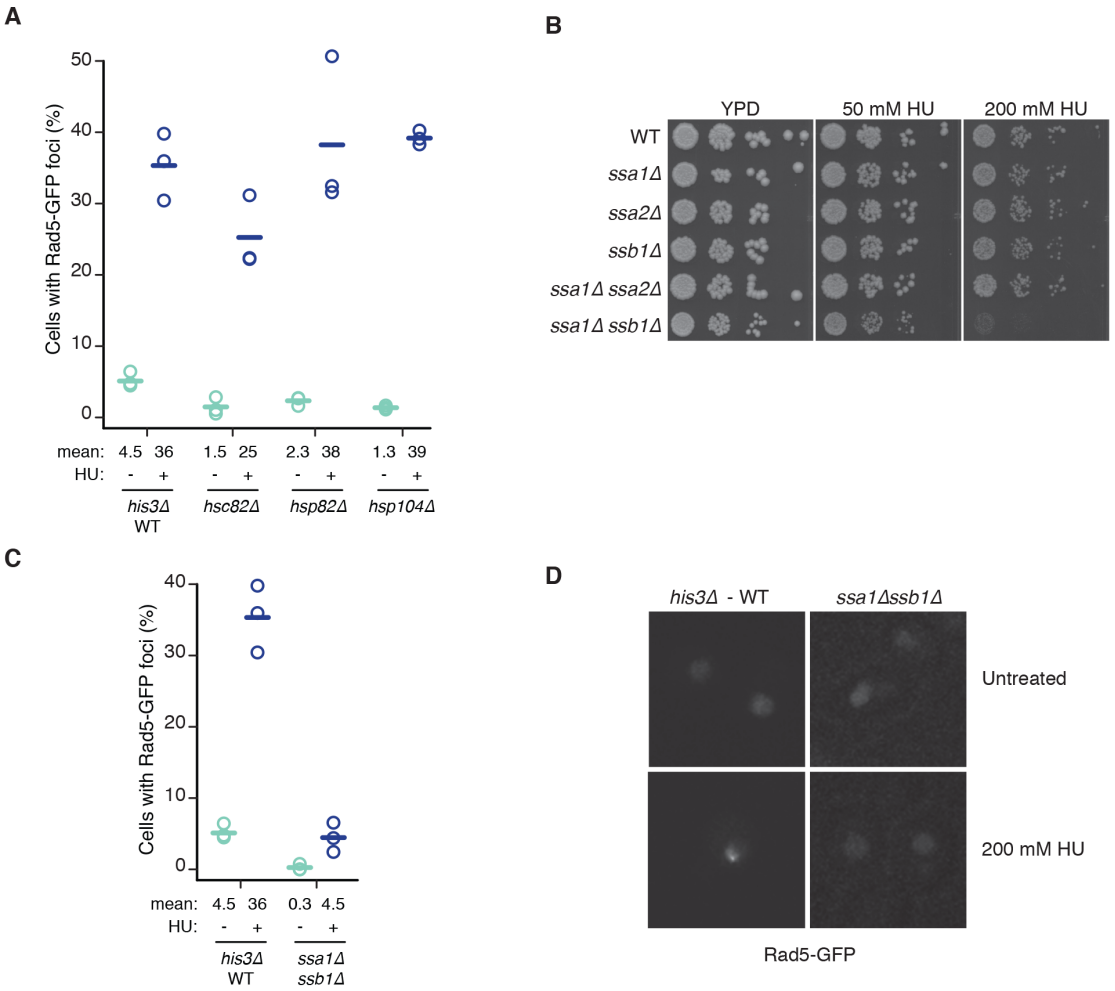

Figure 2.6 The HSP70s Ssa1 and Ssb1 are required for HU resistance and Rad5 focus formation. (A) Mid-logarithmic phase *RAD5-GFP* cells with the indicated gene deletions were treated with 200 mM HU for 60 minutes, harvested and imaged. The percent of cells with at least one focus is plotted for each replicate and the means are shown as solid bars. At least 100 cells of each type were scored for each replicate. (B) The indicated gene deletion mutant strains were grown to saturation, serially diluted, spotted on YPD and HU agar plates, and grown for 3 days at 30°C. (C) Mid-logarithmic phase *RAD5-GFP* cells with the indicated gene deletions were treated with 200 mM HU for 60 minutes, harvested and imaged. The percent of cells with at least one focus is plotted for each replicate and the means are shown as solid bars. At least 100 cells of each type were scored for each replicate. (D) Representative micrographs in the GFP channel of WT and *ssa1*Δ*ssb1*Δ cells before or after treatment with 200 mM HU.

The other enriched biological process that reduces Rad5 focus formation is related to iron transport and was driven by *FET3* and *FTR1*, the only two components of the high-affinity iron permease-oxidase complex (Askwith et al., 1994; Stearman et al., 1996). The function of the Fet3-Ftr1 complex is related the mechanism of HU inhibition. HU works by reducing ferric Fe^{+3} to ferrous Fe^{+2} in the active site of RNR resulting in loss of the iron center and inhibition of dNTP production (Chabes et al., 2000; Nyholm et al., 1993). During iron transport Fet3 oxidizes to Fe^{+2} to Fe^{+3} which allows uptake into the cell by the transmembrane permease Ftr1. To compensate for low Fe^{+3} during HU treatment the yeast activate the Aft regulon which induces

iron uptake (Dubacq et al., 2006). In agreement with my results our lab has also shown that Ftr1-Fet3 protein abundance increases during HU exposure (Tkach et al., 2012). Moreover, *FTR1* and *FET3* deletions have fitness defects in HU (Figure 2.4A). Thus, it is clear that yeast cells need to take up ferric iron to regenerate RNR for dNTP production when challenged with HU. How low cellular ferric iron causes a reduction in Rad5 foci is puzzling to me because inability to regenerate RNR and make dNTPs should increase levels of replication stress and presumably the amount of Rad5 foci. Also, it seems that *FTR1* and *FET3* are in parallel HU resistance pathways with *RAD5* based on their additive HU-induced genetic interactions (Figure 2.4A) However, it does appears that Rad5 is somehow regulated by ferric iron levels in cells. Recently, attention has been given to Fe-S clusters in DNA replication and repair (Fuss et al., 2015; Puig et al., 2017). It is interesting to speculate that changes in iron homeostasis might impact Fe-S cluster formation and possibly, Rad5 function.

2.3.2 A role for HSPs during physiological and stressed DNA replication

My research has identified the HSP40 chaperone Ydj1, HSP70s chaperones Ssa1 and Ssb1 and the HSP90 co-chaperones Pih1 and Sti1 as proteins that promote both Rad5 focus formation and resistance to HU-induced replication stress. There is additional evidence that HSPs function during both physiological and stressed DNA replication.

Studies over the last 30 years have identified roles for HSP40 and HSP70 in DNA replication initiation. The HSP40 DnaJ and HSP70 DnaK in bacteria activate the helicase DnaB to unwind DNA and initiate DNA replication (Alfanos and Mcmacken, 1989; Zylicz et al., 1989). DnaJ and DnaK also stimulate binding of the replication initiation protein RepA to plasmid origins (DasGupta et al., 1993; Kuhlbusch et al., 1991; Wickner et al., 1992). The HSP70s Ssa1-4 and Ssb1-2 in yeast are proposed to participate in DNA replication by physically interacting with Orc4 and assembling the origin recognition complex (ORC) on DNA to initiate replication (Álamo et al., 2010). Furthermore, Hsp70 and the HSP40s Hdj1 and Hdj2 in humans are required for HSV-1 and HPV viral genome replication (Le Gac and Boehmer, 2002; Lin et al., 2002) These studies provide evidence that HSPs are important for DNA replication initiation, a trait that is conserved in all kingdoms of life.

More recently, high-throughput and small-scale studies have elucidated roles for HSPs in the replication stress response. High-throughput genome-wide microscopic analysis of the yeast GFP

collection in our lab identified many HSP proteins that increase in abundance and change localization in response to HU and MMS treatment (Tkach et al., 2012). These changes likely indicate that HSPs are interacting with different clients during replication stress or DNA damage. Indeed, looking at changes in client proteins of Ssa1 and Hsp82 during MMS treatment in yeast revealed increased interaction with Rnr4, a subunit of the RNR complex (Truman et al., 2015). Inhibition HSP70 or HSP90 in yeast and human cells destabilized the RNR complex and sensitized cells to RNR inhibition. In addition to stabilizing RNR, *ssa1*Δ*ssa2*Δ cells exposed to UV have fitness defects attributed to reduced Rad9 phosphorylation and faulty checkpoint activation (Gilbert et al., 2003). Interestingly, Ydj1 also has roles in the UV-induced DNA damage response by facilitating proper stoichiometry of the TFIIH complex required for nucleotide excision repair (NER) of UV-lesions (Moriel-Carretero et al., 2011). Taken together, my work, and others have hinted at the importance of HSPs during the replication stress response.

2.3.3 Conclusions

In this chapter I used a high-throughput genome-wide screen to identify genes that decrease Rad5 recruitment to nuclear foci. Hits from my screen were enriched for genes encoding proteins that mediate protein ubiquitination. This was not entirely surprising given that PRR is mediated by PCNA ubiquitination. The screen also revealed an unexpected role for HSP proteins in Rad5 relocalization. While this is not the first time HSPs have been liked to DNA replication or the replication stress response, I think my findings represent the tip of an iceberg. Follow-up studies should address at the molecular level where HSPs impact PRR and how HSPs regulate the global replication stress response

2.4 Future directions

My results clearly indicate that Rad5 fails to form nuclear foci in *ydj1*Δ and *ssa1*Δ*ssb1*Δ cells. Aside from ruling out Rad5 abundance I have not yet determined how HSP chaperones are mediating Rad5 recruitment to nuclear foci. In addition to affecting Rad5 the literature suggests that HSPs might play a global role in regulating the replication stress response. My future directions address how Ydj1, Ssa1, Ssb1 and other HSP chaperone members specifically affect the PRR pathway and regulate the global replication stress response.

2.4.1 Characterize how Ydj1, Ssa1 and Ssb1 are affecting the PRR pathway

Ydj1, Ssa1 and Ssb1 could impinge on Rad5 recruitment to nuclear foci by indirectly affecting the signaling that recruits Rad5 to foci or by directly recruiting Rad5. In Chapter 3 I determined that $PCNA_{K164}Ub$ is required for Rad5 focus formation and, thus, Ydj1, Ssa1 and Ssb1 could be affecting PCNA monoubiquitination. To test this I will directly monitor the PCNA ubiquitination status in HU treated *ydj1*Δ and *ssa1*Δ*ssb1*Δ cells by SDS-PAGE western blot using α-PCNA antibodies. $PCNA_{K164}Ub$ and $PCNA_{K164}PolyUb$ species migrate as higher molecular weight bands under these conditions. While this method of $PCNA_{K164}Ub$ and $PCNA_{K164}PolyUb$ detection has been successful, it has limited sensitivity due to the plethora of different PCNA posttranslational modifications making identification of the correct bands difficult. If I am unable to quantify PCNA ubiquitination by this method I will purify PCNA from cells expressing endogenously tagged $^{His}PCNA$ (Hoege et al., 2002) before assessing alterations in ubiquitylation. Purified $^{His}PCNA$ species will be subjected to western blots using α-His antibodies to detect $PCNA_{K164}Ub$ and $PCNA_{K164}PolyUb$. If $PCNA_{K164}Ub$ remains robust in HU treated *ydj1*Δ and *ssa1*Δ*ssb1*Δ cells it will suggest that chaperones have a direct role in Rad5 recruitment. If $PCNA_{K164}Ub$ is decreased it will suggest the effect on Rad5 recruitment is indirect. Either way, these results will be important to our understanding of how HSP chaperones regulate the PRR pathway

In addition to PCNA ubiquitination I will test *ydj1*Δ and *ssa1*Δ*ssb1*Δ cells for other Rad5 spontaneous and HU-induced phenotypes. I will test wild type, *rad5*Δ*, ydj1*Δ and *rad5*Δ*ydj1*Δ cells for increased mutation, recombination and GCR rates. If Ydj1 is in pathway with Rad5 then I expect *ydj1*Δ cells to have similar increases in these phenotypes that are epistatic to Rad5. Other Rad5 phenotypes can also be assayed such as sister chromatid junction formation, RPA focus formation, ssDNA accumulation and anaphase bridge formation (I characterized the last three phenotypes for *rad5*Δ cells in Chapter 3). Interesting interactions with *ydj1*Δ can be extended to *ssa1*Δ*ssb1*Δ cells. Together these experiments will pinpoint the role of Ydj1, Ssa1 and Ssb1 in regulating Rad5 relocalization and replication stress resistance.

2.4.2 Identify how HSPs are impacting the global replication stress response

In addition to regulating the PRR pathway HSP chaperones likely regulate other components of the replication stress response. For example, Ydj1 physically interacts with the RPA subunit Rfa1, the TLS polymerases subunits Rev1, Rev3, and Pol32 and the template-switching and HR factor Rad51 (Gong et al., 2009). Furthermore, many GFP-tagged HSPs change localization and/or abundance when cells are treated with MMS or HU (Tkach et al., 2012). These data lead me to hypothesize that HSP chaperones play a global role in regulating the replication stress response. To address this I will take genome-wide high-throughput approaches to look at genetic interactions of HSP genes, physical interactions of HSP proteins and how HSPs affect global protein relocalization during the replication stress response. By taking the overlapping trends from multiple genome-wide approaches I will undoubtedly uncover new and interesting biology about how HSP chaperones regulate the replication stress response. I left the identity of HSPs generic, as the methodology can be applied to any protein of interest, however Ydj1 would be my first choice to take through the pipeline.

2.4.2.1 Determine the genetic interaction network of HSPs during replication stress

Replication stress-induced genetic interactions are useful for elucidating roles for proteins in the replication stress response (Loll-Krippleber and Brown, 2017; Onge et al., 2007). I will use this approach to look for HU-induced genetic interactions with HSP genes. Using SGA I will cross *hsp*Δ queries to the non-essential gene deletion and temperature sensitive essential gene collections. Single and double mutant colonies will be replica pinned to YPD or YPD +HU plates. The plates will be imaged and colony sizes will be measured as a readout for viability. HU-induced genetic interactions will be scored as negative, epistatic or suppressing in nature. Follow-up priority will be given to genes with epistatic or suppressing interactions with *hsp*Δ cells as these are likely functioning in the same HU-resistance pathway. If colony-based fitness measurements are not sensitive enough to tease out HU-induced genetic interactions I will move to a pooled liquid competition based assay using each deletion strains unique barcode to track fitness in the population by barcode sequencing. I anticipate that mapping the HU-induced genetic interactions of HSP chaperones will lead to identification of HSP clients and the replication stress response pathways they regulate.

2.4.2.2 Determine physical interaction network of HSPs during replication stress

Cataloging the clients of molecular chaperones using affinity purification coupled to mass spectrometry (AP-MS) has provided valuable protein-chaperone interaction network under standard growth conditions (Gong et al., 2009). I hypothesize that the protein-HSP chaperone physical interaction network will change during the replication stress response as HSPs engage with clients. To test this I will conduct AP-MS with TAP-tagged HSPs +/- HU treatment. Results will be scored looking for novel and/or increased interactions after HU treatment compared to standard growth conditions. I will follow up on hits using orthogonal approaches to monitor protein-protein interactions such as yeast-2-hybrid or co-immunoprecipitation. These results will provide direct physical evidence that HSP chaperones engage replication stress response proteins as clients.

2.4.2.3 Determine changes global protein relocalization during replication stress

Changes in protein localization are a hallmark of the replication stress response. Our lab has identified ~300 proteins that change localization in response to replication stress induced by either MMS of HU (Tkach et al., 2012). I hypothesize that HSPs are regulating a subset of these protein relocalizations in addition to Ydj1 Ssa1/Ssb1 regulation of Rad5 foci. To test this I will use SGA and cross *hsp*Δ *RPL39pr-TdTomato* queries to a mini-array of proteins that relocalize in HU-induced replication stress. From here an improved methodology to my Rad5 focus screen will be employed to discover proteins that fail to relocalize after HU treatment in *hsp*Δ cells. Cells will be grown to mid-log phase and imaged in a microfluidics chamber (Schmidt et al., 2018). The microfluidics approach will allow me to follow protein relocalization in a single cell temporally using time-lapse microscopy before, during or after HU treatment. I will run the images through image analysis pipelines to quickly identify localization changes in an unbiased manner (Chong et al., 2015). My protein relocalization screens will help identify meaningful HSP clients in the HU-induced replication stress response.

Once all three genome-wide approaches are completed high-confidence hit lists will be compared with each other to identify common themes in the data and guide follow-up studies. An ideal HSP client for follow up would have positive HU-induced genetic interactions,

increased HU-induced physical interactions and an altered HU-induced localization pattern. I am confident that if all three -omics approaches are conducted accurately I will uncover a subset of proteins that are regulated by HSPs in the replication stress response. The role of HSPs in replication stress represents an exciting aspect of HSP function we are just beginning to understand.

2.5 Materials and Methods

2.5.1 Yeast strains and media

All yeast strains used in this chapter (Table 2.2) are derivatives of BY4741 (Brachmann et al., 1998). Standard yeast media and growth conditions were used for all experiments unless otherwise noted. All non-SGA strains were constructed using genetic crosses and standard PCR-based gene disruption and epitope- tagging techniques. For SGA strains standard procedures were used (Tong and Boone, 2006). For the Rad5-GFP reporter SGA DGY2 (*MATα RAD5-GFP::HIS3MX can1Δ::STE2prLEU2::RPL39pr-TdTomato::CaURA3 leu2Δ0 his3Δ1 ura3Δ0 lyp1Δ met15Δ0*) was crossed to the non-essential deletion collection(*MAT***a** *xxxΔ::kanMX6 leu2Δ0 his3Δ1 ura3Δ0 met15Δ0*) (Giaever et al., 2002). For Rad5-FLAG reporter SGA DGY19 (*MAT***a** *RAD5-6His10FLAG::kanMX6 leu2Δ0 his3Δ1 ura3Δ0 met15Δ0*) was crossed to query strains (*MATα xxxΔ::natMX6 can1Δ::STE2pr-SpHIS5 leu2Δ0 his3Δ1 ura3Δ0 met15Δ0 lyp1Δ*). For *rad5ΔxxxΔ* SGA the *rad5Δ* query strain (*MATα rad5Δ::natMX6 can1Δ::STE2pr-SpHIS5 leu2Δ0 his3Δ1 ura3Δ0 met15Δ0 lyp1Δ*) was crossed to non-essential gene deletion strains (*MAT***a** *xxxΔ::kanMX6 leu2Δ0 his3Δ1 ura3Δ0 met15Δ0*).

2.5.2 Manual Rad5-GFP focus formation assay

Cells expressing Rad5-GFP (Figures 2.1A, 2.1B) in the indicated genetic backgrounds were grown in YPD at 30 °C to mid-logarithmic phase (OD_{600} = 0.3-0.6). Cells were either left unperturbed or treated with 200 mM HU for 60 min, washed in low-fluorescence media (1.7g/l LF powder (CAT), 5g/l ammonium sulphate, 1x amino acids, 2% w/v glucose) and resuspended in 25µl LFM per 1 OD600 unit of cells, with or without 200 mM HU. 2 µl was mounted on glass slide with a coverslip and imaged using a Leica DMI6000 confocal using Volocity imaging software (PerkinElmer). Eleven z-stacks with a 0.4 µM step size were collected using fluorescein isothiocyanate, Texas Red, and cell differential interference contrast filter sets (Quorum

Technologies) for Rad5, Nup49 and cell morphology analysis respectively. Images were processed using cell profiler (version 2.2.0) (Kamentsky et al., 2011) by projecting the maximum pixel intensity in the x-y plane from the 11 z-stacks to a single image. Budding index and cells containing one or more Rad5-GFP focus were scored by visual inspection.

2.5.3 High-throughput Rad5-GFP focus formation assay

High-throughput confocal microscopy was done as previously described (Torres and Brown, 2015). Images were visually inspected for decreased Rad5-GFP foci during HU treatment in specific gene deletions compared to the *his3*Δ boarder strains used as a wild type controls.

2.5.4 Gene Ontology (GO) enrichment analysis

GO Term Finder version 0.83 (https://www.yeastgenome.org/cgi-bin/GO/goTermFinder.pl) was used with the default settings to identify enriched terms. The background set of genes was restricted to those encompassing the non-essential gene deletion collection.

2.5.5 Whole cell extracts and immunoblotting

Cells were diluted to OD_{600} = 0.5 in 10% trichloroacetic acid and whole cell extracts were prepared as previously described (Pellicioli et al., 1999). Proteins were resolved on a SDS-PAGE gel and detected by immunoblotting with anti-FLAG M2 (Sigma) 1:10,000 and anti-PGK (Novex 459250) antibodies. Densitometry was performed using ImageJ (https://imagej.nih.gov/ij/).

2.5.6 HU fitness spot assay

Saturated cultures were diluted to OD_{600} = 0.5 in a flat bottom 96-wel plate and 5-fold serial dilutions were prepared using a multi-channel pipette. The spots were plated using a multi-pronged pinning tool onto YPD or YPD + HU. Images were taken after 3 days of growth at 30°C

2.5.7 Ydj1 consensus binding peptide analysis

Identification of the Ydj1 consensus binding peptide in Rad5 and alignments with HLTF were done using Protein BLAST (https://blast.ncbi.nlm.nih.gov/Blast.cgi?PAGE=Proteins).

Table 2.2 Strains used in this chapter

Strain	Genotype	Source
BY4741	*MAT***a** *leu2Δ0 his3Δ1 ura3Δ0 met15Δ0*	Brachmann *et al.* (1998)
DGY1	*MAT*α *RAD5-GFP::HIS3MX6 can1Δ::STE2pr-LEU2::RPL39pr-TdTomato::CaURA3 leu2Δ0 his3Δ1 ura3Δ0 met15Δ0 lyp1Δ*	This study
	*MAT***a** *his3Δ::KanMX6 RAD5-GFP::HIS3MX6 can1Δ::STE2pr-LEU2::RPL39pr-TdTomato::CaURA3 leu2Δ0 his3Δ1 ura3Δ0 met15Δ0 lyp1Δ*	This study
	*MAT***a** *slx8Δ::KanMX6 RAD5-GFP::HIS3MX6 can1Δ::STE2pr-LEU2::RPL39pr-TdTomato::CaURA3 leu2Δ0 his3Δ1 ura3Δ0 met15Δ0 lyp1Δ*	This study
	*MAT***a** *spt8Δ::KanMX6 RAD5-GFP::HIS3MX6 can1Δ::STE2pr-LEU2::RPL39pr-TdTomato::CaURA3 leu2Δ0 his3Δ1 ura3Δ0 met15Δ0 lyp1Δ*	This study
	*MAT***a** *asf1Δ::KanMX6 RAD5-GFP::HIS3MX6 can1Δ::STE2pr-LEU2::RPL39pr-TdTomato::CaURA3 leu2Δ0 his3Δ1 ura3Δ0 met15Δ0 lyp1Δ*	This study
	*MAT***a** *mlo50Δ::KanMX6 RAD5-GFP::HIS3MX6 can1Δ::STE2pr-LEU2::RPL39pr-TdTomato::CaURA3 leu2Δ0 his3Δ1 ura3Δ0 met15Δ0 lyp1Δ*	This study
	*MAT***a** *ftr1Δ::KanMX6 RAD5-GFP::HIS3MX6 can1Δ::STE2pr-LEU2::RPL39pr-TdTomato::CaURA3 leu2Δ0 his3Δ1 ura3Δ0 met15Δ0 lyp1Δ*	This study
	*MAT***a** *lip5Δ::KanMX6 RAD5-GFP::HIS3MX6 can1Δ::STE2pr-LEU2::RPL39pr-TdTomato::CaURA3 leu2Δ0 his3Δ1 ura3Δ0 met15Δ0 lyp1Δ*	This study
	*MAT***a** *pho13Δ::KanMX6 RAD5-GFP::HIS3MX6 can1Δ::STE2pr-LEU2::RPL39pr-TdTomato::CaURA3 leu2Δ0 his3Δ1 ura3Δ0 met15Δ0 lyp1Δ*	This study
	*MAT***a** *pih1Δ::KanMX6 RAD5-GFP::HIS3MX6 can1Δ::STE2pr-LEU2::RPL39pr-TdTomato::CaURA3 leu2Δ0 his3Δ1 ura3Δ0 met15Δ0 lyp1Δ*	This study
	*MAT***a** *pmr1Δ::KanMX6 RAD5-GFP::HIS3MX6 can1Δ::STE2pr-LEU2::RPL39pr-TdTomato::CaURA3 leu2Δ0 his3Δ1 ura3Δ0 met15Δ0 lyp1Δ*	This study
	MAT **a** *bre5* Δ::KanMX6 RAD5-GFP::HIS3MX6 can1Δ::STE2pr-LEU2::RPL39pr-TdTomato::CaURA3 leu2Δ0 his3Δ1 ura3Δ0 met15Δ0 lyp1Δ	This study
	*MAT***a** *vps9Δ::KanMX6 RAD5-GFP::HIS3MX6 can1Δ::STE2pr-LEU2::RPL39pr-TdTomato::CaURA3 leu2Δ0 his3Δ1 ura3Δ0 met15Δ0 lyp1Δ*	This study
	*MAT***a** *sti1Δ::KanMX6 RAD5-GFP::HIS3MX6 can1Δ::STE2pr-LEU2::RPL39pr-TdTomato::CaURA3 leu2Δ0 his3Δ1 ura3Δ0 met15Δ0 lyp1Δ*	This study
	*MAT***a** *snt1Δ::KanMX6 RAD5-GFP::HIS3MX6 can1Δ::STE2pr-LEU2::RPL39pr-TdTomato::CaURA3 leu2Δ0 his3Δ1 ura3Δ0 met15Δ0 lyp1Δ*	This study
	*MAT***a** *mms2Δ::KanMX6 RAD5-GFP::HIS3MX6 can1Δ::STE2pr-LEU2::RPL39pr-TdTomato::CaURA3 leu2Δ0 his3Δ1 ura3Δ0 met15Δ0 lyp1Δ*	This study
	*MAT***a** *mga2Δ::KanMX6 RAD5-GFP::HIS3MX6 can1Δ::STE2pr-LEU2::RPL39pr-TdTomato::CaURA3 leu2Δ0 his3Δ1 ura3Δ0 met15Δ0 lyp1Δ*	This study
	*MAT***a** *ptc6Δ::KanMX6 RAD5-GFP::HIS3MX6 can1Δ::STE2pr-LEU2::RPL39pr-TdTomato::CaURA3 leu2Δ0 his3Δ1 ura3Δ0 met15Δ0 lyp1Δ*	This study
	*MAT***a** *hur1Δ::KanMX6 RAD5-GFP::HIS3MX6 can1Δ::STE2pr-LEU2::RPL39pr-TdTomato::CaURA3 leu2Δ0 his3Δ1 ura3Δ0 met15Δ0 lyp1Δ*	This study
	*MAT***a** *mub1Δ* ::KanMX6 RAD5-GFP::HIS3MX6 can1Δ::STE2pr-LEU2::RPL39pr-TdTomato::CaURA3 leu2Δ0 his3Δ1 ura3Δ0 met15Δ0 lyp1Δ	This study
	*MAT***a** *lsm1Δ::KanMX6 RAD5-GFP::HIS3MX6 can1Δ::STE2pr-LEU2::RPL39pr-TdTomato::CaURA3 leu2Δ0 his3Δ1 ura3Δ0 met15Δ0 lyp1Δ*	This study
	*MAT***a** *dcg1Δ::KanMX6 RAD5-GFP::HIS3MX6 can1Δ::STE2pr-LEU2::RPL39pr-TdTomato::CaURA3 leu2Δ0 his3Δ1 ura3Δ0 met15Δ0 lyp1Δ*	This study
	*MAT***a** *asc1Δ::KanMX6 RAD5-GFP::HIS3MX6 can1Δ::STE2pr-LEU2::RPL39pr-TdTomato::CaURA3 leu2Δ0 his3Δ1 ura3Δ0 met15Δ0 lyp1Δ*	This study
	*MAT***a** *fet3Δ::KanMX6 RAD5-GFP::HIS3MX6 can1Δ::STE2pr-LEU2::RPL39pr-TdTomato::CaURA3 leu2Δ0 his3Δ1 ura3Δ0 met15Δ0 lyp1Δ*	This study
	*MAT***a** *ydj1Δ::KanMX6 RAD5-GFP::HIS3MX6 can1Δ::STE2pr-LEU2::RPL39pr-TdTomato::CaURA3 leu2Δ0 his3Δ1 ura3Δ0 met15Δ0 lyp1Δ*	This study
	*MAT***a** *gas1Δ::KanMX6 RAD5-GFP::HIS3MX6 can1Δ::STE2pr-LEU2::RPL39pr-TdTomato::CaURA3 leu2Δ0 his3Δ1 ura3Δ0 met15Δ0 lyp1Δ*	This study
	*MAT***a** *hsc821Δ::KanMX6 RAD5-GFP::HIS3MX6 can1Δ::STE2pr-LEU2::RPL39pr-TdTomato::CaURA3 leu2Δ0 his3Δ1 ura3Δ0 met15Δ0 lyp1Δ*	This study
	*MAT***a** *hsp104Δ::KanMX6 RAD5-GFP::HIS3MX6 can1Δ::STE2pr-LEU2::RPL39pr-TdTomato::CaURA3 leu2Δ0 his3Δ1 ura3Δ0 met15Δ0 lyp1Δ*	This study
	*MAT***a** *hsp42Δ::KanMX6 RAD5-GFP::HIS3MX6 can1Δ::STE2pr-LEU2::RPL39pr-TdTomato::CaURA3 leu2Δ0 his3Δ1 ura3Δ0 met15Δ0 lyp1Δ*	This study
	*MAT***a** *hsp82Δ::KanMX6 RAD5-GFP::HIS3MX6 can1Δ::STE2pr-LEU2::RPL39pr-TdTomato::CaURA3 leu2Δ0 his3Δ1 ura3Δ0 met15Δ0 lyp1Δ*	This study
	*MAT***a** *ssa1Δ::KanMX6 ssb1Δ::natMX6 RAD5-GFP::HIS3MX6 can1Δ::STE2pr-LEU2::RPL39pr-TdTomato::CaURA3 leu2Δ0 his3Δ1 ura3Δ0 met15Δ0 lyp1Δ*	This study
DGY19	*MAT***a** *RAD5-6His10FLAG::kanMX6 leu2Δ0 his3Δ1 ura3Δ0 met15Δ0*	This study
	*MAT***a** *his3Δ::natMX6 RAD5-6His10FLAG::kanMX6 can1Δ::STE2pr-SpHIS5 leu2Δ0 his3Δ1 ura3Δ0 met15Δ0 lyp1Δ*	This study
	*MAT***a** *slx8Δ::natMX6 RAD5-6His10FLAG::kanMX6 can1Δ::STE2pr-SpHIS5 leu2Δ0 his3Δ1 ura3Δ0 met15Δ0 lyp1Δ*	This study
	*MAT***a** *spt8Δ::natMX6 RAD5-6His10FLAG::kanMX6 can1Δ::STE2pr-SpHIS5 leu2Δ0 his3Δ1 ura3Δ0 met15Δ0 lyp1Δ*	This study
	*MAT***a** *asf1Δ::natMX6 RAD5-6His10FLAG::kanMX6 can1Δ::STE2pr-SpHIS5 leu2Δ0 his3Δ1 ura3Δ0 met15Δ0 lyp1Δ*	This study
	*MAT***a** *mlo50Δ::natMX6 RAD5-6His10FLAG::kanMX6 can1Δ::STE2pr-SpHIS5 leu2Δ0 his3Δ1 ura3Δ0 met15Δ0 lyp1Δ*	This study
	*MAT***a** *ftr1Δ::natMX6 RAD5-6His10FLAG::kanMX6 can1Δ::STE2pr-SpHIS5 leu2Δ0 his3Δ1 ura3Δ0 met15Δ0 lyp1Δ*	This study
	*MAT***a** *pho13Δ::natMX6 RAD5-6His10FLAG::kanMX6 can1Δ::STE2pr-SpHIS5 leu2Δ0 his3Δ1 ura3Δ0 met15Δ0 lyp1Δ*	This study
	*MAT***a** *pih1Δ::natMX6 RAD5-6His10FLAG::kanMX6 can1Δ::STE2pr-SpHIS5 leu2Δ0 his3Δ1 ura3Δ0 met15Δ0 lyp1Δ*	This study
	*MAT***a** *pmr1Δ::natMX6 RAD5-6His10FLAG::kanMX6 can1Δ::STE2pr-SpHIS5 leu2Δ0 his3Δ1 ura3Δ0 met15Δ0 lyp1Δ*	This study
	*MAT***a** *bre5Δ::natMX6 RAD5-6His10FLAG::kanMX6 can1Δ::STE2pr-SpHIS5 leu2Δ0 his3Δ1 ura3Δ0 met15Δ0 lyp1Δ*	This study
	*MAT***a** *vps9Δ::natMX6 RAD5-6His10FLAG::kanMX6 can1Δ::STE2pr-SpHIS5 leu2Δ0 his3Δ1 ura3Δ0 met15Δ0 lyp1Δ*	This study
	*MAT***a** *sti1Δ::natMX6 RAD5-6His10FLAG::kanMX6 can1Δ::STE2pr-SpHIS5 leu2Δ0 his3Δ1 ura3Δ0 met15Δ0 lyp1Δ*	This study
	*MAT***a** *snt1Δ::natMX6 RAD5-6His10FLAG::kanMX6 can1Δ::STE2pr-SpHIS5 leu2Δ0 his3Δ1 ura3Δ0 met15Δ0 lyp1Δ*	This study
	*MAT***a** *mms2Δ::natMX6 RAD5-6His10FLAG::kanMX6 can1Δ::STE2pr-SpHIS5 leu2Δ0 his3Δ1 ura3Δ0 met15Δ0 lyp1Δ*	This study
	*MAT***a** *mga2Δ::natMX6 RAD5-6His10FLAG::kanMX6 can1Δ::STE2pr-SpHIS5 leu2Δ0 his3Δ1 ura3Δ0 met15Δ0 lyp1Δ*	This study
	*MAT***a** *ptc6Δ::natMX6 RAD5-6His10FLAG::kanMX6 can1Δ::STE2pr-SpHIS5 leu2Δ0 his3Δ1 ura3Δ0 met15Δ0 lyp1Δ*	This study
	*MAT***a** *hur1Δ::natMX6 RAD5-6His10FLAG::kanMX6 can1Δ::STE2pr-SpHIS5 leu2Δ0 his3Δ1 ura3Δ0 met15Δ0 lyp1Δ*	This study
	*MAT***a** *mub1Δ::natMX6 RAD5-6His10FLAG::kanMX6 can1Δ::STE2pr-SpHIS5 leu2Δ0 his3Δ1 ura3Δ0 met15Δ0 lyp1Δ*	This study
	*MAT***a** *lsm1Δ::natMX6 RAD5-6His10FLAG::kanMX6 can1Δ::STE2pr-SpHIS5 leu2Δ0 his3Δ1 ura3Δ0 met15Δ0 lyp1Δ*	This study
	*MAT***a** *dcg1Δ::natMX6 RAD5-6His10FLAG::kanMX6 can1Δ::STE2pr-SpHIS5 leu2Δ0 his3Δ1 ura3Δ0 met15Δ0 lyp1Δ*	This study
	*MAT***a** *asc1Δ::natMX6 RAD5-6His10FLAG::kanMX6 can1Δ::STE2pr-SpHIS5 leu2Δ0 his3Δ1 ura3Δ0 met15Δ0 lyp1Δ*	This study
	*MAT***a** *fet3Δ::natMX6 RAD5-6His10FLAG::kanMX6 can1Δ::STE2pr-SpHIS5 leu2Δ0 his3Δ1 ura3Δ0 met15Δ0 lyp1Δ*	This study
	*MAT***a** *ydj1Δ::natMX6 RAD5-6His10FLAG::kanMX6 can1Δ::STE2pr-SpHIS5 leu2Δ0 his3Δ1 ura3Δ0 met15Δ0 lyp1Δ*	This study
	*MAT***a** *gas1Δ::natMX6 RAD5-6His10FLAG::kanMX6 can1Δ::STE2pr-SpHIS5 leu2Δ0 his3Δ1 ura3Δ0 met15Δ0 lyp1Δ*	This study
	*MAT*α *rad5Δ::natMX6 can1Δ::STE2pr-SpHIS5 leu2Δ0 his3Δ1 ura3Δ0 met15Δ0 lyp1Δ*	Boone lab
	*MAT***a** *his3Δ::kanMX6 rad5Δ::natMX6 can1Δ::STE2pr-SpHIS5 leu2Δ0 his3Δ1 ura3Δ0 met15Δ0 lyp1Δ*	This study
	*MAT***a** *slx8Δ::kanMX6 rad5Δ::natMX6 can1Δ::STE2pr-SpHIS5 leu2Δ0 his3Δ1 ura3Δ0 met15Δ0 lyp1Δ*	This study
	*MAT***a** *asf1Δ::kanMX6 rad5Δ::natMX6 can1Δ::STE2pr-SpHIS5 leu2Δ0 his3Δ1 ura3Δ0 met15Δ0 lyp1Δ*	This study
	*MAT***a** *mlo50Δ::kanMX6 rad5Δ::natMX6 can1Δ::STE2pr-SpHIS5 leu2Δ0 his3Δ1 ura3Δ0 met15Δ0 lyp1Δ*	This study
	*MAT***a** *ftr1Δ::kanMX6 rad5Δ::natMX6 can1Δ::STE2pr-SpHIS5 leu2Δ0 his3Δ1 ura3Δ0 met15Δ0 lyp1Δ*	This study
	*MAT***a** *lip1Δ::kanMX6 rad5Δ::natMX6 can1Δ::STE2pr-SpHIS5 leu2Δ0 his3Δ1 ura3Δ0 met15Δ0 lyp1Δ*	This study
	*MAT***a** *pho13Δ::kanMX6 rad5Δ::natMX6 can1Δ::STE2pr-SpHIS5 leu2Δ0 his3Δ1 ura3Δ0 met15Δ0 lyp1Δ*	This study
	*MAT***a** *pih1Δ::kanMX6 rad5Δ::natMX6 can1Δ::STE2pr-SpHIS5 leu2Δ0 his3Δ1 ura3Δ0 met15Δ0 lyp1Δ*	This study
	*MAT***a** *pmr1Δ::kanMX6 rad5Δ::natMX6 can1Δ::STE2pr-SpHIS5 leu2Δ0 his3Δ1 ura3Δ0 met15Δ0 lyp1Δ*	This study
	*MAT***a** *bre5Δ::kanMX6 rad5Δ::natMX6 can1Δ::STE2pr-SpHIS5 leu2Δ0 his3Δ1 ura3Δ0 met15Δ0 lyp1Δ*	This study
	*MAT***a** *vps9Δ::kanMX6 rad5Δ::natMX6 can1Δ::STE2pr-SpHIS5 leu2Δ0 his3Δ1 ura3Δ0 met15Δ0 lyp1Δ*	This study
	*MAT***a** *sti1Δ::kanMX6 rad5Δ::natMX6 can1Δ::STE2pr-SpHIS5 leu2Δ0 his3Δ1 ura3Δ0 met15Δ0 lyp1Δ*	This study
	*MAT***a** *snt1Δ::kanMX6 rad5Δ::natMX6 can1Δ::STE2pr-SpHIS5 leu2Δ0 his3Δ1 ura3Δ0 met15Δ0 lyp1Δ*	This study
	*MAT***a** *mms2Δ::kanMX6 rad5Δ::natMX6 can1Δ::STE2pr-SpHIS5 leu2Δ0 his3Δ1 ura3Δ0 met15Δ0 lyp1Δ*	This study
	*MAT***a** *mga2Δ::kanMX6 rad5Δ::natMX6 can1Δ::STE2pr-SpHIS5 leu2Δ0 his3Δ1 ura3Δ0 met15Δ0 lyp1Δ*	This study
	*MAT***a** *ptc6Δ::kanMX6 rad5Δ::natMX6 can1Δ::STE2pr-SpHIS5 leu2Δ0 his3Δ1 ura3Δ0 met15Δ0 lyp1Δ*	This study
	*MAT***a** *hur1Δ::kanMX6 rad5Δ::natMX6 can1Δ::STE2pr-SpHIS5 leu2Δ0 his3Δ1 ura3Δ0 met15Δ0 lyp1Δ*	This study
	*MAT***a** *mub1Δ::kanMX6 rad5Δ::natMX6 can1Δ::STE2pr-SpHIS5 leu2Δ0 his3Δ1 ura3Δ0 met15Δ0 lyp1Δ*	This study
	*MAT***a** *lsm1Δ::kanMX6 rad5Δ::natMX6 can1Δ::STE2pr-SpHIS5 leu2Δ0 his3Δ1 ura3Δ0 met15Δ0 lyp1Δ*	This study
	*MAT***a** *dcg1Δ::kanMX6 rad5Δ::natMX6 can1Δ::STE2pr-SpHIS5 leu2Δ0 his3Δ1 ura3Δ0 met15Δ0 lyp1Δ*	This study
	*MAT***a** *asc1Δ::kanMX6 rad5Δ::natMX6 can1Δ::STE2pr-SpHIS5 leu2Δ0 his3Δ1 ura3Δ0 met15Δ0 lyp1Δ*	This study
	*MAT***a** *fet3Δ::kanMX6 rad5Δ::natMX6 can1Δ::STE2pr-SpHIS5 leu2Δ0 his3Δ1 ura3Δ0 met15Δ0 lyp1Δ*	This study
	*MAT***a** *ydj1Δ::kanMX6 rad5Δ::natMX6 can1Δ::STE2pr-SpHIS5 leu2Δ0 his3Δ1 ura3Δ0 met15Δ0 lyp1Δ*	This study
	*MAT***a** *gas1Δ::kanMX6 rad5Δ::natMX6 can1Δ::STE2pr-SpHIS5 leu2Δ0 his3Δ1 ura3Δ0 met15Δ0 lyp1Δ*	This study
DGY78	*MAT***a** *RAD5-GFP::HIS3MX6 leu2Δ0 his3Δ1 ura3Δ0 met15Δ0*	Huh *et al.* (2003)
DGY236	*MAT***a** *rad5Δ::kanMX6 leu2Δ0 his3Δ1 ura3Δ0 met15Δ0*	This study
DGY290	*MAT***a** *RAD5-GFP::HIS3MX6 pol32Δ::kanMX6 leu2Δ0 his3Δ1 ura3Δ0 met15Δ0*	This study
DGY366	*MAT***a** *RAD5-GFP::HIS3MX6 NUP49-mCherry::CaURA3 can1Δ::STE2pr-LEU2 leu2Δ0 his3Δ1 ura3Δ0 met15Δ0 lyp1Δ*	Tkach *et al.* (2012)
DGY372	*MAT***a** *ssa1Δ::KanMX6 leu2Δ0 his3Δ1 ura3Δ0 met15Δ0*	This study
DGY373	*MAT***a** *ssa2Δ::KanMX6 leu2Δ0 his3Δ1 ura3Δ0 met15Δ0*	This study
DGY374	*MAT***a** *ssb1Δ::KanMX6 leu2Δ0 his3Δ1 ura3Δ0 met15Δ0*	This study
DGY375	*MAT***a** *ssa1Δ::KanMX6 ssa2Δ::natMX6 leu2Δ0 his3Δ1 ura3Δ0 met15Δ0*	This study
DGY376	*MAT***a** *ssa1Δ::KanMX6 ssb1Δ::natMX6 leu2Δ0 his3Δ1 ura3Δ0 met15Δ0*	This study

Chapter 3
Rad5 recruits TLS polymerases for mutagenic repair of ssDNA gaps on undamaged templates

CONTRIBUTION OF WORK:

TaeHyung Kim and Yoona park (Zhang lab) performed ChIP-seq analysis, Banabas Szakal (Branzei lab) performed two-dimensional gel analysis, Xanita Saayman performed copy number variation analysis and Ashrut Narula constructed the *rad5-IA* and *rad5-YYAA* stains.

ACKNOWLEGEMENTS:

I would like to thank Helle Ulrich for *RAD5-IA* plasmids, Hugo Wurtele for the HWY536 strain, Xiaolan Zhao for the parent *rad5-QD* strain, and all past and present Brown lab members for technical assistance and project conceptualization during consumption of alcohol.

3 Rad5 recruits TLS polymerases for mutagenic repair of ssDNA gaps on undamaged templates

3.1 Summary

In the previous chapter I described an unbiased genome-wide approach to look for regulators of Rad5 and PRR during HU-induced replication stress. In this chapter, I describe a candidate approach to dissect how PRR pathway components affect Rad5 recruitment. I dove deeper into the functional significance of Rad5 foci and characterized the defects of *rad5*Δ cells during both physiological and replication stress conditions. I found that Rad5 forms nuclear foci during normal S-phase and after exposure to types of replication stress where DNA base lesions are likely absent. Rad5 binds to stressed DNA replication forks, where it recruits TLS polymerases to repair ssDNA gaps. Absence of Rad5 at stressed replication forks results in accumulation of ssDNA leading to a hyper-activated checkpoint, mitotic defects and chromosome breaks. Importantly, my data indicate that Rad5 is the central effector of PRR signaling at stressed replication forks, where Rad5 promotes mutagenic repair of undamaged ssDNA that arises during physiological and exogenous replication stress.

3.2 Results

3.2.1 Rad5 forms foci in S-phase in response to DNA replication stress

To understand how Rad5 is functioning in the replication stress response I looked at where Rad5 foci are forming during cell cycle progression. In budding yeast the bud size roughly correlates with cell cycle position, with a small bud emerging at the G1/S transition and growing larger until G2 where it buds off to a new daughter cell after mitosis. Microscopic inspection of unperturbed cells expressing Rad5-GFP from the *RAD5* locus revealed that foci form in 10% of S-phase (small-budded) cells and less than 1% of G1 (unbudded) or G2 phase (large-budded) cells (Figure 3.1A). Applying DNA replication stress by depleting dNTP pools using the RNR inhibitor hydroxyurea (HU) or by destabilizing polymerase δ (*pol32*Δ) (Karras and Jentsch, 2010) caused an increase in S-phase foci to 46% and 48% respectively, with only a slight increase in foci in G1 or G2 cells (Figure 3.1B). Although Rad5 foci were not previously detected during HU stress (Fan et al., 2018; Ortiz-Bazán et al., 2014), my results indicate that Rad5 foci form in response to diverse types of replication stress, including physiological

replication stress. Consistent with an important role of Rad5 in resisting endogenous DNA replication stress, *rad5*Δ cells have on average a 10% increase in generation time (Figure 3.1C). Furthermore, HU-induced replication stress results in pronounced growth defects in *rad5*Δ cells (Figure 2.4A) (Daee et al., 2012). Thus, Rad5 responds to DNA replication stress, both exogenous and physiological, and is important for robust cell division cycles in the presence of DNA replication stress.

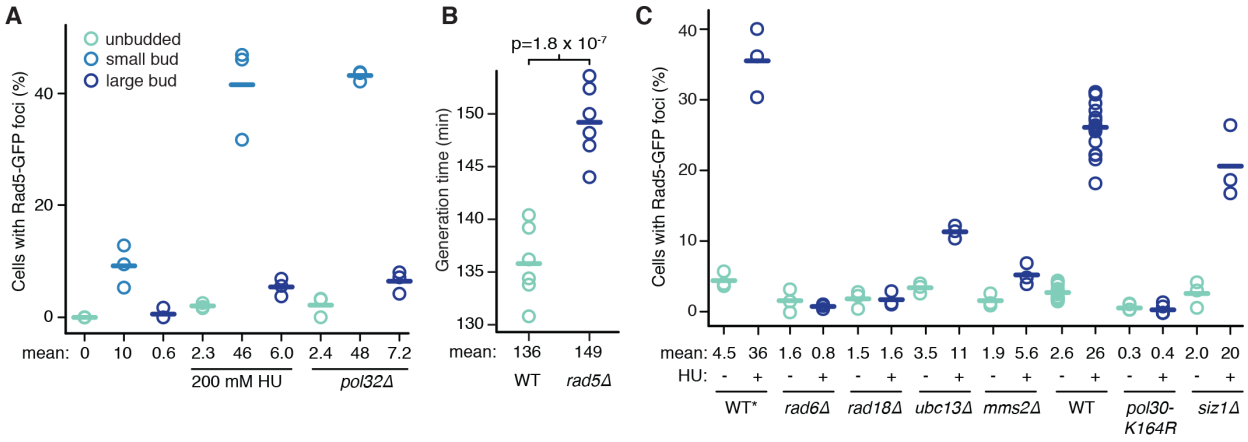

Figure 3.1 Rad5 forms PCNA$_{K164}$Ub dependent nuclear foci during S phase and in response to replication stress. (A) Mid-logarithmic phase *RAD5-GFP* and *RAD5-GFP pol32*Δ cells were left unperturbed or treated with 200 mM HU for 60 minutes and imaged as in A. The percent of unbudded, small budded and large budded cells with at least one focus is plotted for each replicate and the means are shown as solid bars. At least 100 cells of each type were scored for each replicate. (B) Generation times of wild type (WT) and rad5Δ cells during logarithmic growth are plotted for each replicate and the means are shown as solid bars. The p-value was calculated using a 2-tailed t-test. (C) Mid-logarithmic phase *RAD5-GFP* cells with the indicated mutations were left unperturbed or were treated with 200 mM HU for 60 minutes, harvested and imaged by confocal microscopy in the GFP and DIC channels. The percent of unbudded, small budded and large budded cells with at least one focus is plotted for each replicate and the means are shown as solid bars. At least 100 cells were scored for each replicate. WT* is DGY367, the isogenic background for the *rad6*Δ, *rad18*Δ, *ubc13*Δ and *mms2*Δ strains.

To identify how Rad5 is recruited to nuclear foci I interrogated the role of PCNA modification by mono- and poly-ubiquitination and by sumoylation (Figure 3.1D). Cells were treated with 200 mM HU for 1hr to increase the fraction of cells with Rad5 foci to 26 – 36%, depending on genetic background. Abolishing PCNA$_{K164}$ monoubiquitination by deletion of *RAD6* or *RAD18*, or the *pol30-K164R* mutation, substantially reduced the number of cells with Rad5 foci (Figure 1E). Abolishing PCNA$_{K164}$SUMO by deletion of *SIZ1* (Hoege et al., 2002) did not reduce Rad5 focus formation. Finally, blocking PCNA$_{K164}$ polyubiquitination by deletion of *UBC13* or *MMS2* yielded intermediate phenotypes, with Rad5 foci being reduced but not eliminated. Taken together, these results indicate that PCNA$_{K164}$Ub is required for Rad5 re-localization to nuclear foci during DNA replication stress.

3.2.2 Rad5 is recruited to stressed replication forks by $PCNA_{K164}Ub$

Based on the observation that replisomes form clusters visualized as nuclear foci (Saner et al., 2013) and the known roles of PRR at the replication fork, I hypothesized that Rad5 foci correspond to stressed replication forks. I used chromatin immunoprecipitation coupled to deep sequencing (ChIP-seq) to assess Rad5 binding genome-wide during synchronous progression through S-phase in the presence of 200 mM HU. Under these conditions, replisomes stall in close proximity to early-firing replication origins, enabling detection of proteins associated with stressed replication forks. To produce a genome-wide view of enrichment in the ChIP-seq experiments, Simon Kim calculated median ChIP-seq enrichment values for 50 kb on either side of the 108 annotated early-firing yeast origins (Figure 3.2A). We defined the position of the DNA replication machinery by immunoprecipitating the DNA polymerase ε subunit Dpb3. After 60 min of release into S-phase in the presence of HU, Dpb3 formed two tight peaks flanking early-firing replication origins (Figure 3.2A). At 120 min and 180 min post-release the Dpb3 peaks are found increasingly distal to the early origins, consistent with bi-directional replication fork movement away from the origins. Rad5 has a very similar enrichment profile, indicating that Rad5 is recruited to chromatin during DNA replication stress, and that the location of Rad5 is indistinguishable from that of the DNA replication machinery (Figure 3.2B). Simon confirmed that the Dpb3 and Rad5 enrichment peaks correspond to DNA replication by plotting the median increase in DNA copy number over the same 100 kb window (Figure 3.2C and 2D). Next, I tested if the dependencies for Rad5 recruitment to stressed replication forks are the same as for Rad5 focus formation. As expected, deletion of *RAD18* or introduction of *pol30-K164R* drastically reduced Rad5 recruitment to stressed-replication forks (Figure 3.2E) while deletion of *SIZ1, UBC13* or *MMS2* caused only minor recruitment defects (Figure 3.2F and 3.2G) Decreases in Rad5 recruitment were not due to dissociation of replisomes in these mutants as Dpb3 recruitment remained robust (Figure 3.3A, 3.3B, and 3.3C), or to decreased Rad5 levels (Figure 3.3D). Therefore, my ChIP-seq results reveal that Rad5 is recruited and retained at stressed DNA replication forks by $PCNA_{K164}Ub$.

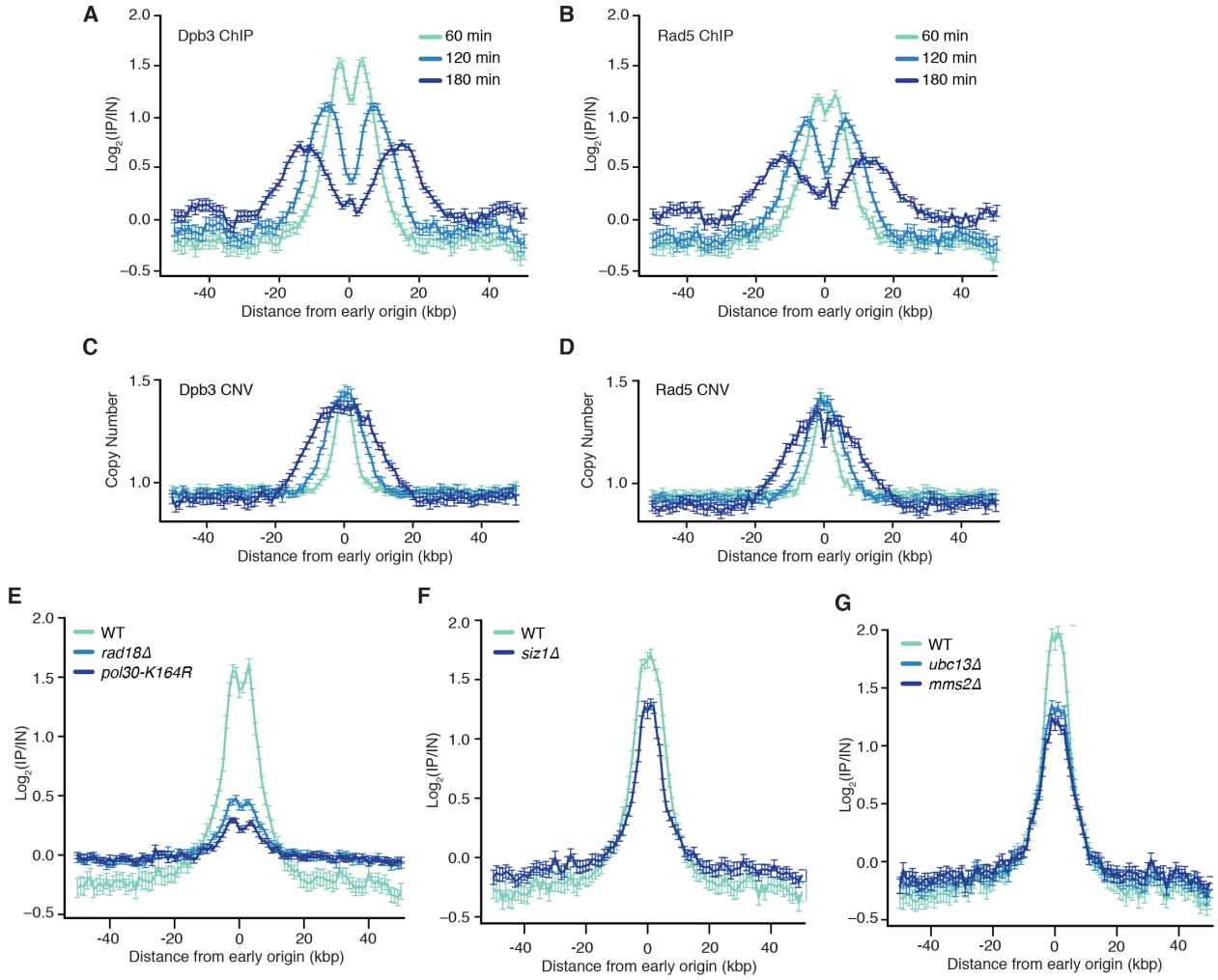

Figure 3.2 Rad5 is recruited and retained at HU-stressed replication forks in a PCNA$_{K164}$Ub dependent manner. ChIP-seq analysis was performed on (A) *DPB3-FLAG* or (B) *RAD5-FLAG* cells at 60, 120, and 180 min following synchronous release into S phase in the presence of 200 mM HU. The median (± standard error) ChIP enrichment scores across n = 108 early-firing origins are plotted. (C) DNA replication profiles comparing the copy number of DNA sequences in samples from A to a sample of G1 arrested cells, with median relative DNA copy number (± standard error) across 108 early-firing origins plotted. (D) DNA replication profiles of DNA sequences in samples from B. (E,F,G) ChIP-seq analysis was performed on *RAD5-FLAG* cells carrying the indicated mutations, 60 min following synchronous release into S phase in the presence of 200 mM HU. The median (± standard error) ChIP enrichment scores across 108 early-firing origins are plotted.

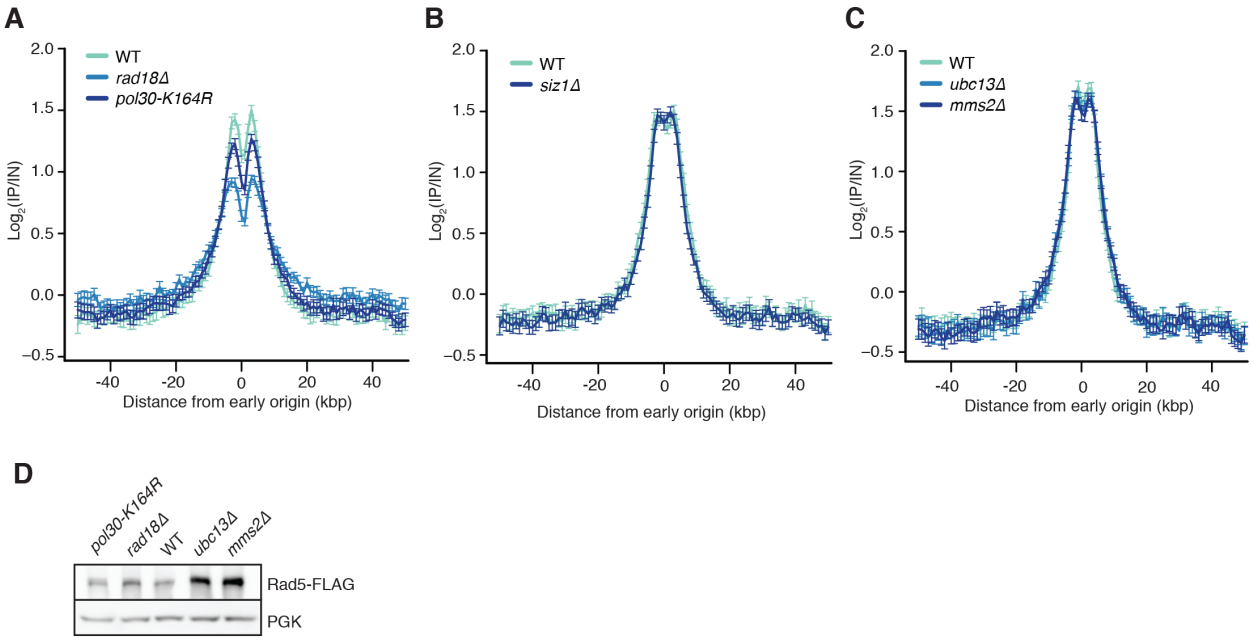

Figure 3.3 Dpb3 recruitment to stressed-replication forks is unaffected in PCNA$_{K164}$ modification mutants. *DPB3-FLAG* cells with (A) *rad18*Δ or *pol30-K164R* (B) *siz1*Δ and (C) *ubc13*Δ or *mms2*Δ mutations were synchronously released into S-phase in the presence of 200 mM HU before harvesting samples for ChIP-seq at 60 min. The median (± standard error) ChIP enrichment scores across 108 early-firing origins are plotted. (D) Mid-logarithmic phase *RAD5-FLAG* cells with the indicated mutations were immunoblotted with FLAG- or PGK-specific antibodies.

3.2.3 Rad5 suppresses the accumulation of ssDNA at stressed replication forks

Having established that Rad5 is recruited to stressed replication forks by PCNA monoubiquitination, I shifted my attention to uncovering Rad5 function at the stressed fork. I first tested whether the kinetics of DNA replication were altered in *rad5*Δ. Flow cytometry, copy number analysis, and DNA combing all revealed an increase in the rate of DNA replication early in S phase in *rad5*Δ (Figure 3.4A, 3.4B, 3.4C). However, when I made similar measurements later in S phase, I found that replication fork rate reverted to the wild type rate after the initial increase (Figure 3.4D), and that under-replicated regions were not evident in the population (Figure 3.4F). I conclude that the initial increased replication rate in *rad5*Δ is an indirect effect of increased dNTP pools (Davidson et al., 2012; Poli et al., 2012) and not a direct effect of fork reversal as suggested for the Rad5 mammalian homolog HLTF (Kile et al., 2015). Consistent with my interpretation, increased expression of the ribonucleotide reductase subunit Rnr3 is readily detectable in *rad5*Δ (Figure 3.4E).

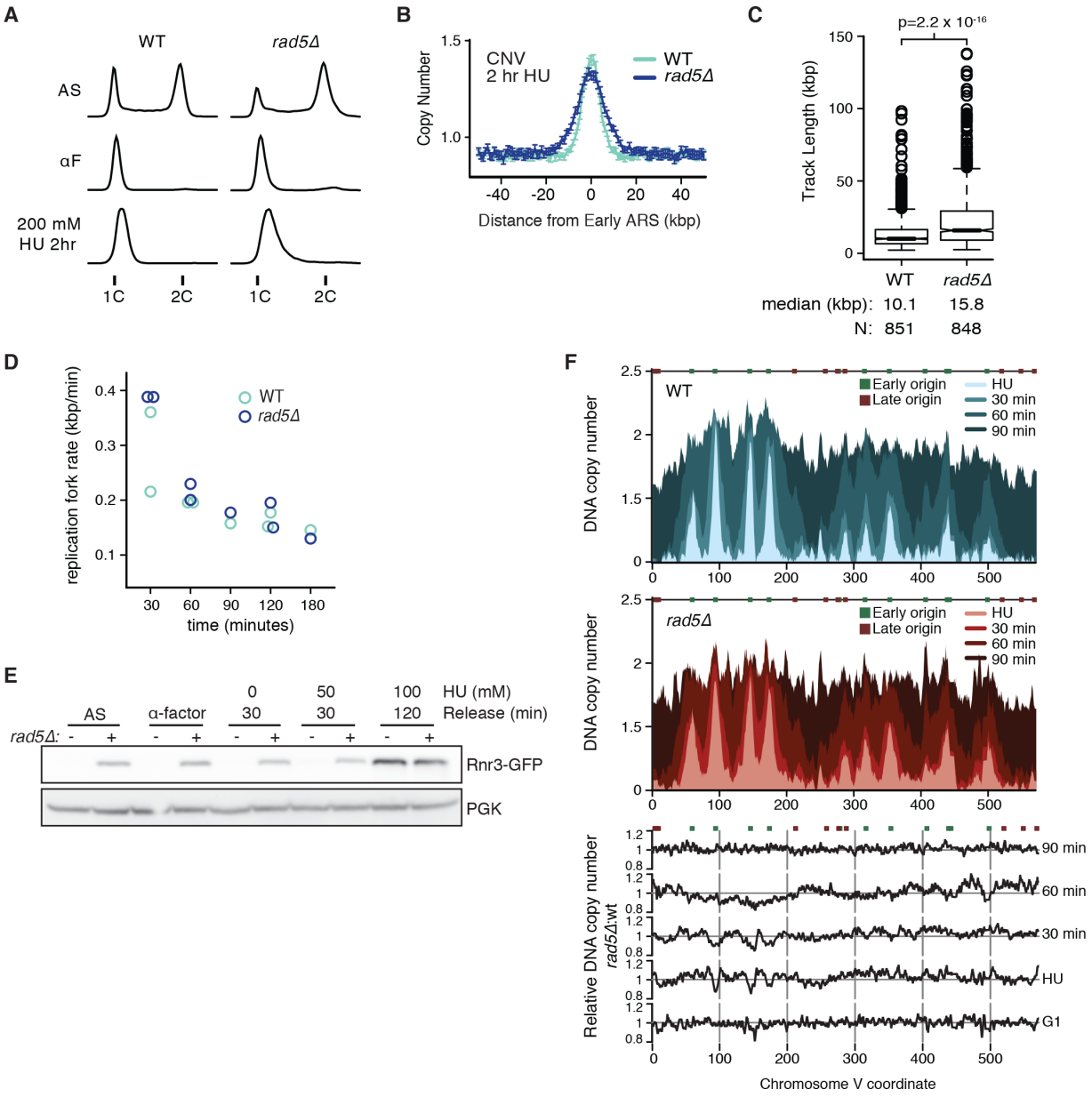

Figure 3.4 Deletion of *RAD5* accelerates early S phase but does not cause under-replication. (A) Mid-logarithmic phase (AS) wild type (WT) or rad5Δ cells were arrested in G1 phase (AF), and released synchronously into S phase in the presence of 200 mM HU for 2 hr. Cultures were sampled for analysis of DNA contents by flow cytometry, which are plotted as histograms, with the positions of 1C and 2C DNA contents indicated. (B) DNA replication profiles comparing the copy number of DNA sequences in samples from A to a sample of G1 arrested cells, with median relative DNA copy number (± standard error) across 108 early-firing origins plotted. (C) Wild type (WT) or *rad5*Δ cells were released synchronously into S phase in 50 mM HU + BrdU and sampled for DNA combing after 30 min. Boxplots of nascent DNA track lengths are shown with horizontal bars indicating the medians. Boxes span the first through third quartiles, whiskers extending to the last data points within 1.5 times the interquartile range, and outliers are plotted as circles. The p-value was calculated using a 2-tailed Mann-Whitney U-test.(D) Wild type and *rad5*Δ cells were synchronously released into S-phase in the presence of 200 mM HU + BrdU and sampled for DNA combing at the indicated times. Median replication fork rates are plotted for two replicates. (E) Mid-logarithmic phase *RNR3-GFP* cells ± *rad5*Δ were immunoblotted with GFP- or PGK-specific antibodies. (F) WT or *rad5*Δ cells were synchronously released into S phase in the presence of 200 mM HU for 120 min, washed and re-suspended in fresh media. Cultures were sampled at indicated times and genomic DNA was extracted. DNA replication profiles compare the relative copy number of DNA sequences in each sample to a sample of G1 arrested cells. Profiles for chromosome V are shown. Relative DNA copy number was calculated by dividing the copy number of *rad5*Δ by WT to detect any under-replicated regions.

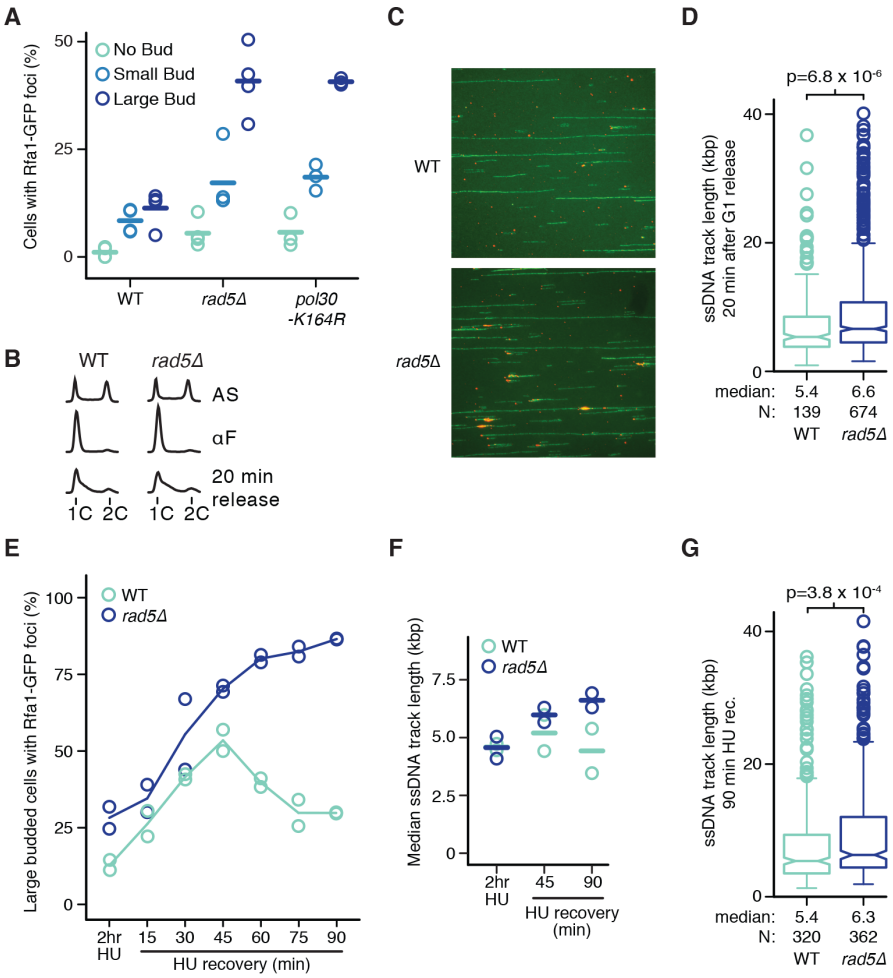

Figure 3.5 Rad5 prevents the accumulation of ssDNA during S phase. (A) Mid-logarithmic phase *RFA1-GFP* cells with the indicated mutations were fixed and imaged by confocal microscopy in the GFP and DIC channels. The percent of unbudded, small budded and large budded cells with at least one focus is plotted for each replicate and the means are shown as solid bars. At least 200 cells were scored for each replicate. (B) Wild type (WT) or *rad5*Δ cells were released synchronously into S phase and sampled for DNA molecular combing after 20 min. Cultures were sampled at the indicated times for analysis by flow cytometry. DNA contents are plotted as histograms, and the positions of 1C and 2C DNA contents are indicated. (C) Representative images of combed native DNA stained with YOYO-1 (green) and anti-ssDNA antibody (red) are shown. (D) Boxplots of ssDNA track lengths from B are shown with horizontal bars indicating the medians. Boxes span the first through third quartiles, whiskers extending to the last data points within 1.5 times the interquartile range, and outliers are plotted as circles. P-values were calculated using a 2-tailed Mann-Whitney U-test. (E) *RFA1-GFP* WT or *rad5*Δ cells were released synchronously into S phase in the presence of 200 mM HU for 120 min, washed and re-suspended in fresh media. Cells were sampled at the indicated times and processed as in A. The percent of large budded cells with at least one Rfa1-GFP focus is plotted. (F) WT or *rad5*Δ cells were released synchronously into S phase in the presence of 200 mM HU for 120 min, washed, re-suspended in fresh media, and sampled for DNA molecular combing at the indicated times. Median ssDNA track lengths from each replicate are plotted and the mean values are shown as solid bars. (G) ssDNA track lengths for one replicate from E are shown as boxplots, as in C.

I next tested for more subtle effects on DNA replication by measuring the presence of ssDNA in *rad5*Δ. I used RPA focus formation as a proxy for ssDNA (Bélanger et al., 2016; Lisby et al., 2004), monitoring Rfa1-I find 1.1% of G1-, 8.4% of S- and 11.3% of G2-phase cells have at least

one RPA focus. In *rad5*Δ the number cells with RPA foci increases to 5.5% in G1, 17.2% in S- and 40.8% in G2-phase. To establish that the presence of Rad5 at stressed replication forks is important for preventing the formation of ssDNA I tested *pol30-K164R*, which is unable to recruit Rad5 (Figure 3.2E). When Rad5 is not present at the stressed fork, RPA foci increase substantially (Figure 3.5A), consistent with Rad5 action at replication forks being important for preventing the formation of ssDNA.

Although RPA foci are a reasonable proxy for ssDNA, I tested directly whether ssDNA was increased in *rad5*Δ mutants. I used a modified DNA combing protocol to directly visualize ssDNA on DNA fibers isolated from wild type and *rad5*Δ cells (Figure 3.5C, 3.5D) (García-Rodríguez et al., 2018). Following synchronous release into S phase (Figure 3.5B) we found that the median length of ssDNA tracks increased from 5.4kb in wild type to 6.6kb in *rad5*Δ (Figure 3.5D). Since ssDNA and RPA foci could result from DNA resection at double-strand breaks (DSBs) (Lisby et al., 2004) or from gapped regions, we quantified the fraction of ssDNA tracks that were present at DNA ends, and therefore could originate from processing of DSBs. We found that 67% (wild type) and 80% (*rad5*Δ) of ssDNA tracks were not at a DNA end, and therefore originate from gapped internal DNA regions rather than from DSB processing.

Rad5 suppression of ssDNA accumulation could reflect Rad5 function in preventing ssDNA formation at replication forks, or in promoting repair of ssDNA. To distinguish these possibilities I used HU to induce replication stress and monitored Rfa1-GFP foci and ssDNA following recovery from replication stress (Figure 3.5E). After 2 hours of HU treatment the fraction of cells with RPA foci is greater in *rad5*Δ (28% in *rad5*Δ vs 13% in wild type). Upon removal of HU, both wild type and *rad5*Δ cells accumulate RPA foci for 45 min (increasing to 53.5% for wild type and 70.3% for *rad5*Δ), suggesting that the formation of ssDNA occurs in both wild type and *rad5*Δ cells. After 45 minutes, RPA foci start to decrease in the wild type cells, whereas RPA foci continue to increase in *rad5*Δ cells (Figure 3.5E), suggesting that ssDNA is not repaired effectively in *rad5*Δ. We measured ssDNA directly, again using DNA combing, and detected the same trend. After HU treatment the length of ssDNA tracks in wild type and *rad5*Δ was initially indistinguishable (Figure 3.5F and 3.6). Again, ssDNA increased for 45 minutes after removal of HU (to 5.2 kbp for wild type and 6.0 kbp for *rad5*Δ), followed by a decrease in wild type (to 4.5 kbp) and continued increase in *rad5*Δ (6.6 kbp) (Figure 3.5G). We conclude that Rad5 promotes

repair of ssDNA that accumulates during S phase, both in the presence and absence of exogenous DNA replication stress.

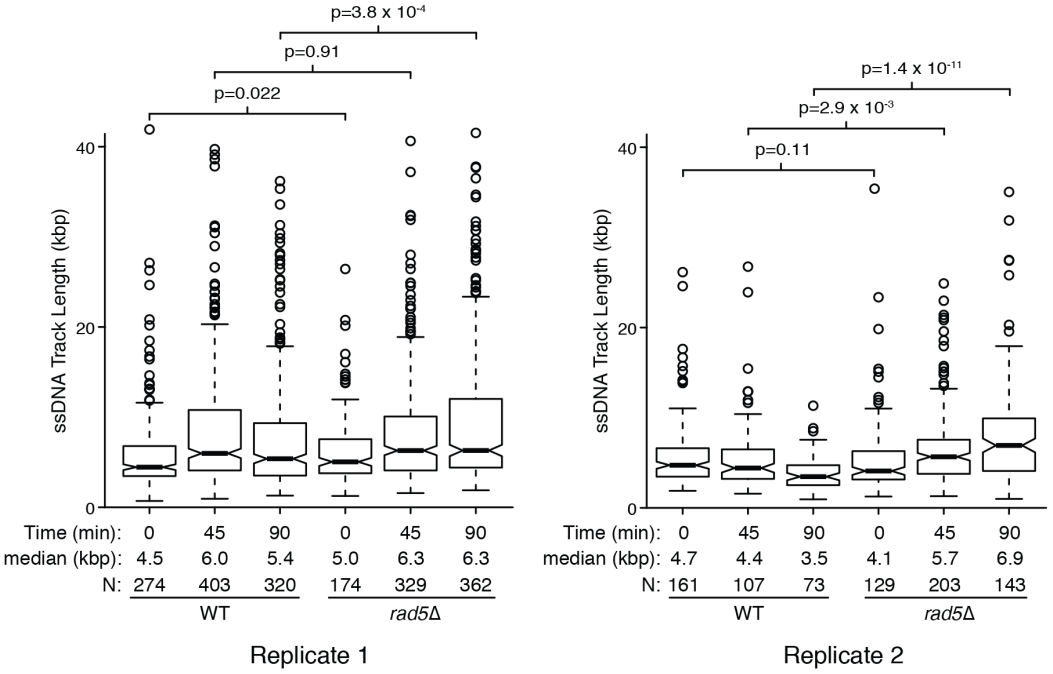

Figure 3.6 *RAD5* is required to suppress the accumulation of ssDNA following recovery from HU-induced replication stress. Mid-logarithmic phase wild type (WT) or *rad5*Δ cells were synchronously released into S-phase in the presence of 200 mM HU for 120 min, washed, re-suspended into fresh media and sampled for ssDNA molecular combing at the indicated times after HU removal. Boxplots of ssDNA track lengths are shown with a horizontal bars indicating the medians, boxes spanning the first through third quartiles, whiskers extending to the last data points within 1.5 times the interquartile range and outliers plotted as circles. P-values were calculated using a 2-tailed Mann-Whitney U-test. 2 independent replicates are shown.

3.2.4 Rad5-dependant clearance of ssDNA prevents mitotic delay, checkpoint activation and chromosome rearrangements

During my HU recovery experiments I noticed that *rad5*Δ cells fail to progress through mitosis into the next cell cycle (Figure 3.7A, where a 1C/G1 peak is absent at 90 minutes in *rad5*Δ). To directly test if *rad5*Δ accumulates in G2/M, I scored the nuclear morphology and budding index of wild type and *rad5*Δ cells recovering from HU (Figure 3.7B and 3.7C). I detected a dramatic increase in the fraction of cells with a large bud and one nucleus or with an anaphase bridge (DAPI-stained DNA connecting two separated nuclei in a large budded cell) in *rad5*Δ (Figure 3.7B and 3.7C). The patterns of accumulation in G2/M are strikingly similar to the patterns of ssDNA accumulation that I observed: G2/M cells with a single nucleus or an anaphase bridge are increased after 45 minutes in both wild type and *rad5*Δ, followed by a decrease in wild type and persistent accumulation in *rad5*Δ (Figure 3.7C). We detect an increase in G2/M cells with a

single nucleus or an anaphase bridge in *rad5*Δ (and in *pol30-K164R*) even without the application of HU (Figure 3.7D), indicating that Rad5 is important to prevent abnormal mitoses in an unperturbed cell cycle. Finally, in *rad5*Δ 70% of cells with anaphase bridges also have a RPA focus, compared to only 19% in wild type (Figure 3.7E), indicating a link between ssDNA and anaphase bridges, and further demonstrating that ssDNA persists in *rad5*Δ independently of exogenous DNA replication stress.

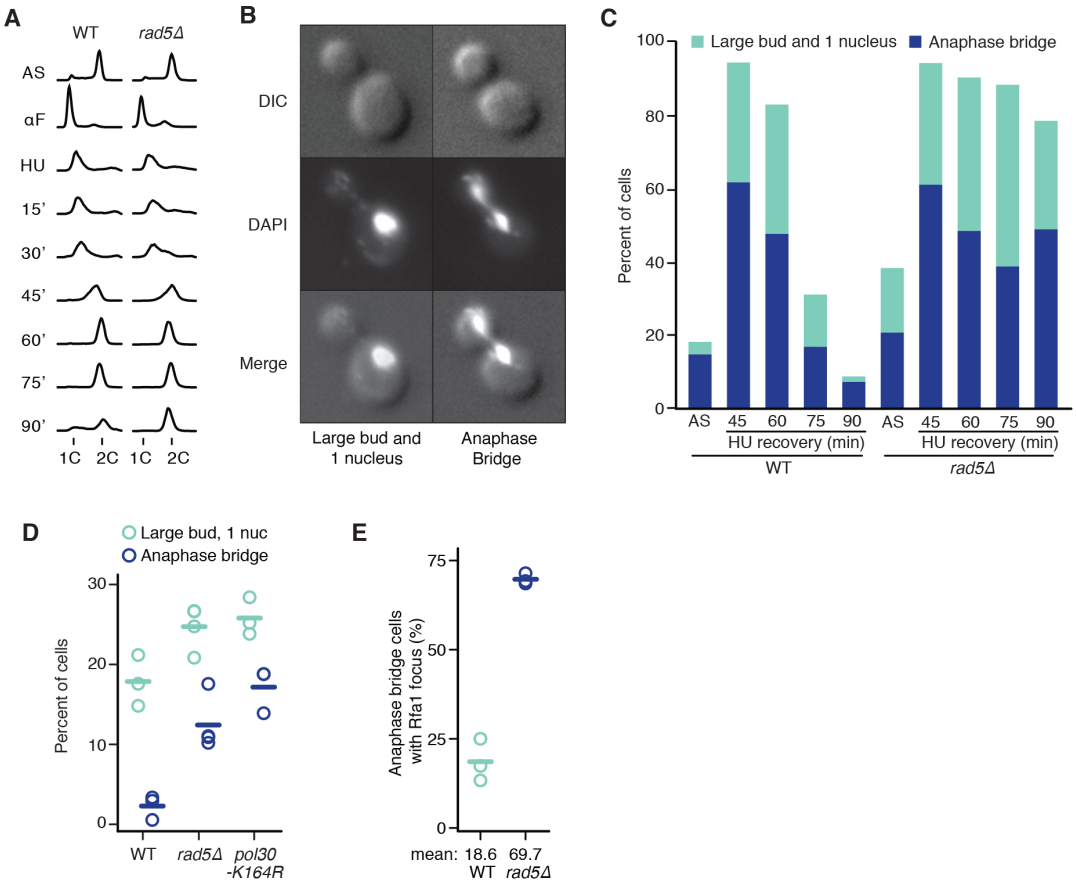

Figure 3.7 ssDNA accumulation in *rad5*Δ cells leads to anaphase bridges. (A) Mid-logarithmic phase (AS) wild type (WT) or *rad5*Δ cells were arrested in G1 phase (aF), released synchronously into S phase in the presence of 200 mM HU for 120 min (HU), washed and re-suspended in fresh media. Cultures were sampled at the indicated times for analysis by flow cytometry. DNA contents are plotted as histograms, and the positions of 1C and 2C DNA contents are indicated. (B) Samples from A were DAPI stained and imaged by brightfield and fluorescence microscopy. Representative micrographs in the DIC and DAPI channels of a cell with a large bud 1 nucleus and an anaphase bridge are shown. (C) The percent of cells from A with a large bud and 1 nucleus or anaphase bridges is shown as a stacked bar plot. At least 200 total cells were scored for each time point. (D) Mid-logarithmic phase wild type, *rad5*Δ or *pol30-K164R* cells were fixed and treated as in B. The percent of cells with a large bud and one nucleus, or with an anaphase bridge, is plotted for each replicate and the means are shown as solid bars. At least 200 cells were scored for each replicate. (E) Mid-logarithmic phase *RFA1-GFP* wild type or *rad5*Δ cells were fixed, DAPI stained and imaged by confocal microscopy in the GFP, DAPI and DIC channels. The percent of cells with an anaphase bridge with an associated Rfa1 focus is plotted for each replicate and the means are shown as solid bars. At least 17 anaphase bridge containing cells were scored for each replicate.

The G2/M phenotypes I observe in *rad5*Δ cells are indicative of a hyper-activated DNA damage checkpoint (Sanchez et al., 1999; Yang et al., 1997). RPA coated ssDNA is the major activator of the DNA damage checkpoint (Branzei and Foiani, 2009; Zou and Elledge, 2003) and PRR defective cells have a hyper-activated checkpoint when recovering from replication stress induced by *pol32*Δ (Karras and Jentsch, 2010; Karras et al., 2013), UV (Daigaku et al., 2010) or MMS (Huang et al., 2013). I confirmed that the DNA damage checkpoint is activated, as measured by Rad9 phosphorylation, in asynchronous *rad5*Δ cultures (Figure 3.8A, compare AS lanes) and is hyper-activated during HU recovery (Figure 3.8A, compare 90 minute HU recovery lanes). Furthermore, deleting *RAD9* in *rad5*Δ cells causes an increase in the fraction of G1 cells with RPA foci (Figure 3.8B), consistent with *RAD9* preventing *rad5*Δ cells with ssDNA from proceeding through mitosis. In line with this reasoning, *rad5*Δ *rad9*Δ double mutant cells have wild type levels of anaphase bridges (Figure 3.8C) yet have a large HU-induced fitness defect (Figure 3.8D). We conclude that the DNA damage checkpoint restricts ssDNA to G2 phase to allow repair and promote survival of *rad5*Δ cells.

I hypothesized that the persistent ssDNA that we detect in *rad5*Δ could contribute to the increased chromosome rearrangements seen in *rad5*Δ cells (Motegi et al., 2006; Putnam et al., 2010). If this is the case, imposing additional replication stress by applying a low dose of HU should increase the rate of chromosome rearrangements. I used the classic gross chromosomal rearrangement (GCR) assay (Srivatsan et al., 2018) to monitor chromosome rearrangements in wild type and *rad5*Δ cells in unperturbed and mild replication stress conditions (Figure 3.8E). In wild type cells, HU increased the GCR rate by 3-fold, whereas GCR increased by 4-fold in *rad5*Δ. I infer that HU-induced replication stress causes chromosome rearrangements, and this is exacerbated by deletion of *rad5*, consistent with chromosome breakage in *rad5*Δ cells that survive HU treatment.

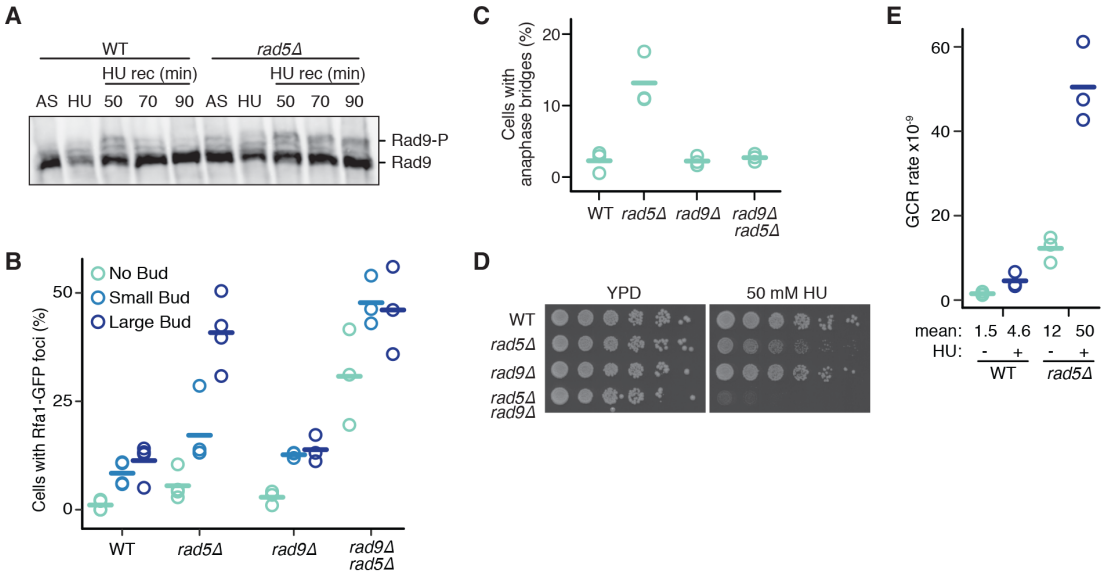

Figure 3.8 The DNA damage checkpoint restricts mitosis when ssDNA is present and promotes survival of *rad5*Δ cells. (A) Mid-logarithmic phase (AS) *RAD9-FLAG* wild type (WT) or *rad5*Δ cells were released synchronously into S phase in the presence of 200 mM HU for 120 min (HU), washed and re-suspended in fresh media. Cultures were sampled at indicated times and immunoblotted with FLAG-specific antibodies. The positions corresponding to unmodified Rad9 and to slower migrating phosphorylated Rad9 are indicated. (B) Mid-logarithmic phase *RFA1-GFP* cells with the indicated gene deletions were fixed and imaged by confocal microscopy in the GFP and DIC channels. The percent of unbudded, small budded and large budded cells with at least one focus is plotted for each replicate and the means are shown as solid bars. At least 200 cells were scored for each replicate. (C) Mid-logarithmic phase cells with the indicated gene deletions were fixed, stained with DAPI, and imaged by brightfield and fluorescence microscopy. The percent of cells with an anaphase bridge is plotted for each replicate and the means are shown as solid bars. At least 200 cells were scored for each replicate. (D) Cells with the indicated gene deletions were grown to saturation, serially diluted, spotted on YPD or YPD+50 mM HU agar plates and grown for 3 days at 30°C. (E) WT and *rad5*Δ cells with a GCR reporter were grown in YPD or YPD+25 mM HU to saturation and plated on selective media to measure gross chromosomal rearrangements. The GCR rate is plotted for each replicate and the means are shown as solid bars.

3.2.5 Rad51-mediated HR does not cause anaphase bridges in *rad5*Δ cells

Anaphase bridges can result from recombination intermediates caused by the replication stress response (García-Luis and Machín, 2014; Germann et al., 2014; Mohebi et al., 2015; Sofueva et al., 2011) or from the simple presence of unreplicated parental DNA regions (Ait Saada et al., 2017; Amaral et al., 2016; Germann et al., 2014; Sabatinos et al., 2015). To test whether recombination intermediates accumulate at replication forks in *rad5*Δ cells Banabas Szakal from Dana Branzei's lab performed 2D gel electrophoresis on WT and *rad5*Δ cells synchronously released into HU challenged S phase. After 60 minutes in HU, they could detect signals characteristic of X-shaped recombination structures near the early-firing replication origin *ARS305* in wild type cells (Figure 3.9A). Surprisingly, *rad5*Δ had few if any X-shaped molecules detected, indicating that *rad5*Δ mutants have less recombination near stressed forks than do wild type cells. The decrease in recombination intermediates is likely due to defective Rad5-mediated template switching repair of ssDNA early in S phase (Branzei et al., 2008; Gonzalez-Huici et al.,

2014; Karras et al., 2013; Minca and Kowalski, 2010). I tested whether the ssDNA accumulation observed in *rad5*Δ was due to homologous recombination, and found that deleting *RAD51* resulted in more RPA foci in *rad5*Δ, rather than less (Figure 3.9B). Similarly, the fraction of cells with anaphase bridges or in G2/M with a single nucleus increased upon deletion of *RAD51* in *rad5*Δ (Figure 3.9C and 3.9D), further indicating that Rad51-dependent recombination processes do not generate the ssDNA, the anaphase bridges, or the mitotic delay observed in *rad5*Δ. Finally, the HU sensitivity of *rad5*Δ is worsened, not suppressed, by *rad51*Δ (Figure 3.9E).

3.2.6 Activation of HR in S-phase prevents ssDNA accumulation in *rad5*Δ

Since my experiments indicated that loss of HR exacerbated all of the *rad5*Δ replication stress phenotypes, I assessed the effect of promoting HR in S phase. The anti-recombinase protein Srs2 inhibits HR at replication forks (Hoege et al., 2002; Krejci et al., 2003; Veaute et al., 2003), and so I deleted *SRS2* and measured RPA foci, anaphase bridges, and HU sensitivity (Figure 3.9B, 3.9C, and 3.9E). Deletion of *SRS2* in *rad5*Δ rescued all of the phenotypes to near wild type levels. Hence, relieving Srs2 inhibition at replication forks allows more efficient Rad51-dependent but Rad5-independent HR suppression of ssDNA accumulation, thereby bypassing the requirement for Rad5 to repair ssDNA resulting from DNA replication stress.

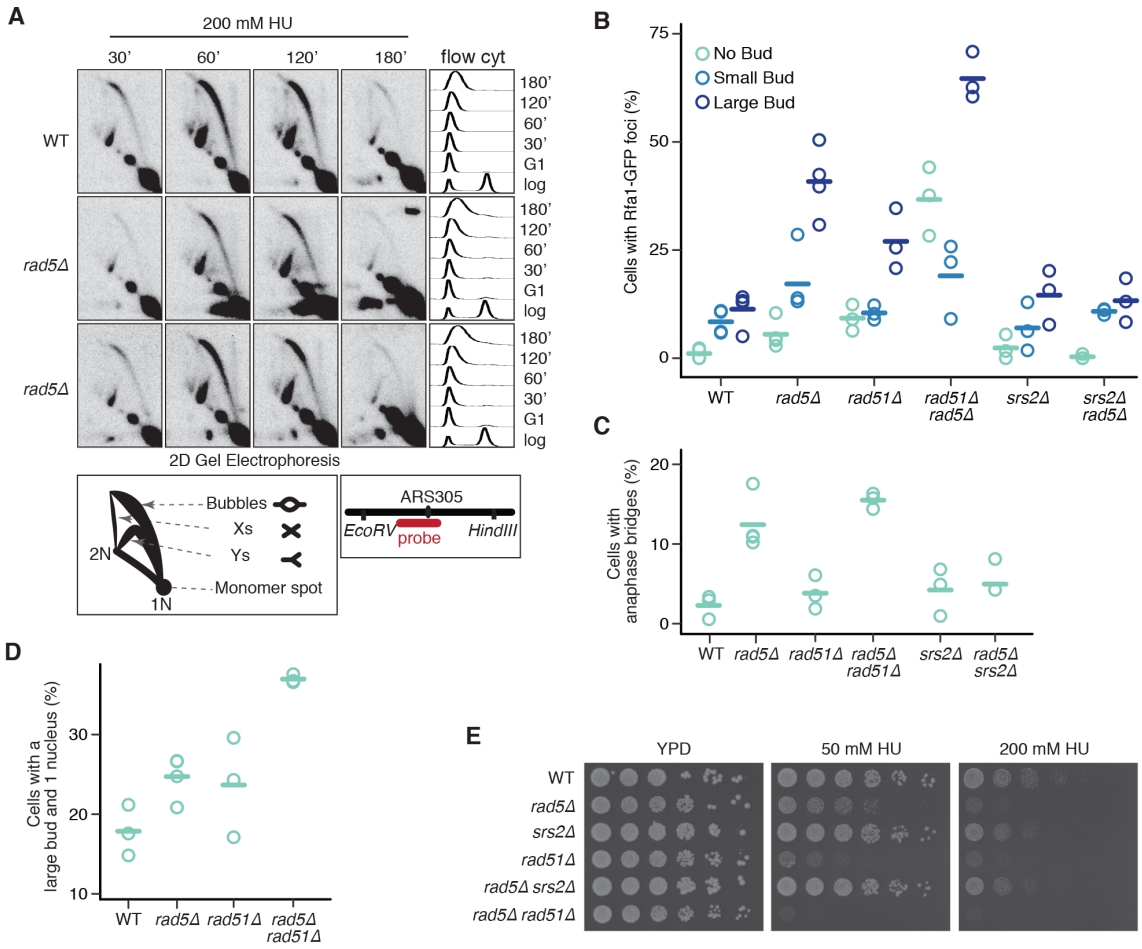

Figure 3.9 Activating Rad51-mediated recombination repairs ssDNA in *rad5*Δ. (A) Wild type (WT) or *rad5*Δ cells were synchronously released into S phase in the presence of 200 mM HU before sampling at the indicated times for 2D gel and flow cytometric analysis. Autoradiograms of the 2D gels for wild type and 2 replicates of *rad5*Δ are shown. The DNA contents of cells from the 2D gel analysis were measured by flow cytometry and the histograms are plotted on the right. A schematic of the expected migration positions for different DNA structures is shown below, as is the location of the *ARS305* probe (red) relative to the corresponding locus (black). (B) Mid-logarithmic phase *RFA1-GFP* cells with the indicated gene deletions were fixed and imaged by confocal microscopy in the GFP and DIC channels. The percent of unbudded, small budded and large budded cells with at least one focus is plotted for each replicate and the means are shown as solid bars. At least 200 cells were scored for each replicate. (C) Mid-logarithmic phase cells with the indicated gene deletions were fixed, stained with DAPI, and imaged by brightfield and fluorescence microscopy. The percent of cells with an anaphase bridge is plotted for each replicate and the means are shown as solid bars. At least 200 cells were scored for each replicate. (D) The cells in C were scored for the fraction with a large bud and 1 nucleus. The percent of cells is plotted for each replicate and the means are shown as solid bars. (E) Cells with the indicated gene deletions were grown to saturation, serially diluted, spotted on YPD, YPD+50 mM HU, or YPD+200 mM HU agar plates and grown for 3 days at 30°C.

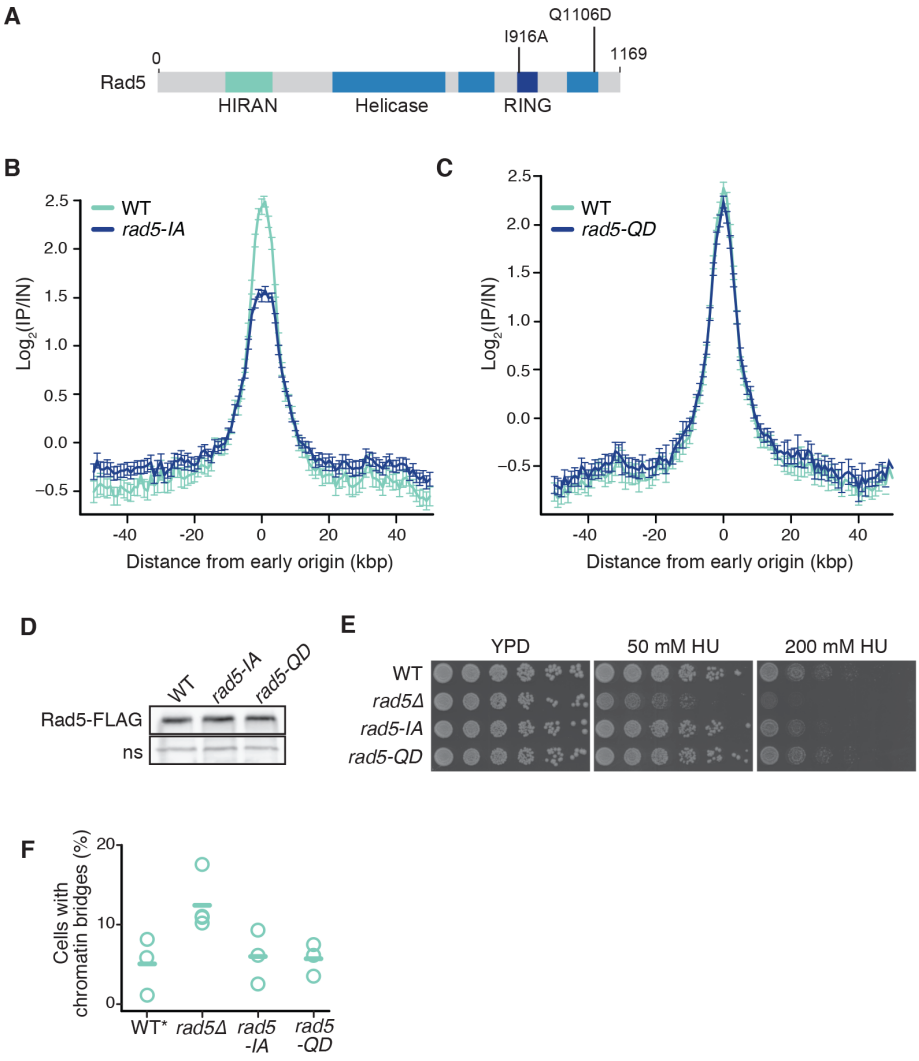

Figure 3.10 Mutations that disrupt Rad5 ubiquitin ligase, helicase or ATPase activity do not affect recruitment to stressed replication forks and do not share *rad5*Δ phenotypes. (A) Domain structure of Rad5 highlighting the HIRAN, helicase and RING finger domains, and the mutations reported to disrupt ubiquitin ligase activity (I916A) and helicase activity (Q1106D). (B) ChIP-seq analysis was performed on *RAD5-FLAG* and *rad5-IA-FLAG* or (C) *RAD5-FLAG* and *rad5-QD-FLAG* cells, 60 min after synchronous release into S phase in the presence of 200 mM HU. The median (± standard error) ChIP enrichment scores across 108 early-firing origins are plotted. (D) Mid-logarithmic phase *RAD5-FLAG, rad5-IA-FLAG* and *rad5-QD-FLAG* cells were immunoblotted with FLAG-specific antibodies. A non-specific (ns) species recognized by the FLAG antibody in the BY4741 strain background is shown as a loading control. (E) Cells with the indicated gene mutations were grown to saturation, serially diluted, spotted on YPD, YPD+50 mM HU, or YPD+200 mM HU agar plates and grown for 3 days at 30°C. (F) Mid-logarithmic phase wild type, *rad5*Δ, *rad5-IA* or *rad5-QD* cells were fixed, DAPI stained and imaged by brightfield and fluorescence microscopy. . The percent of cells with an anaphase bridge is plotted for each replicate and the means are shown as solid bars. At least 200 cells were scored for each replicate.

3.2.7 Rad5 recruits TLS polymerases to stressed replication forks to repair ssDNA

I was interested in defining the Rad5 function or domain that mediates ssDNA repair during replication stress. First, I tested ubiquitin ligase (*rad5-IA*) (Ulrich, 2003), and DNA helicase

(*rad5-QD*) (Choi et al., 2015) defective mutants (Figure 3.10A) in our battery of phenotypic assays. *rad5-IA* was slightly defective for recruitment to stressed-DNA replication forks (Figure 3.10B), while *rad5-QD* was indistinguishable from wild type (Figure 3.10C). Neither of the mutants had decreased fitness during HU-induced replication stress (Figure 3.10E) or increased anaphase bridges (Figure 3.10F). I conclude there must be either elusive enzymatic functions or a structural role for Rad5 in repair of ssDNA. In line with the latter, Rad5 physically interacts with Rev1 (Fan et al., 2018; Kuang et al., 2013; Pagès et al., 2008; Xu et al., 2016) and this interaction is important for UV-induced Rev1-dependent mutagenesis (Xu et al., 2016).

I hypothesized that Rad5 could be recruiting Rev1 to stressed replication forks to assist in filling the ssDNA gaps that I detect. Deletion of *REV1* has little effect on RPA foci on its own, or when combined with *rad5*Δ (Figure 3.11A), which could indicate that *REV1* and *RAD5* function in the same pathway to prevent ssDNA accumulation. As I noted, deletion of *RAD51* exacerbates the *rad5*Δ phenotype, and of particular interest I find that deletion of *RAD51* causes a synergistic increase in RPA foci in *rev1*Δ (Figure 3.11A), to a level similar to that seen in *rad5*Δ *rad51*Δ. When I examine cell fitness during HU exposure, I find the same result, that *RAD5* and *REV1* display a markedly greater negative genetic interaction with *RAD51* than they do with each other (Figure 3.11B). The triple mutant *rad5*Δ *rad51*Δ *rev1*Δ experiences no further decrease in fitness. I also note that *rev3*Δ phenocopies *rev1*Δ, consistent with Rev1 functioning in concert with Rev3/7 (DNA Pol ζ) (Acharya et al., 2005; Kikuchi et al., 2012). Since the genetic interactions of *rev1*Δ with *rad51*Δ mimic those of *rad5*Δ, I conclude that *RAD5* and *REV1* are in the same genetic pathway to prevent accumulation of ssDNA resulting from stressed DNA replication forks, and that this pathway is parallel to *RAD51*.

I explored the physical basis for the genetic interactions, by performing ChIP-seq for Rad5 and Rev1 in DNA replication stress. Rad5 recruitment to HU-stressed replication forks does not change when *REV1* is deleted (Figure 3.11C). By contrast Rev1, which is clearly recruited to stressed forks, depends heavily on *RAD5* for its recruitment (Figure 3.11D). These data are consistent with a model in which Rad5 recruits Rev1 to stressed forks, a striking finding given that Rad5 action is typically believed to promote template switching at the expense of TLS DNA synthesis, and that there is little precedent for TLS polymerase recruitment to DNA replication forks, or to regions of nascent DNA synthesis, in the absence of DNA base lesions.

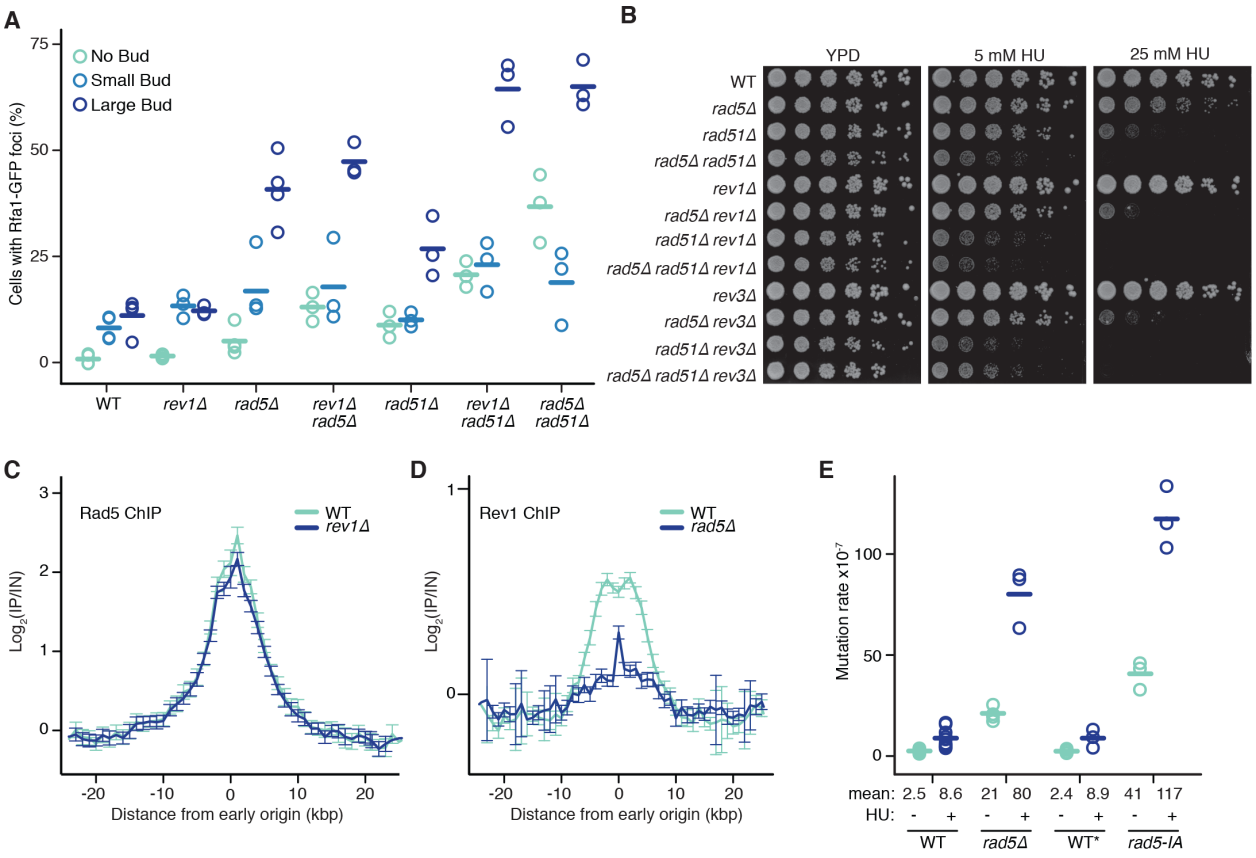

Figure 3.11 Rad5 recruits TLS polymerases at stressed replication forks to repair ssDNA. (A) Mid-logarithmic phase *RFA1-GFP* cells with the indicated gene deletions were fixed and imaged by confocal microscopy in the GFP and DIC channels. The percent of unbudded, small budded and large budded cells with at least one focus is plotted for each replicate and the means are shown as solid bars. At least 200 cells were scored for each replicate. (B) Cells with the indicated gene deletions were grown to saturation, serially diluted, spotted on YPD, YPD+5 mM HU, or YPD+25 mM HU agar plates and grown for 3 days at 30°C. (C) ChIP-seq analysis was performed on *RAD5-FLAG* or (D) *REV1-FLAG* cells carrying the indicated mutations, 60 min after synchronous release into S phase in the presence of 200 mM HU. The median (± standard error) ChIP enrichment scores across 108 early-firing origins are plotted. (E) Mutation rates are plotted for wild type (WT), *rad5*Δ, WT*(*RAD5-FLAG*) and *rad5-FLAG-IA*. The three replicates are plotted and the mean values are shown as solid bars.

Recruitment of TLS polymerases during replication stress suggests that mutagenic DNA synthesis should be taking place. The absence of *RAD5* should increase mutagenesis by the canonical TLS pathway, as ssDNA can no longer be repaired by Rad5-dependent template switching. In line with this expectation, I see a clear increase in HU-induced mutagenesis when *RAD5* is deleted (Figure 3.11E). Following the same reasoning, introduction of the *rad5-IA* allele, which cannot promote template switching (Ulrich, 2003), should result in the same HU-induced mutation rate as *rad5*Δ. However, I find an even higher mutation rate in *rad5-IA* (Figure 3.11E), indicating that Rad5 promotes mutagenic DNA synthesis, consistent with a model in which Rad5 recruits TLS polymerases to stressed forks. Indeed, the Rad5-IA mutant protein is still recruited to stressed forks (Figure 3.10B), and the *rad5-IA* mutant does not induce formation

of chromatin bridges or sensitivity to HU (Figure 3.10E and 3.10F). Finally, the mutagenesis pattern, where wild type < *rad5*Δ < *rad5-IA* is evident in the absence of HU (Figure 3.11E), consistent with Rad5 performing a similar recruitment of TLS polymerase to fill ssDNA gaps in response to physiological DNA replication stress.

3.3 Discussion

By carefully analyzing Rad5 foci during physiological and induced replication stress conditions I revealed that PRR signaling recruits Rad5 and the Rev1-Polζ TLS DNA polymerase to repair an undamaged ssDNA template. I propose a model (Figure 3.12) in which replication fork slowing during endogenous replication stress or nucleotide depletion results in exposed ssDNA. Rapid coating of the ssDNA by RPA, in concert with PCNA, recruits Rad18/Rad6 to catalyze PCNA monoubiquitination. $PCNA_{K164}Ub$ recruits the effector scaffold Rad5 which supports both template-switching- and TLS-mediated repair of the undamaged ssDNA. In the TLS branch, Rad5 recruits Rev1-Polζ to repair ssDNA with accompanying mutagenesis. In the template-switching branch, Rad5-Ubc13-Mms3 catalyzes $PCNA_{K164}$PolyUbi chains that signal repair by Rad51-mediated HR in an error free manner. I propose that Rad5 is the main effector of PCNA signaling at stressed replication forks, that there is a mutagenic TLS pathway downstream of Rad5, and that Rev1-Polζ promotes repair of exposed yet undamaged ssDNA.

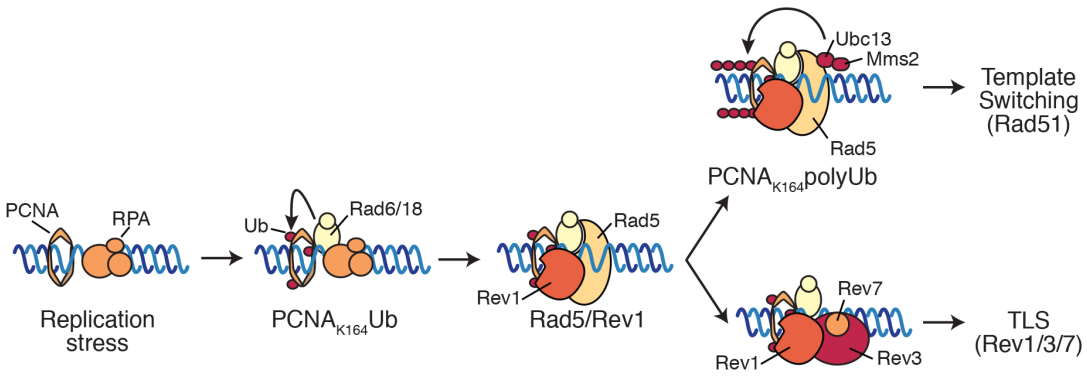

Figure 3.12 Model of Rad5 function in DNA replication stress to promote mutagenic repair of ssDNA gaps. Replication stress results in exposed ssDNA that is coated by RPA and signals for ubiquitination of $PCNA_{K164}$ by Rad6/Rad18. $PCNA_{K164}Ub$ recruits Rad5-Rev1, which either cooperates with Ubc13/Mms2 to form $PCNA_{K164}$PolyUb chains, or with Rev3/7 (DNA polymerase ζ) to catalyze mutagenic repair of ssDNA.

3.3.1 Rad5 is recruited by $PCNA_{K164}Ub$ during lesion-less DNA replication stress

The function of Rad5 in responding to DNA base lesions to promote the template-switching mode of lesion bypass has been studied extensively. Here I revealed that Rad5 responds to DNA replication stress by forming nuclear foci and by localizing to chromatin in a pattern that is identical to the chromatin association of the DNA replication machinery. Of particular interest, my data indicate that the function of Rad5 in the DNA replication stress response is not limited to exogenous stress or to dNTP pool depletion. Rad5 nuclear foci form in S-phase cells even under physiological conditions. Similar to Rad5 recruitment to replication forks in HU, Rad5 foci are dependent on $PCNA_{K164}Ub$ (Figure 1E), suggesting that Rad5 recruitment is signaled by a structure common to different forms of DNA replication stress, likely ssDNA. Other groups have reported that Rad5 forms nuclear foci (Fan et al., 2018; Ortiz-Bazán et al., 2014). A subset of Rad5 foci co-localize with telomeres (Fallet et al., 2014), raising the possibility that Rad5 also responds to stressed replication forks at telomeres. Whether Rad5 foci represent a functional form of Rad5 remains an open question, although I find that focus formation and recruitment to replication forks *in vivo* have the same genetic requirements.

An independent line of evidence supporting the hypothesis that Rad5 is recruited to stressed DNA replication forks in the absence of DNA base lesions lies in analysis of PCNA ubiquitination. PCNA ubiquitination is important during DNA replication under physiological conditions in both budding and fission yeast. In budding yeast, the genetic interaction profile of *PCNA-K164R* has very high correlation with mutants that are defective in lagging-strand DNA synthesis (Becker et al., 2015). Since similarity in genetic interaction profiles often indicates similar function, the genetic data indicate that PCNA ubiquitination promotes normal DNA replication. $PCNA_{K164}$ ubiquitination is induced by defective DNA replication in *mcm10-1* cells, a scenario where the presence of base lesions is unlikely, and *mcm10-1* cells display Pol ζ-dependent mutagenesis (Becker et al., 2014). In fission yeast, loss of PCNA ubiquitination results in slow S-phase progression, defects in late-replicating regions and increased frequency of replication gaps (Daigaku et al., 2017). Interestingly, *RAD5* genetic interaction profiles are highly correlated with *PCNA-K164R* and *RAD18* (Costanzo et al., 2016), suggesting similar function during physiological cell cycles. I find that *PCNA-K164R* shows the same accumulation

of RPA foci and anaphase bridges as *rad5*Δ (Figure 3.5A and 3.7D), reinforcing the notion that the functions of Rad5 and $PCNA_{K164}Ub$ at stressed forks are inter-related.

The Rad5 regions that are important for its recruitment to stressed DNA replication forks remain to be identified. I found that neither ubiquitin ligase nor helicase activity was required. The HIRAN domain of Rad5 is reported to be important for formation of Rad5 nuclear foci (Ding and Forsburg, 2014; Fan et al., 2018), and so is a reasonable candidate. Structural studies of the HIRAN domain of HLTF, a mammalian homolog of Rad5, revealed a binding pocket for the free 3'-OH of ssDNA (Kile et al., 2015). Interaction between the HIRAN binding pocket and the free 3'-OH is required for HLTF to bind ssDNA and to reverse HU-stressed replication forks. It is intriguing to speculate that the HIRAN domain of Rad5 binds the free 3'OH at ssDNA gaps, possibly protecting it and allowing for extension by Pol ζ or for the D-loop formation that precedes template switching. Detailed mutagenic studies of the Rad5 HIRAN domain would be an asset in this respect, as the key Rad5 residues for DNA binding remain to be identified.

3.3.2 Rad5 scaffolds both template-switching- and TLS-mediated repair of undamaged ssDNA

The canonical description of TLS-mediated DNA lesion bypass signaled by PCNA monoubiquitination places TLS upstream of Rad5, such that Rad5 signals for recombination-mediated repair in competition with TLS (Branzei and Szakal, 2016; Garcia-Rodriguez et al., 2016). In addition to the canonical pathway, I provide several lines of evidence indicating that a distinct TLS pathway exists downstream of Rad5, responding to replication stress to repair undamaged ssDNA. Genetic analyses indicate that *RAD5* and *REV1* are in the same pathway, parallel to canonical *RAD51* homologous recombination, for ssDNA repair and for replication stress resistance (Figure 3.11A and 3.11B). The *RAD5* mutant *rad5-IA*, which disrupts Rad5-Ubc13 physical interaction and inactivates the E3 ubiquitin ligase activity of Rad5 without blocking Rad5 recruitment to stressed forks, reveals an increase in mutagenesis above that seen when only TLS upstream of Rad5 is active (Figure 3.11E). Most importantly, my ChIP-seq results provide strong evidence that *RAD5* is needed for Rev1 recruitment to stressed replication forks, whereas Rad5 recruitment is independent of *REV1* (Figure 3.11C and 3.11D). Surprisingly, *rev1*Δ cells show no obvious accumulation of RPA foci (Figure 3.11A) and are not sensitive to DNA replication stress (Figure 3.11B). Considering that $PCNA_{K164}$PolyUb defective

rad5-IA cells have near wild type fitness in HU (Figure 3.10E) and wild type anaphase bridge levels (Figure 3.10F), it appears that the error-prone and error-free branch of PRR can equally compensate in each other's absence to repair replication stress-induced ssDNA.

3.3.3 TLS polymerases function on undamaged templates

One important implication of my study is that TLS polymerases can function on an undamaged DNA template *in vivo.* In doing so, TLS polymerases of course carry out mutagenic DNA synthesis, and so the potential for TLS polymerases to cause mutation is far greater than would be the case if TLS function was restricted to damaged DNA templates. My finding that Rev1 (and presumably Pol ζ) is found at DNA replication forks *in vivo* when dNTP pools are depleted (Figure 3.11D) and that a fraction of HU-induced mutagenesis can be assigned to the ability of Rad5 to recruit Rev1 (Figure 3.11E) are strong indications that TLS polymerases can replicate undamaged templates *in vivo.* My findings are consistent with contributions of Pol ζ to DNA replication in replication gene mutants (Northam et al., 2006) and to HU-induced mutagenesis (Northam et al., 2010).

Emerging evidence suggests that functional recruitment of TLS polymerases and activation of error-free PRR at undamaged DNA is also important in more complex eukaryotes. Pol η colocalizes in nuclear foci with the recombination repair factors BRCA2 and PALB2 upon dNTP pool depletion in human cells, and readily extends a primed D-loop in concert with either BRCA2 or PALB2 *in vitro* (Buisson et al., 2014). Depletion of Pol ζ subunits results in anaphase bridges in human cells (Bhat et al., 2013), similar to what I observe in *rad5*Δ, and results in chromosome breaks during replication stress (Bhat et al., 2013). Pol ζ is essential for proliferation in both mouse (Lange et al., 2012) and human cells (Hart et al., 2015; Lange et al., 2012; Wang et al., 2015) and in preventing replication-dependent DNA breaks in mouse cells (Lange et al., 2012), consistent with a role during physiological DNA replication stress. Finally, the Rad5 homologue HTLF modulates DNA replication in response to HU-induced replication stress, and so might also act on undamaged DNA templates (Kile et al., 2015).

While safeguarding wild type cells from replication stress prevents genomic instability it could also allow survival of cancer cells with chronic replication stress. Recent studies have begun to address this notion. Replication stress induced by either inhibition of the DNA replication

inhibitor geminin or over-expression of the oncogene Cyclin E results in replication fork slowing, Rad18-dependent PCNA ubiquitination and TLS-dependent re-replication (Sekimoto et al., 2015). Cyclin E over-expression or Wee1 inhibition causes an increase in RPA foci, chromatin-bound RPA, PCNA ubiquitination, and Polκ recruitment in cancer cell lines (Yang et al., 2017). These results are consistent with PCNA ubiquitination serving to recruit TLS polymerases in response to DNA replication stress. I speculate that TLS recruitment by PRR pathways could represent a therapeutic target to kill tumor cells that are experiencing DNA replication stress. Consistent with this notion, combining a Wee1 inhibitor with Rad18 depletion decreases tumor cell line fitness (Yang et al., 2017). It will be exciting to see if depletion or inhibition of HLTF and SHPRH in cancer cells experiencing replication stress yields similar results.

3.3.4 Conclusions

In this chapter I have revealed 3 important aspects of PRR and Rad5 function in budding yeast. First, the PRR pathway is activated during lesion-less and physiological replication stress to repair ssDNA gaps. Second, Rad5 is the central effector of PRR signaling at stressed replication forks and orchestrates both error-free and error prone PRR branches. Third, TLS polymerases participate in mutagenic repair of ssDNA gaps on undamaged DNA templates. My findings are surely significant to the PRR, DNA replication and cancer fields. However, my PhD work has only began to unravel the molecular interplay of error-prone and error-free PRR regulation. Futures studies should address the structural features of Rad5 that mediates its recruitment and function during the replication stress response. It will also be interesting to test the role of HTLF in suppressing ssDNA and recruiting TLS polymerases in human cells. Finally, studying the PRR pathway during oncogene- or therapeutic-induced replication stress will lead to a better understanding of cancer progression and chemoresistance mechanisms.

3.4 Future directions

My results clearly indicate that Rad5 is recruited to stressed replication forks where it recruits TLS polymerases for mutagenic repair of ssDNA. Yet, the structural requirements of Rad5 that mediate TLS recruitment remain unidentified. I have also only presented indirect evidence that TLS polymerases repair ssDNA. My future directions will address these key knowledge gaps.

Finally, I will describe my approach to test if these Rad5 functions are conserved in HLTF and how this applies to oncogene- or therapeutically-induced replication stress in cancer.

3.4.1 Reinforce the evidence that TLS polymerases repair ssDNA on undamaged templates

My findings demonstrate that Rad5 recruits Rev1 to stressed replication forks and when Rad5 ubiquitin ligase activity is compromised there is an increase in spontaneous and HU-induced mutagenesis. This is a strong indication that Rad5 recruits TLS polymerases to undamaged templates. These findings can be reinforced with additional experiments to provide direct evidence that TLS polymerases repair ssDNA on undamaged templates at stressed replication forks.

3.4.1.1 Confirm that *rev1*Δ has increased ssDNA in a template-switching defective background

An important feature of my model is that Rad5 promotes both template-switching and TLS repair of ssDNA. However, *rev1*Δ alone does not have increased RPA foci (Figure 3.11A) or increased HU sensitivity (Figure 3.11B) and *rad5-IA* cells do not have increased anaphase bridges (Figure 3.10F) or increased HU sensitivity (Figure 3.10E). This suggests that template-switching and TLS are redundant for ssDNA repair. Accordingly, *rad5-IA* cells have an increased spontaneous and HU-induced mutation rate, suggesting that Rev1 and possibly Pol ζ or Pol η are repairing ssDNA in template-switching defective cells. To test this directly I will look at RPA foci, HU sensitivity and anaphase bridge formation in *rad5-IA* and *rad5-IA rev1*Δ cells. I will also test if *ubc13*Δ and *mms2*Δ phenocopy *rad5-IA* interactions with *rev1*Δ. Likewise, to confirm that Rev1 is recruiting Pol ζ (see below) for mutagenic ssDNA repair I will test if *rad5-IA rev3*Δ cells have increased RPA foci, HU sensitivity and anaphase bridge formation. If there are increased RPA foci in any of these strains I will directly confirm the presence of ssDNA by DNA combing. Finally, I will measure the mutation rate *rad5-IA rev1*Δ and *rad5-IA rev3*Δ cells +/- HU to confirm that that TLS is responsible for the increased mutagenesis. These results will nail down the claim that TLS polymerases are repairing ssDNA gaps on undamaged templates.

3.4.1.2 Test if Pol ζ is recruited to stressed replication forks

My data provide direct evidence that Rad5 is recruiting Rev1 to HU-stressed replication forks. Based on the extremely low processivity of Rev1 and ability of Rev1 to only incorporate dCTP, it is unlikely to be the only TLS polymerase responsible for ssDNA repair (Vaisman and Woodgate, 2017). Rev1 physically interacts with the Rev7 subunit of Pol ζ and is required for Pol ζ mutagenesis (Murakumo et al., 2001). To test if Rad5 is recruiting Pol ζ via Rev1 to stressed replication forks I conducted ChIP-seq of Rev7 in *rad5*Δ cells (Figure 3.13). Unfortunately, The enrichment of Rev7-FLAG at HU -stressed replication forks was weak, although *rad5*Δ appears to reduce the signal. To optimize the Pol ζ ChIP I will try different crosslinking conditions or performing ChIP with affinity purification tags on the other Pol ζ subunits. Combined with the genetic approaches from the previous section these experiments will confirm that Rad5 recruits Pol ζ to stressed replication forks for mutagenic ssDNA repair.

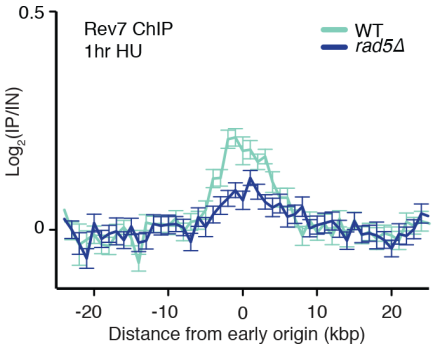

Figure 3.13 *REV7-FLAG* has a weak ChIP-seq enrichment signal. ChIP-seq analysis was performed on *REV7-FLAG* WT or *rad5*Δ cells, 60 min after synchronous release into S phase in the presence of 200 mM HU. The median (± standard error) ChIP enrichment scores across 108 early-firing origins are plotted.

3.4.1.3 Search for TLS mutations near replication origins

If my model of TLS ssDNA gap filling is correct it predicts increased mutation rates in genomic loci near stressed replication forks. Indeed, Rev1/Pol ζ dependent mutations are observed at DNA hairpins in budding yeast (Northam et al., 2014). To test this I will construct a reporter to measure mutation rates near HU-stressed replication forks. The *URA3MX6* cassette, which compliments BY4741 to form a functional uracil biosynthetic pathway, will be integrated to sequences flanking the early and efficient firing origin *ARS305*. As a control I will also construct a separate strain with *URA3MX6* integrated near a late-firing origin where DNA replication is inhibited by the DNA replication checkpoint during HU-induced replication stress. Cultures of each reporter strain will be synchronously released into HU-challenged S-phase for 2hr, washed, resuspended into fresh YPD, harvested after completion of S-phase and plated on media

containing 5-Fluoroorotic Acid (5-FOA). Cells with a functional uracil biosynthetic pathway convert 5-FOA to a toxic intermediate and die. Therefore, cells with *URA3MX6* mutations will form colonies on 5-FOA plates. I expect to see an increase in 5-FOA resistant colonies if the reporter is placed near an early-firing origin compared to a late-firing origin. If no mutations are observed I will use a MMR defective strain background to inhibit repair of TLS-induced mutations. Once 5-FOA resistant colonies are isolated I will, PCR amplify the *URA3MX6* cassette from individual clones and conduct Sanger sequencing to identify TLS mutational signatures. The assay can be repeated in *rev1*Δ*, rev3*Δ*, rad5*Δ or any functional mutants identified in the previous aims to directly assess the contribution of any component of my model. These results will confirm that TLS polymerases replicate DNA from undamaged templates at stressed replication forks.

3.4.2 Identify features of Rad5 required for ssDNA repair

I have presented evidence that Rad5 acts as a scaffold at stressed replication forks to mediate repair of ssDNA. Recruitment of Rad5 depends on $PCNA_{K164}Ub$ and in turn recruitment of Rev1 depends on Rad5. However, I have not identified the structural features of Rad5 that mediate these transactions. My future efforts will focus on identifying these structural features of Rad5.

3.4.2.1 Identify features required for recruitment to stressed replication forks

The N-terminal HIRAN domain of Rad5 in budding yeast (Fan et al., 2018) and fission yeast (Ding and Forsburg, 2014) is required for Rad5 recruitment to nuclear foci making it a likely candidate for mediating recruitment to stressed replication forks. However, in these studies the HIRAN domain was completely removed from Rad5 and therefore lack any functional information about how the HIRAN domain mediates recruitment. The crystal structure of the HLTF HIRAN domain in complex with ssDNA revealed two well conserved tyrosine residues that form base stacking interactions with the DNA helix and are required for HLTF recruitment and activity. To test their requirement for Rad5 recruitment, Ashrut Narula made analogous tyrosine mutations in *RAD5* (*rad5-YYAA*) and I tested this mutant for recruitment to HU-stressed replication forks and HU sensitivity. While *rad5-YYAA* recruitment to HU stressed replication forks was slightly decreased (Figure 3.14A), cells were resistant to HU (Figure 3.14B) indicating

that other residues in the HIRAN or elsewhere in Rad5 are responsible for recruitment to stressed replication forks.

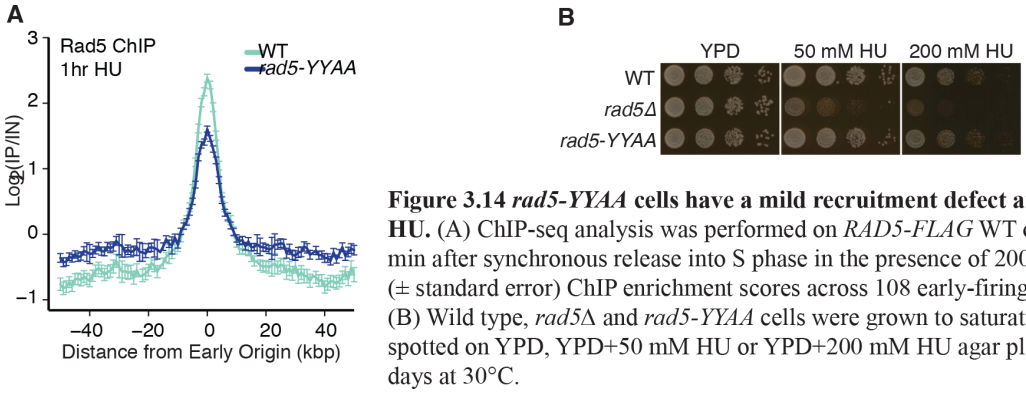

Figure 3.14 *rad5-YYAA* cells have a mild recruitment defect and are not sensitive to HU. (A) ChIP-seq analysis was performed on *RAD5-FLAG* WT or *rad5-YYAA* cells 60 min after synchronous release into S phase in the presence of 200 mM HU. The median (± standard error) ChIP enrichment scores across 108 early-firing origins are plotted. (B) Wild type, *rad5*Δ and *rad5-YYAA* cells were grown to saturation, serially diluted, spotted on YPD, YPD+50 mM HU or YPD+200 mM HU agar plates and grown for 3 days at 30°C.

To discover Rad5 point mutants that are important for recruitment to stressed replication forks and for replication stress resistance I will conduct a deep mutational scan of *RAD5* and screen for increased HU sensitivity using a technique called DMS-BarSeq. Deep mutational scanning combines screening for protein function using a library of point mutants with high-throughput sequencing to create rich functional maps (Fowler et al., 2014). First, I will create a high coverage single amino acid mutation library of Rad5 using POPCode (Weile et al., 2017) and clone it *en masse* into a pool of randomly-barcoded plasmids. The barcoded plasmids will be sequenced to link barcodes with individual mutants and pooled to create the library. Next, I will transform the pooled library into *rad5*Δ cells such that there is one plasmid/cell. The cultures will be grown up, sampled at time 0 and divided into YPD or YPD+HU for outgrowth. The cultures will be sampled at regular intervals and subjected to DMS-BarSeq to identify the mutants present in the population. HU-sensitive *RAD5* mutants will not complement *rad5*Δ and will drop out of the YPD+HU culture. One caveat with this approach I foresee is the limited dynamic range of the *rad5*Δ fitness defect. To circumvent this I can screen the DMS-BarSeq libraries in a HU-sensitized background by mutating *POL32* (Figure 3.15). *RAD5* mutants recovered from the screen will likely be recruitment defective considering *PCNA-K164R*, which cannot recruit Rad5 to stressed replication forks, shares the same HU-induced phenotypes as *rad5*Δ cells (Figures 3.5A, 3.7D) and *rad5-IA* (ligase dead) or *rad5-QD* (helicase dead) are not sensitive to HU (Figure 3.10E). Following identification of HU sensitive *RAD5* mutants I will test them against my battery of Rad5 functional assays, most notably ChIP-seq to directly assess recruitment.

Results from DMS-BarSeq will allow me to identify the key features of Rad5 that mediate recruitment to stressed replication forks.

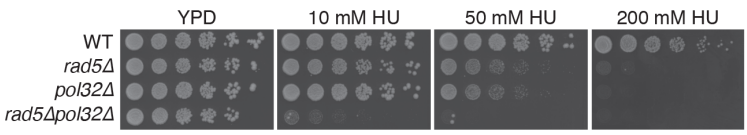

Figure 3.15 *rad5*Δ and *pol32*Δ cells have additive growth defects in HU. Wild type, *rad5*Δ, *pol32*Δ and *rad5*Δ*pol32*Δ cells were grown to saturation, serially diluted, spotted on YPD, YPD+10 mM HU, YPD+50 mM HU or YPD+200 mM HU agar plates and grown for 3 days at 30°C.

3.4.2.2 Identify features required for recruitment of TLS polymerases

The crystal structure of Rad5(5-20) and Rev1(876-985) was recently solved and indicated that Rad5 F13 and N14 are required for Rad5-Rev1 physical interactions in the context of these protein fragments (Xu et al., 2016). To test if these Rad5 residues are important for Rev1 recruitment to stressed replication forks I conducted ChIP-seq of Rev1 in a *rad5-FNAA* mutant background. *rad5-FNAA* was present at stressed replication forks (Figure 3.16A) and Rev1 recruitment was largely unaffected by *rad5-FNAA* at 60 min (Figure 3.16B) and only slightly decreased after 120 min (Figure 3.16C) indicating that these two residues have at best a minor role in retention of Rev1 at stressed replication forks. Consistent with Rev1 being recruited to stressed forks, *rad5-FNAA* does not increase RPA foci (Figure 3.16D) or HU sensitivity (Figure 3.16E) of *rad51*Δ cells. Thus, there must be as yet undiscovered resides or functions of Rad5 mediating Rev1 recruitment to stressed replication forks.

To identify features of Rad5 that mediate Rev1 recruitment to stressed replication forks I will use the *RAD5* DMS-BarSeq libraries with a similar screening approach to above. Considering *rev1*Δ increase the HU sensitivity of *rad51*Δ (Figure 3.16E), which I hypothesize is due to failed ssDNA repair, I believe a subset of Rad5 mutants that fail to compliment the HU resistance of *rad5*Δ*rad51*Δ will be Rev1 recruitment defective. Of course some of the Rad5 mutants could be Rad5 recruitment defective, but these will be identified in the previous analysis and can be removed from downstream analysis. The remaining Rad5 mutants will be assayed for Rev1 recruitment at stressed replication forks and genetic interactions in *rad51*Δ cells. I anticipate the DMS-BarSeq approach will create a rich functional map of the Rad5-Rev1 interaction interface and guide further structure-function studies of Rad5 and Rev1.

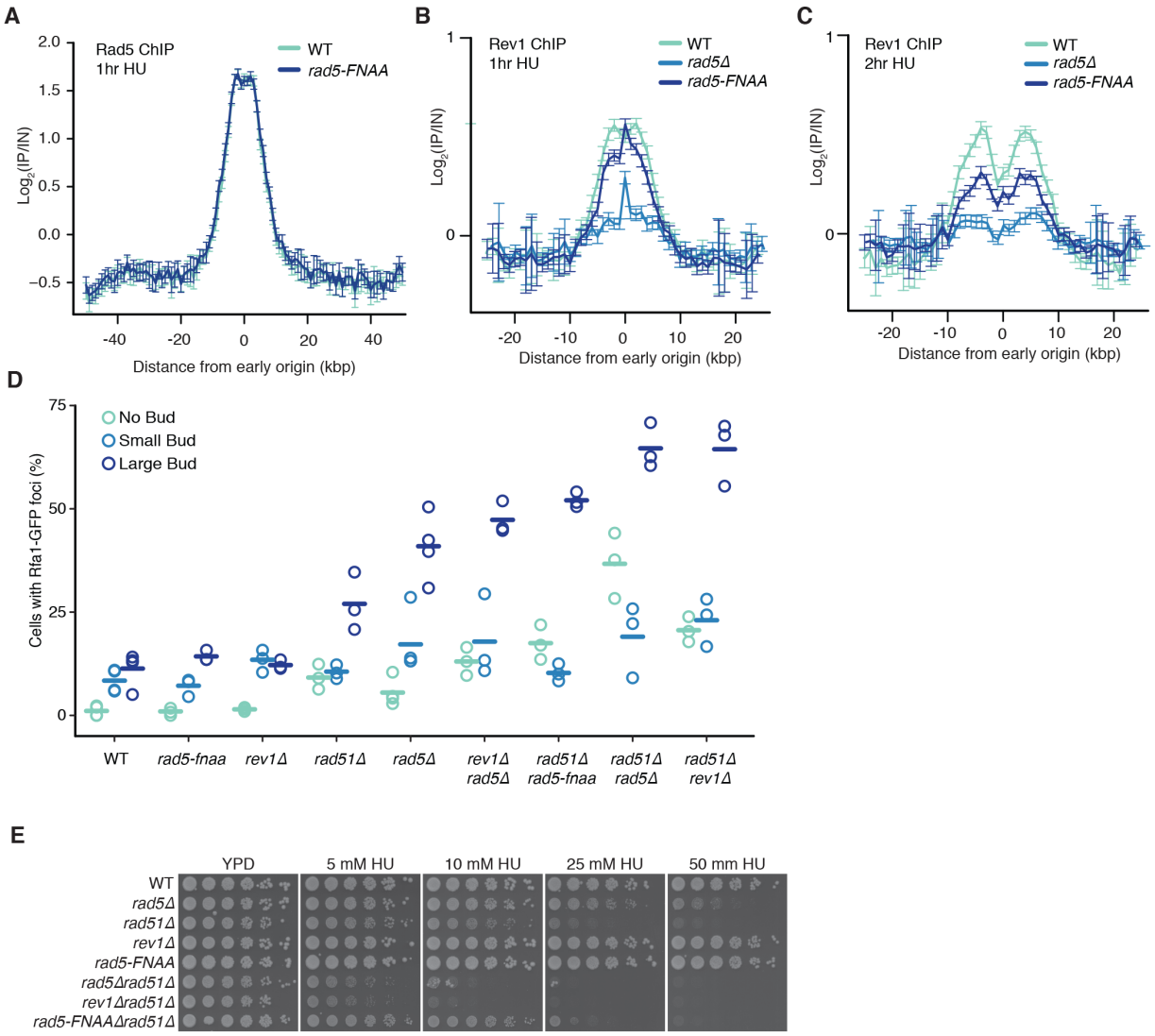

Figure 3.16 *rad5-FNAA* has a mild Rev1 recruitment defect and does not mimic *rev1*Δ for replication-stress induced phenotypes. ChIP-seq analysis was performed on (A) *RAD5-FLAG* WT or *rad5-FNAA* and (B-C) *REV1-FLAG* WT, *rad5*Δ or *rad5-FNAA* cells at the indicated times after synchronous release into S phase in the presence of 200 mM HU. The median (± standard error) ChIP enrichment scores across 108 early-firing origins are plotted. (D) Mid-logarithmic phase *RFA1-GFP* cells with the indicated gene deletions were fixed and imaged by confocal microscopy in the GFP and DIC channels. The percent of unbudded, small budded and large budded cells with at least one focus is plotted for each replicate and the means are shown as solid bars. At least 200 cells were scored for each replicate. (E) Cells with the indicated gene deletions were grown to saturation, serially diluted, spotted on YPD, YPD+5 mM HU, or YPD+25 mM HU agar plates and grown for 3 days at 30°C.

3.4.3 Characterize if Rad5 function is conserved in HLTF

I have implicated Rad5 as being a central effector of PRR signaling and an important suppressor of replication stress-induced ssDNA in budding yeast. Since PRR is evolutionarily conserved, I will test if HLTF can suppress ssDNA caused by physiological and exogenous replication stress and if HLTF can recruit TLS polymerases or any other proteins to stressed replication forks. Additionally, upregulation of PRR is linked to oncogene-induced cancer progression and TLS

polymerases increase mutagenesis and chemoresistance in tumors. Therefore, I will also test what role HLTF plays in oncogene-induced replication stress and chemoresistance.

3.4.3.1 Determine if HLTF suppresses ssDNA accumulation

To test if HLTF is responsible for ssDNA accumulation in mammalian I will look for increased RPA foci and ssDNA by DNA combing. First, I will construct CRISPR *HLTF* KOs in U2OS cell lines (Kile et al., 2015). Wild type and *HLTF* KO cells will be left unperturbed or treated with low doses of HU to induce mild replication stress. Cells will be fixed and subjected to immunofluorescences using α-RPA antibodies. The number of RPA foci and intensity of signal will be scored using automated image analysis software. I expect to see an increase in RPA in *HLTF* KO cells in both untreated and HU conditions, similar to *rad5*Δ cells. I can also conduct these experiments after HU recovery to test if RPA foci persist in *HLTF* KO cells. Next, I will directly test for ssDNA in *HLTF* cells using the ssDNA combing assay. Again, wild type and *HLTF* KO cells will be with left unperturbed or treated with low doses of HU before harvesting and DNA combing. Additionally, a pulse of EdU can be added to the media before harvesting allowing me to directly localize ssDNA to active DNA replication tracks. Again, I expect *HLTF* KO cells will have increased amounts and lengths of ssDNA tracks that co-localize with active DNA replication. These results will confirm that HLTF suppresses ssDNA accumulation from physiological and exogenous replication stress.

If *HLTF* KO cells have increased exposed ssDNA they should also have the hyper-activated checkpoint and mitotic defects I observe in *rad5*Δ cells. In mammalian cells activation of the DNA replication checkpoint leads to phosphorylation of ATR, CHK1, CHK2 and γ-H2AX (Mec1, Chk1, Rad53 and H2A in budding yeast). To test for a hyper-activated checkpoint I will make extracts from wild type and *HLTF* KO cells +/- HU and conduct SDS-PAGE western blotting using α-pATM, α-pATR, α-pCHK1, α-pCHK2 and α-γH2AX antibodies to detect checkpoint kinase activation. Increased signal form the phosopho-blots will confirm that increased ssDNA leads to checkpoint activation in *HLTF* KO cells. I will also test if increased ssDNA leads to mitotic defects by looking at mitotic bridges in *HLTF* KO cells. Mitotic bridges can be sub-grouped into chromatin bridges that are dsDNA and ultrafine bridges that are ssDNA. If HLTF is suppressing ssDNA then I expect *HLTF* KO cells will have increased ssDNA ultrafine bridges following HU treatment. If there is a drastic increase in ultrafine bridges I will

extend this analysis to unperturbed cells to assess the contribution of HLTF to suppressing ssDNA from physiological replication stress. Taken together, these experiments will demonstrate if HLTF suppresses ssDNA accumulation in mammalian cells, and if so, it will be exciting for the replication stress community.

3.4.3.2 Determine if HLTF recruits TLS polymerases or other proteins to stressed replication forks

HLTF is present at unperturbed replication forks in U2OS cells (Kile et al., 2015). I will confirm that HLTF is at unperturbed and stressed replication forks using the recently described assay, quantitative in situ analysis of interactions at DNA replication forks (SIRF) (Roy et al., 2018). Cells will be pulse-labeled with the thymidine analog EdU to mark nascent DNA, followed by DNA-protein crosslinking. The EdU moiety will be covalently linked to biotin followed by incubation with α-biotin and α-HLTF primary antibodies and specialized secondary antibodies that enable rolling circle amplification of plasmid with binding sites for a fluorescent probe, technology borrowed from the proximity ligation assay (PLA). SIRF will be conducted before and after treatment with HU to confirm that HLTF is at unperturbed replication forks and test whether it is present at stressed replication forks. Next, I will test if HLTF is physically interacting with TLS polymerases at stressed replication forks. To do this I will test for HLTF physical interactions before and after HU treatment using proximity-dependent biotin identification (BioID) (Roux et al., 2012). HLTF will be fused to the mutant biotin ligase BirA* and grown +/- HU and in the presence of biotin to facilitate biotinylation of proteins in close proximity. The cells will be lysed and biotin will be pulled down using streptavidin. Pulled down proteins will be subjected to mass spectrometry for identification, and proximal proteins before and after HU treatment will be compared. In addition to identifying HLTF-TLS interactions, BioID will also identify the suite of proteins that interact with HLTF during unperturbed conditions and in HU-induced replication stress. If TLS polymerases or other interesting proteins are identified by BioID, I will test if they are at replication forks using SIRF, and I will test if their fork association decreases in *HLTF* KO cells to determine whether their fork association depends on HTLF. By using these methods to identify HLTF physical interactions, I will uncover whether HLTF recruits TLS polymerases in mammalian cells and possibly identify new players at stressed replication forks.

3.4.3.3 Characterize the role of HLTF in oncogene-induced replication stress and chemoresistance

Recent findings implicate Rad18 in mediating survival of cancer cells during oncogene-induced replication stress and TLS polymerases in causing increased mutation rates leading to chemoresistance in tumors (Sekimoto et al., 2015; Xie et al., 2010; Yang et al., 2017). If my findings in yeast are conserved I hypothesize that HLTF is contributing to both oncogene-induced replication stress survival and increased mutagenesis in cancer development. To test this I will induce replication stress by over expression of the oncogene Cyclin E or treatment with a Wee1 inhibitor in wild type and *HLTF* KO cells. This will be conducted in normal fibroblast cells in an attempt to limit the confounding effects of transformed or tumor derived cell lines. To test if HLTF increases chemoresistance, wild type and *HLTF* KO cells will be treated with cisplatin and analyzed for increased sensitivity and decreased ability to form resistant clones. I am excited to see if HLTF is also the central effector of PRR signaling in mammalian cells and promotes oncogene-induced replication stress survival and chemoresistance in tumors.

3.5 Materials and Methods

3.5.1 Yeast strains and media

All yeast strains used in this study (Table 3.1) are derivatives of BY4741 (Brachmann et al., 1998) or W303. Standard yeast media and growth conditions were used for all experiments unless otherwise noted. Strains were constructed using genetic crosses and standard PCR-based gene disruption and epitope- tagging techniques.

3.5.2 Focus formation assay

Cells expressing Rad5-GFP (Figures 3.1A, 3.1B, 3.1D) in the indicated genetic backgrounds were grown in YPD at 30 °C to mid-logarithmic phase (OD_{600} = 0.3-0.6). Cells were either left unperturbed or treated with 200 mM HU for 60 min, washed in low-fluorescence media (1.7g/l LF powder (CAT), 5g/l ammonium sulphate, 1x amino acids, 2% w/v glucose) and resuspended in 25µl LFM per 1 OD600 unit of cells, with or without 200 mM HU. Alternatively, for Rfa1-GFP expressing cells (Figures 3.5A, 3.5E, 3.7E, 3.8B, 3.9B, 3.11A, 3.16D), cultures at OD_{600} = 0.3 – 0.9 were harvested and fixed in 4% paraformaldehyde, 3.4% sucrose solution at room temperature for 15 min. The reaction was quenched by addition of glycine (200 mM final) at

room temperature for 10 min. The cells were washed twice in PPSB (0.1M KPO_4, 1.2M sorbitol) and resuspended in 5-10 µL of Vectashield mounting medium containing DAPI. For either live or fixed cells, 2 µl was mounted on glass slide with a coverslip and imaged using a Leica DMI6000 confocal using Volocity imaging software (PerkinElmer). Eleven z-stacks with a 0.4 µM step size were collected using fluorescein isothiocyanate, Texas Red, and cell differential interference contrast filter sets (Quorum Technologies) for Rad5, Nup49 and cell morphology analysis respectively. Images were processed using cell profiler (version 2.2.0) (Kamentsky et al., 2011) by projecting the maximum pixel intensity in the x-y plane from the 11 z-stacks to a single image. Budding index and cells containing one or more Rad5-GFP focus were scored by visual inspection.

3.5.3 Generation time measurement

Saturated cultures were diluted to OD_{600} = 0.05 in 100 µL of YPD in flat bottom 96-well plates. Plates were incubated at 30 °C under agitation in TECAN microplate analyzer and the OD_{600} was measured every 10 min for 24 – 48 hrs. The maximum slope (m_{max}) during logarithmic phase growth was calculated using the growth rate algorithm in R designed by Danielle Carpenter (https://scholar.princeton.edu/sites/default/files/botsteinlab/files/growth-rate-using-r.pdf). The maximum growth rate was then calculated using using $\ln(2)/m_{max}$.

3.5.4 HU fitness spot assay

Saturated cultures were diluted to OD_{600} = 0.5 in a flat bottom 96-well plate and 5-fold serial dilutions were prepared using a multi-channel pipette. The dilutions were plated using a multi-pronged bolt pinning tool onto YPD or YPD + HU. Images were taken after 3 days of growth at 30°C

3.5.5 Cell synchronization and HU treatment/recovery

Logarithmically growing cells at 23 °C (ChIP-seq) or 30 °C, and OD_{600} = 0.2-0.3 were arrested in G1 by addition of alpha factor to 1.2 µM, and further incubation for 2.5 hrs. To release cells into S phase, Pronase was added to 100 µg/ml immediately followed by addition of HU to 200 mM, and further incubation for 60-180 min. For HU recovery experiments cells were harvested, washed once in ddH_2O, and resuspended in fresh YPD.

3.5.6 Chromatin immunoprecipitation

Chromatin immunoprecipitation (ChIP) was performed using FLAG epitope tagged versions of each indicated protein, as described (Balint et al., 2015).

3.5.7 Deep sequencing of ChIP samples

Sequencing libraries were generated using the Nextera XT DNA Sample Preparation Kit (Illumina) with custom index primers for the PCR amplification step. Libraries were quantified using a 2100 Bioanalyzer (Agilent) and the KAPA SYBR FAST Universal qPCR Kit (KAPA Biosystems) or the NEBNext Library Quant Kit for Illumina, and sequenced using the NextSeq500 with High Output Kit (Illumina) by multiplexing 18-28 samples per lane, the HiSeq2500 (Illumina) by multiplexing 12–18 samples per lane, or the MiSeq (Illumina) by multiplexing 8 samples, to generate at least 7.5 million reads per sample. Sequencing statistics are summarized in Table 3.1.

3.5.8 ChIP sequencing data analysis

All sequencing data are deposited in the Sequence Read Archive (https://www.ncbi.nlm.nih.gov/sra; Study accession SRP139947). The quality of the raw reads was assessed using FastQC (https://www.bioinformatics.babraham.ac.uk/projects/fastqc/). After the quality control step, we used bowtie2 (Langmead and Salzberg, 2012) to map each read to the reference genome (WS220) downloaded from the *Saccharomyces* Genome Database (Cherry et al., 2012; Engel et al., 2014). The ratio of the total number of reads between the IP sample and the input sample was used to normalize the data, to reduce bias from different sequencing depths of different samples. A second normalization was applied, using the ratio of the number of reads in unreplicated regions between the IP and the input samples. Unreplicated regions were defined by removing regions where the cumulative log2 of IP to input (after the first normalization) from the centre of each ARS is maximized.

To visualize protein binding across all early- and late-firing regions, we extracted enrichment values for 1-kb bins across 50 kb upstream and downstream of each replication origin coordinate (centered at the replication origins), as described (Balint et al., 2015). Each point represents the median of enrichment scores within the bin, and each error bar represents standard error.

3.5.9 DNA copy number analysis

DNA copy number in wild type and *rad5*Δ cells was analyzed during synchronous progression through S phase in the presence of HU, as described (Saayman et al., 2018).

3.5.10 Molecular combing of DNA

WT (HWY534) and *rad5*Δ (DGY223) were used for all ssDNA measurements (Figures 3.3B, 3.3C, 3.3E, 3.3F) and for BrdU track length measurements in 200mM HU and during recovery (Figure S2D). WT (E1670) and *rad5*Δ (DGY31) were used for BrdU track length measurements in 50 mM HU (Figure 3.4C). Synchronization and HU recovery was performed as described above. Plug preparation, digestion, melting and combing were performed as described (Gallo et al., 2016). For detection of ssDNA, coverslips were dehydrated by sequential incubation in 70%, 90% and 99% EtOH and allowed to air dry for 15 min. The NaOH denaturation step was omitted to retain YOYO-1 staining and preserve dsDNA. The coverslip was incubated with 21 µL of blocking solution (PBST (phosphate-buffered saline, pH 7.4, 0.05% Tween-20), 5% w/v BSA (Sigma A4503)) in a humid chamber at 37 °C for 30 min. The coverslip was briefly washed in PBS-T, incubated with 21 µL of α-ssDNA antibody solution (α-ssDNA antibody (Millipore MAB3034) diluted 1:50 in blocking solution), in a humid chamber at 37 °C for 60 min. The coverslip was washed 3 x 5 min in PBST and incubated with 21 µL of α-mouse secondary solution (goat-α-mouse Alexa Fluor 546 (ThermoFisher A11030) diluted 1:50 in blocking solution) in a humid chamber at 37 °C for 60 min. The coverslip was washed 3 x 5 min in PBST and mounted with 15 µL of ProLong Gold Antifade. DNA fibers were imaged using an Axio Imager microscope with a 63× objective, a fluorescein isothiocyanate filter for dsDNA and a CY3 filter for ssDNA. Individual coverslips were blinded before image acquisition to avoid bias in the analysis. Images were processed to maximize signal intensity, and fluorescent tracks were measured in ImageJ v1.50i (https://imagej.nih.gov/ij/). Track lengths were converted from pixels to kilobase pairs using a conversion factor based on combing λ-DNA. To determine replication fork rates, cells were labeled with BrdU and combing was performed as described (Gallo et al., 2016), detecting BrdU with α-BrdU antibody (BD Biosciences 347580) and ssDNA with α-ssDNA antibody (Millipore MAB3034), as described (Gallo et al., 2016).

3.5.11 Flow cytometry

Samples for flow cytometry were collected at the indicated times, fixed in 70% ethanol, washed in ddH_2O, resuspended in 0.5 mL of 50 mM Tris (pH 8.0) containing 2 mg/ml RNaseA, and incubated for 2 hrs at 37°C. Cells were harvested, resuspended in 0.5 ml of 50 mM Tris (pH 7.5) containing 1 mg/ml proteinase K, and incubated for 40 min at 50 °C. Cells were harvested and resuspended in FACS buffer (200 mM Tris (pH 7.5), 200 mM NaCl, and 78 mM $MgCl_2$.). 0.1 mL of cell suspension was added to 0.5 ml of 50 mM Tris (pH 7.5) containing 2x SYBR green, sonicated briefly, and analyzed on a Becton Dickinson FACSCalibur or FACSCanto II, with 10,000 events collected. Histograms were generated using FlowJo software versions 9.7.5 and 10.0.8.

3.5.12 Budding index and nuclear DNA microscopy

Cultures at OD_{600} = 0.3 – 0.9 were harvested and fixed in 70% EtOH. Cells were washed in ddH_2O and resuspended in 5-10 µL of Vectashield mounting medium containing DAPI. 2 µl was mounted on glass slide with a coverslip and imaged using an Axio Imager microscope with a 63× objective, DAPI filters for DNA and cell differential interference contrast filter sets for cell morphology. Budding index and nuclear morphology were scored by visual inspection.

3.5.13 Whole cell extracts and immunoblotting

Cells were diluted to OD_{600} = 0.5 in 10% trichloroacetic acid and whole cell extracts were prepared as described (Pellicioli et al., 1999). Proteins were resolved on a SDS-PAGE gel and detected by immunoblotting with anti-FLAG M2 (Sigma; diluted 1:10,000) and anti-PGK (Novex 459250) antibodies.

3.5.14 GCR assay

GCR assays were carried out as described (Srivatsan et al., 2018). For HU-induced GCR rates, single colonies from YPD plates were transferred to YPD or YPD + 25 mM HU for liquid growth.

3.5.15 Two-dimensional gel electrophoresis

Purification of DNA intermediates for 2D gel analysis was performed as described (Fumasoni et al., 2015). 200 ml cultures (2 to 4 x 10^9 cells) were arrested by addition of 0.1% sodium azide

(final concentration) and cooled on ice before proceeding with psoralen crosslinking. Cells were washed, resuspended in 5ml of cold water in small petri dishes and kept on ice. 300 µl of 4,5',8-tri-methyl-psoralen solution (0.2 mg/ml in EtOH 100%) was added prior to extensive resuspension by pipetting, followed by 5 min of incubation in the dark and then 10 min of UV irradiation at 365 nm. The procedure was repeated 3 times to ensure extensive crosslinking. Cells were harvested by centrifugation, washed in cold water, and incubated in spheroplasting buffer (1M sorbitol, 100 mM EDTA (pH 8.0), 0.1% β-mercaptoethanol, and 50U/ml zymolyase) for 1.5 h at 30ºC. Spheroplasts were harvested, and 2 ml water, 200 µl RNase A (10 µg/ml), and 2.5 ml Solution I (2% w/v cetyl-trimethyl-ammonium-bromide (CTAB), 1.4M NaCl, 100 mM Tris–HCl (pH 7.6), and 25 mM EDTA (pH 8.0)) were sequentially added to the spheroplast pellets, followed by incubation for 30 min at 50ºC. 200 µl Proteinase K (20 mg/ml) was added and the incubation was continued at 50°C for 90 min, and then shifted to 30°C overnight. The sample was then centrifuged at 4000 rpm. for 10 min. The cellular debris pellet was kept for further extraction, while the supernatant was extracted with 2.5 ml chloroform/isoamylalcohol (24:1) and the DNA in the upper phase was precipitated by addition of 2 volumes Solution II (1% w/v CTAB, 50 mM Tris–HCl (pH 7.6), and 10 mM EDTA) and centrifugation at 8500 rpm for 10 min. The pellet was resuspended in 2 ml Solution III (1.4 M NaCl, 10 mM Tris–HCl (pH 7.6), and 1 mM EDTA). Residual DNA in the cellular debris pellet was extracted by resuspension in 2 ml Solution III and incubation at 50ºC for 30 min, followed by extraction in 1 ml chloroform/isoamylalcohol (24:1). The upper phase was pooled together with the main DNA prep. DNA was then precipitated with 1 volume of isopropanol, washed with 70% ethanol, air-dried, and resuspended in TE. Signals were detected following 2D gel electrophoresis and standard southern blot procedures, using a probe against *ARS305* (Chr III 39002-40063).

3.5.16 Mutation rate assay

Mutation rates at the *CAN1* locus were determined using fluctuation tests and the Poisson distribution (Lang and Murray, 2008). Single colonies of indicated strains were grown to saturation in SD + all amino acids or SD + all amino acids + 25 mM HU, and then diluted to 1 x 10^4 cells/ml. 30 µl ($N_{(0)}$ = 300 cells) were added to each of 48 wells of a 96 well round-bottom plate to create 48 individual cultures and allowed to grow for 16-20 hrs. The average number of cells in each culture N(t) was determined by pooling 4 cultures and counting in a hemocytometer. The remaining 44 cultures were individually spotted onto extra dry SD-arginine

+ canavanine (60 mg/L) and grown at 30°C for 3 days. The proportion of cultures with 0 colonies P_0 was recorded and carried forward if $0 < P_0 < 1$. Mutation rate μ was calculated according to the Poisson distribution using the formula:

$$\mu = -\ln(P_0) / (N(t) - N_0)$$

Table 3.1 Strains used in this chapter

Strain	Genotype	Source
BY4741	*MAT* **a** *leu2Δ0 his3Δ1 ura3Δ0 met15Δ0*	Brachmann *et al.* (1998)
ANY37	*MAT* **a** *RAD5-YY195,235AA-6His10FLAG::kanMX6 leu2Δ0 his3Δ1 ura3Δ0 met15Δ0*	This study
ANY38	*MAT* **a** *RAD5-Q1106D-6His10FLAG::kanMX6 leu2Δ0 his3Δ1 ura3Δ0 met15Δ0*	This study
ANY40	*MAT* **a** *RAD5-I916A-6His10FLAG::kanMX6 leu2Δ0 his3Δ1 ura3Δ0 met15Δ0*	This study
DGY19	*MAT* **a** *RAD5-6His10FLAG::kanMX6 leu2Δ0 his3Δ1 ura3Δ0 met15Δ0*	This study
DGY31	*MAT* **a** *rad5Δ::KanMX6 ade2-1 trp1-1 can1-100 his3-11,15 leu2-3,112 RAD5+ GAL psi+ ura3::URA3/GPD-TK(7x)*	This study
DGY78	*MAT* **a** *RAD5-GFP::HIS3MX6 leu2Δ0 his3Δ1 ura3Δ0 met15Δ0*	Huh *et al.* (2003)
DGY83	*MAT* **a** *POL30-K164R::natMX6 leu2Δ0 his3Δ1 ura3Δ0 met15Δ0*	This study
DGY94	*MAT* **a** *DPB3-6His10FLAG::kanMX6 POL30-K164R::natMX6 leu2Δ0 his3Δ1 ura3Δ0 met15Δ0*	This study
DGY95	*MAT* **a** *RAD5-6His10FLAG::kanMX6 POL30-K164R::natMX6 leu2Δ0 his3Δ1 ura3Δ0 met15Δ0*	This study
DGY98	*MAT* **a** *DPB3-6His10FLAG::kanMX6 rad18Δ::natMX6 leu2Δ0 his3Δ1 ura3Δ0 met15Δ0*	This study
DGY99	*MAT* **a** *RAD5-6His10FLAG::kanMX6 rad18Δ::natMX6 leu2Δ0 his3Δ1 ura3Δ0 met15Δ0*	This study
DGY102	*MAT* **a** *RAD5-GFP::HIS3MX6 POL30-K164R::natMX6 leu2Δ0 his3Δ1 ura3Δ0 met15Δ0*	This study
DGY149	*MAT* **a** *RAD5-6His10FLAG::kanMX6 ubc13Δ::natMX6 leu2Δ0 his3Δ1 ura3Δ0 met15Δ0*	This study
DGY150	*MAT* **a** *RAD5-6His10FLAG::kanMX6 mms2Δ::natMX6 leu2Δ0 his3Δ1 ura3Δ0 met15Δ0*	This study
DGY157	*MAT* **a** *DPB3-6His10FLAG::kanMX6 ubc13Δ::natMX6 leu2Δ0 his3Δ1 ura3Δ0 met15Δ0*	This study
DGY158	*MAT* **a** *DPB3-6His10FLAG::kanMX6 mms2Δ::natMX6leu2Δ0 his3Δ1 ura3Δ0 met15Δ0*	This study
DGY165	*MAT* **a** *rev1Δ::kanMX6 leu2Δ0 his3Δ1 ura3Δ0 met15Δ0*	This study
DGY167	*MAT* **a** *rev3Δ::HIS3MX6 leu2Δ0 his3Δ1 ura3Δ0 met15Δ0*	This study
DGY178	*MAT* **a** *rev3Δ::HIS3MX6 rad5Δ::kanMX6 leu2Δ0 his3Δ1 ura3Δ0 met15Δ0*	This study
DGY183	*MAT* **a** *REV7-6His10FLAG::kanMX6 leu2Δ0 his3Δ1 ura3Δ0 met15Δ0*	This study
DGY190	*MAT* **a** *REV7-6His10FLAG::kanMX6 rad5Δ::natMX6 leu2Δ0 his3Δ1 ura3Δ0 met15Δ0*	This study
DGY199	*MAT* **a** *REV1-6His10FLAG::kanMX6 leu2Δ0 his3Δ1 ura3Δ0 met15Δ0*	This study
DGY200	*MAT* **a** *RAD5-6His10FLAG::kanMX6 rev1Δ::natMX6 leu2Δ0 his3Δ1 ura3Δ0 met15Δ0*	This study
DGY216	*MAT* **a** *REV1-6His10FLAG::kanMX6 rad5Δ::natMX6 leu2Δ0 his3Δ1 ura3Δ0 met15Δ0*	This study
DGY223	*MAT* **a** *his3Δ1::HIS3-ADH1pr-hENT-GPDpr-HSV-TK rad5Δ::kanMX leu2Δ0 ura3Δ0 met15Δ0*	This study
DGY230	*MAT* **a** *srs2Δ::kanMX6 leu2Δ0 his3Δ1 ura3Δ0 met15Δ0*	This study
DGY231	*MAT* **a** *rad51Δ::kanMX6 leu2Δ0 his3Δ1 ura3Δ0 met15Δ0*	This study
DGY236	*MAT* **a** *rad5Δ::kanMX6 leu2Δ0 his3Δ1 ura3Δ0 met15Δ0*	This study
DGY252	*MAT* **a** *rad9Δ::natMX6 leu2Δ0 his3Δ1 ura3Δ0 met15Δ0*	This study
DGY253	*MAT* **a** *rad5Δ::kanMX6 rad9Δ::natMX6 leu2Δ0 his3Δ1 ura3Δ0 met15Δ0*	This study
DGY254	*MAT* **a** *DPB3-6His10FLAG::kanMX6 siz1Δ::natMX6 leu2Δ0 his3Δ1 ura3Δ0 met15Δ0*	This study
DGY255	*MAT* **a** *RAD5-6His10FLAG::kanMX6 siz1Δ::natMX6 leu2Δ0 his3Δ1 ura3Δ0 met15Δ0*	This study
DGY256	*MAT* **a** *RAD5-GFP::HIS3MX6 siz1Δ::natMX6 leu2Δ0 his3Δ1 ura3Δ0 met15Δ0*	This study
DGY264	*MAT* **a** *srs2Δ::URA3MX6 rad5Δ::kanMX6 leu2Δ0 his3Δ1 ura3Δ0 met15Δ0*	This study
DGY265	*MAT* **a** *rad51Δ::URA3MX6 rad5Δ::kanMX6 leu2Δ0 his3Δ1 ura3Δ0 met15Δ0*	This study
DGY268	*MAT* **a** *RAD9-6His10FLAG::natMX6 leu2Δ0 his3Δ1 ura3Δ0 met15Δ0*	This study
DGY269	*MAT* **a** *RAD9-6His10FLAG::natMX6 rad5Δ::kanMX6 leu2Δ0 his3Δ1 ura3Δ0 met15Δ0*	This study
DGY274	*MAT* **a** *RFA1-GFP::HIS3MX6 leu2Δ0 his3Δ1 ura3Δ0 met15Δ0*	Huh *et al.* (2003)
DGY275	*MAT* **a** *RFA1-GFP::HIS3MX6 rad5Δ::kanMX6 leu2Δ0 his3Δ1 ura3Δ0 met15Δ0*	This study
DGY276	*MAT* **a** *RFA1-GFP::HIS3MX6 rad9Δ::natMX6 leu2Δ0 his3Δ1 ura3Δ0 met15Δ0*	This study
DGY277	*MAT* **a** *RFA1-GFP::HIS3MX6 rad5Δ::kanMX6 rad9Δ::natMX6 leu2Δ0 his3Δ1 ura3Δ0 met15Δ0*	This study
DGY278	*MAT* **a** *RFA1-GFP::HIS3MX6 srs2Δ::URA3MX6 leu2Δ0 his3Δ1 ura3Δ0 met15Δ0*	This study
DGY279	*MAT* **a** *RFA1-GFP::HIS3MX6 srs2Δ::URA3MX6 rad5Δ::kanMX6 leu2Δ0 his3Δ1 ura3Δ0 met15Δ0*	This study
DGY280	*MAT* **a** *RFA1-GFP::HIS3MX6 rad51Δ::URA3MX6 leu2Δ0 his3Δ1 ura3Δ0 met15Δ0*	This study
DGY281	*MAT* **a** *RFA1-GFP::HIS3MX6 rad51Δ::URA3MX6 rad5Δ::kanMX6 leu2Δ0 his3Δ1 ura3Δ0 met15Δ0*	This study
DGY284	*MAT* **a** *RFA1-6His10FLAG::kanMX6 leu2Δ0 his3Δ1 ura3Δ0 met15Δ0*	This study
DGY285	*MAT* **a** *RFA1-6His10FLAG::kanMX6 rad5Δ::natMX6 leu2Δ0 his3Δ1 ura3Δ0 met15Δ0*	This study
DGY288	*MAT* **a** *pol32Δ::kanMX6 leu2Δ0 his3Δ1 ura3Δ0 met15Δ0*	This study
DGY289	*MAT* **a** *pol32Δ::kanMX6 rad5Δ::natMX6 leu2Δ0 his3Δ1 ura3Δ0 met15Δ0*	This study
DGY290	*MAT* **a** *RAD5-GFP::HIS3MX6 pol32Δ::kanMX6 leu2Δ0 his3Δ1 ura3Δ0 met15Δ0*	This study
DGY324	*MAT* **a** *hxt13Δ::URA3MX6 leu2Δ0 his3Δ1 ura3Δ0 met15Δ0*	This study
DGY325	*MAT* **a** *hxt13Δ::URA3MX6 rad5Δ::kanMX6 leu2Δ0 his3Δ1 ura3Δ0 met15Δ0*	This study
DGY332	*MAT* **a** *rev3Δ::HIS3MX6 rad51Δ::URA3MX6 leu2Δ0 his3Δ1 ura3Δ0 met15Δ0*	This study
DGY333	*MAT* **a** *rev3Δ::HIS3MX6 rad5Δ::kanMX6 rad51Δ::URA3MX6 leu2Δ0 his3Δ1 ura3Δ0 met15Δ0*	This study
DGY338	*MAT* **a** *rev1Δ::natMX6 rad5Δ::kanMX6 leu2Δ0 his3Δ1 ura3Δ0 met15Δ0*	This study
DGY339	*MAT* **a** *rev1Δ::natMX6 rad51Δ::URA3MX6 leu2Δ0 his3Δ1 ura3Δ0 met15Δ0*	This study
DGY340	*MAT* **a** *rev1Δ::natMX6 rad5Δ::kanMX6 rad51Δ::URA3MX6 leu2Δ0 his3Δ1 ura3Δ0 met15Δ0*	This study
DGY341	*MAT* **a** *RFA1-GFP::HIS3MX6 rev1Δ::natMX6 leu2Δ0 his3Δ1 ura3Δ0 met15Δ0*	This study
DGY342	*MAT* **a** *RFA1-GFP::HIS3MX6 rev1Δ::natMX6 rad5Δ::kanMX6 leu2Δ0 his3Δ1 ura3Δ0 met15Δ0*	This study
DGY343	*MAT* **a** *RFA1-GFP::HIS3MX6 rev1Δ::natMX6 rad51Δ::URA3MX6 leu2Δ0 his3Δ1 ura3Δ0 met15Δ0*	This study
DGY349	*MAT* **a** *REV1-6His10FLAG::kanMX6 RAD5-FN13,14AA::kanMX leu2Δ0 his3Δ1 ura3Δ0 met15Δ0*	This study
DGY350	*MAT* **a** *RAD5-FN13,14AA::kanMX leu2Δ0 his3Δ1 ura3Δ0 met15Δ0*	This study
DGY352	*MAT* **a** *RAD5-FN13,14AA::kanMX rad51Δ::URA3MX6 leu2Δ0 his3Δ1 ura3Δ0 met15Δ0*	This study
DGY354	*MAT* **a** *RAD5-FN13,14AA-6His10FLAG::kanMX6 leu2Δ0 his3Δ1 ura3Δ0 met15Δ0*	This study
DGY356	*MAT* **a** *RFA1-GFP::HIS3MX6 RAD5-FN13,14AA::kanMX leu2Δ0 his3Δ1 ura3Δ0 met15Δ0*	This study
DGY358	*MAT* **a** *RFA1-GFP::HIS3MX6 RAD5-FN13,14AA::kanMX rad51Δ::URA3MX6 leu2Δ0 his3Δ1 ura3Δ0 met15Δ0*	This study
DGY360	*MAT* **a** *RFA1-GFP::HIS3MX6 POL30-K164R::natMX6 leu2Δ0 his3Δ1 ura3Δ0 met15Δ0*	This study
DGY366	*MAT* **a** *RAD5-GFP::HIS3MX6 NUP49-mCherry::CaURA3 can1Δ::STE2pr-LEU2 leu2Δ0 his3Δ1 ura3Δ0 met15Δ0 lyp1Δ*	This study
DGY367	*MAT* **a** *RAD5-GFP::HIS3MX6 his3Δ::kanMX6 can1Δ::STE2prLEU2::RPL39pr-TdTomato::CaURA3 leu2Δ0 his3Δ1 ura3Δ0 met15Δ0 lyp1Δ*	This study
DGY368	*MAT* **a** *RAD5-GFP::HIS3MX6 rad6Δ::kanMX6 can1Δ::STE2prLEU2::RPL39pr-TdTomato::CaURA3 leu2Δ0 his3Δ1 ura3Δ0 met15Δ0 lyp1Δ*	This study
DGY369	*MAT* **a** *RAD5-GFP::HIS3MX6 rad18Δ::kanMX6 can1Δ::STE2prLEU2::RPL39pr-TdTomato::CaURA3 leu2Δ0 his3Δ1 ura3Δ0 met15Δ0 lyp1Δ*	This study
DGY370	*MAT* **a** *RAD5-GFP::HIS3MX6 ubc13::kanMX6 can1Δ::STE2prLEU2::RPL39pr-TdTomato::CaURA3 leu2Δ0 his3Δ1 ura3Δ0 met15Δ0 lyp1Δ*	This study
DGY371	*MAT* **a** *RAD5-GFP::HIS3MX6 mms2Δ::kanMX6 can1Δ::STE2prLEU2::RPL39pr-TdTomato::CaURA3 leu2Δ0 his3Δ1 ura3Δ0 met15Δ0 lyp1Δ*	This study
DGY372	*MAT* **a** *RNR3-GFP::HIS3MX6 can1Δ::STE2prLEU2::RPL39pr-TdTomato::CaURA3 leu2Δ0 his3Δ1 ura3Δ0 met15Δ0 lyp1Δ*	This study
DGY373	*MAT* **a** *RNR3-GFP::HIS3MX6 rad5Δ::kanMX6 can1Δ::STE2prLEU2::RPL39pr-TdTomato::CaURA3 leu2Δ0 his3Δ1 ura3Δ0 met15Δ0 lyp1Δ*	This study
E1670	*MAT* **a** *ade2-1 trp1-1 can1-100 his3-11,15 leu2-3,112 RAD5+ GAL psi+ ura3::URA3/GPD-TK(7x)*	Lengronne *et al. (* 2001)
HWY534	*MAT* **a** *his3Δ1::HIS3-ADH1pr-hENT-GPDpr-HSV-TK leu2Δ0 ura3Δ0 met15Δ0*	H. Wurtele
JOY128	*MAT* **a** *DPB3-6His10FLAG::kanMX6 leu2Δ0 his3Δ1 ura3Δ0 met15Δ0*	Ballint *et al.* (2015)

Table 3.2 Sequencing library statistics

Genotype	Strain	Sample Type	Sample Name	Sequencing Type	# of reads	Sequencing Coverage	Alignment Rate	ChIP Average Plot	CNV Histogram	CNV Average Plot	SRA Accession Number
WT (G1-arrested)	BY4741	Input	AB1	Single-end (50 bp)	16269022	63.17	96.11%	---	---	---	SRR1986232
DPB3-FLAG (60min HU)	JOY128	Input	DG29	Single-end (50 bp)	13481060	33.42	97.42%	Figure 3.2A	---	Figure 3.2C	SRR7000968
DPB3-FLAG (60min HU)	JOY128	ChIP	DG30	Single-end (50 bp)	11276516	28.04	97.45%	Figure 3.2A	---	---	SRR7000969
DPB3-FLAG (120min HU)	JOY128	Input	DG31	Single-end (50 bp)	11317418	28.21	98.20%	Figure 3.2A	---	Figure 3.2C	SRR7000970
DPB3-FLAG (120min HU)	JOY128	ChIP	DG32	Single-end (50 bp)	10845948	26.86	97.23%	Figure 3.2A	---	---	SRR7000971
DPB3-FLAG (180min HU)	JOY128	Input	DG33	Single-end (50 bp)	17620348	43.23	95.69%	Figure 3.2A	---	Figure 3.2C	SRR7000964
DPB3-FLAG (180min HU)	JOY128	ChIP	DG34	Single-end (50 bp)	14604435	36.07	96.89%	Figure 3.2A	---	---	SRR7000965
RAD5-FLAG (60min HU)	DGY19	Input	DG11	Single-end (100 bp)	17832278	90.88	51.41%	Figure 3.2B	---	Figure 3.2D	SRR7000906
RAD5-FLAG (60min HU)	DGY19	ChIP	DG12	Single-end (100 bp)	17017130	98.32	58.71%	Figure 3.2B	---	---	SRR7000967
RAD5-FLAG (120min HU)	DGY19	Input	DG13	Single-end (100 bp)	18551749	112.55	61.12%	Figure 3.2B	---	Figure 3.2D	SRR7000961
RAD5-FLAG (120min HU)	DGY19	ChIP	DG14	Single-end (100 bp)	15154999	88.53	58.85%	Figure 3.2B	---	---	SRR7000963
RAD5-FLAG (180min HU)	DGY19	Input	DG15	Single-end (100 bp)	13876730	96.03	69.00%	Figure 3.2B	---	Figure 3.2D	SRR7000927
RAD5-FLAG (180min HU)	DGY19	ChIP	DG16	Single-end (100 bp)	15491805	94.32	61.35%	Figure 3.2B	---	---	SRR7000928
RAD5-FLAG (60min HU)	DGY19	Input	DG73	Single-end (50 bp)	23385435	92.87	96.42%	Figure 3.2E	---	---	SRR7000929
RAD5-FLAG (60min HU)	DGY19	ChIP	DG74	Single-end (50 bp)	23721350	94.69	97.42%	Figure 3.2E	---	---	SRR7000930
RAD5-FLAG rad18Δ (60min HU)	DGY99	Input	DG75	Single-end (50 bp)	25912446	102.40	96.16%	Figure 3.2E	---	---	SRR7000931
RAD5-FLAG rad18Δ (60min HU)	DGY99	ChIP	DG76	Single-end (50 bp)	19170364	78.17	97.90%	Figure 3.2E	---	---	SRR7000932
RAD5-FLAG pol30-K164R (60min HU)	DGY95	Input	DG77	Single-end (50 bp)	18607918	72.99	95.71%	Figure 3.2E	---	---	SRR7000933
RAD5-FLAG pol30-K164R (60min HU)	DGY95	ChIP	DG78	Single-end (50 bp)	16044710	65.06	97.60%	Figure 3.2E	---	---	SRR7000934
RAD5-FLAG (60min HU)	DGY19	Input	DG181	Single-end (75 bp)	24336937	108.90	88.73%	Figure 3.2F	---	---	SRR7000919
RAD5-FLAG (60min HU)	DGY19	ChIP	DG182	Single-end (75 bp)	16064458	72.18	89.32%	Figure 3.2F	---	---	SRR7000920
RAD5-FLAG siz1Δ (60min HU)	DGY255	Input	DG183	Single-end (75 bp)	29171504	121.45	88.91%	Figure 3.2F	---	---	SRR7000953
RAD5-FLAG siz1Δ (60min HU)	DGY255	ChIP	DG184	Single-end (75 bp)	16684226	69.09	88.98%	Figure 3.2F	---	---	SRR7000952
RAD5-FLAG (60min HU)	DGY19	Input	DG109	Single-end (75 bp)	17916549	83.16	80.16%	Figure 3.2G	---	---	SRR7000955
RAD5-FLAG (60min HU)	DGY19	ChIP	DG110	Single-end (75 bp)	7997045	47.68	97.07%	Figure 3.2G	---	---	SRR7000954
RAD5-FLAG ubc13Δ (60min HU)	DGY149	Input	DG111	Single-end (75 bp)	18282726	102.58	93.12%	Figure 3.2G	---	---	SRR7000949
RAD5-FLAG ubc13Δ (60min HU)	DGY149	ChIP	DG112	Single-end (75 bp)	13903837	74.05	89.95%	Figure 3.2G	---	---	SRR7000948
RAD5-FLAG mms2Δ (60min HU)	DGY150	Input	DG113	Single-end (75 bp)	12399294	71.36	94.92%	Figure 3.2G	---	---	SRR7000951
RAD5-FLAG mms2Δ (60min HU)	DGY150	ChIP	DG114	Single-end (75 bp)	10029585	57.74	94.98%	Figure 3.2G	---	---	SRR7000950
DPB3-FLAG (60min HU)	JOY128	Input	DG67	Single-end (50 bp)	27773853	110.68	96.51%	Figure 3.3A	---	---	SRR7000960
DPB3-FLAG (60min HU)	JOY128	ChIP	DG68	Single-end (50 bp)	17482380	71.81	98.31%	Figure 3.3A	---	---	SRR7000959
DPB3-FLAG rad18Δ (60min HU)	DGY98	Input	DG69	Single-end (50 bp)	23597646	93.00	96.11%	Figure 3.3A	---	---	SRR7000925
DPB3-FLAG rad18Δ (60min HU)	DGY98	ChIP	DG70	Single-end (50 bp)	16281189	64.73	95.07%	Figure 3.3A	---	---	SRR7000926
DPB3-FLAG pol30-K164R (60min HU)	DGY94	Input	DG71	Single-end (50 bp)	30701647	107.25	89.20%	Figure 3.3A	---	---	SRR7000923
DPB3-FLAG pol30-K164R (60min HU)	DGY94	ChIP	DG72	Single-end (50 bp)	19147802	78.05	97.92%	Figure 3.3A	---	---	SRR7000924
DPB3-FLAG (60min HU)	JOY128	Input	DG177	Single-end (75 bp)	21510862	96.80	89.44%	Figure 3.3B	---	---	SRR7000921
DPB3-FLAG (60min HU)	JOY128	ChIP	DG178	Single-end (75 bp)	26216984	110.58	86.09%	Figure 3.3B	---	---	SRR7000922
DPB3-FLAG siz1Δ (60min HU)	DGY254	Input	DG179	Single-end (75 bp)	20474806	92.92	90.24%	Figure 3.3B	---	---	SRR7000962
DPB3-FLAG siz1Δ (60min HU)	DGY254	ChIP	DG180	Single-end (75 bp)	16080369	72.21	89.80%	Figure 3.3B	---	---	SRR7000966
DPB3-FLAG (60min HU)	JOY128	Input	DG103	Single-end (75 bp)	18538214	90.97	84.29%	Figure 3.3C	---	---	SRR7000936
DPB3-FLAG (60min HU)	JOY128	ChIP	DG104	Single-end (75 bp)	11893880	64.66	90.97%	Figure 3.3C	---	---	SRR7000937
DPB3-FLAG ubc13Δ (60min HU)	DGY157	Input	DG105	Single-end (75 bp)	11391314	66.36	95.67%	Figure 3.3C	---	---	SRR7000974
DPB3-FLAG ubc13Δ (60min HU)	DGY157	ChIP	DG106	Single-end (75 bp)	11319585	66.01	96.16%	Figure 3.3C	---	---	SRR7000972
DPB3-FLAG mms2Δ (60min HU)	DGY158	Input	DG107	Single-end (75 bp)	19989493	105.17	88.85%	Figure 3.3C	---	---	SRR7000913
DPB3-FLAG mms2Δ (60min HU)	DGY158	ChIP	DG108	Single-end (75 bp)	7539546	45.29	97.65%	Figure 3.3C	---	---	SRR7000973
DPB3-FLAG (120min HU)	JOY128	Input	DG197	Single-end (75 bp)	45085087	199.00	88.87%	---	---	Figure 3.4B	SRR7000917
DPB3-FLAG rad5Δ (120min HU)	JOY128	Input	DG201	Single-end (75 bp)	35299085	159.00	90.28%	---	---	Figure 3.4B	SRR7000911
RFA1-FLAG (G1-arrested)	DGY284	Input	DG229	Single-end (75 bp)	16131330	74.55	91.98%	---	Figure 3.4F	---	SRR7000907
RFA1-FLAG (120min HU)	DGY284	Input	DG231	Single-end (75 bp)	15427453	71.14	91.85%	---	Figure 3.4F	---	SRR7000975
RFA1-FLAG (30min HU rec.)	DGY284	Input	DG233	Single-end (75 bp)	28210106	129.92	92.41%	---	Figure 3.4F	---	SRR7000958
RFA1-FLAG (60min HU rec.)	DGY284	Input	DG235	Single-end (75 bp)	18090576	83.78	92.25%	---	Figure 3.4F	---	SRR7000957
RFA1-FLAG (90min HU rec.)	DGY284	Input	DG237	Single-end (75 bp)	21347238	98.98	92.96%	---	Figure 3.4F	---	SRR7000915
RFA1-FLAG rad5Δ (G1-arrested)	DGY285	Input	DG241	Single-end (75 bp)	19770536	90.03	92.58%	---	Figure 3.4F	---	SRR7000916
RFA1-FLAG rad5Δ (120min HU)	DGY285	Input	DG243	Single-end (75 bp)	20685138	95.86	92.46%	---	Figure 3.4F	---	SRR7000956
RFA1-FLAG rad5Δ (30min HU rec.)	DGY285	Input	DG245	Single-end (75 bp)	21979004	101.46	92.84%	---	Figure 3.4F	---	SRR7000918
RFA1-FLAG rad5Δ (60min HU rec.)	DGY285	Input	DG247	Single-end (75 bp)	17877597	82.34	92.35%	---	Figure 3.4F	---	SRR7000935
RFA1-FLAG rad5Δ (90min HU rec.)	DGY285	Input	DG249	Single-end (75 bp)	18226082	84.14	92.21%	---	Figure 3.4F	---	SRR7000912
RAD5-FLAG (60min HU)	DGY19	Input	DG91	Single-end (50 bp)	26064258	105.76	97.42%	Figures 3.10B, 3.10C, 3.14	---	---	SRR7000938
RAD5-FLAG (60min HU)	DGY19	ChIP	DG92	Single-end (50 bp)	12147307	49.80	98.16%	Figures 3.10B, 3.10C, 3.14	---	---	SRR7000914
RAD5-IA-FLAG (60min HU)	ANY40	Input	DG97	Single-end (50 bp)	21897532	89.56	98.11%	Figure 3.10B	---	---	SRR7000909
RAD5-IA-FLAG (60min HU)	ANY40	ChIP	DG98	Single-end (50 bp)	15716892	64.03	97.85%	Figure 3.10B	---	---	SRR7000910
RAD5-QD-FLAG (60min HU)	ANY38	Input	DG95	Single-end (50 bp)	31840595	126.72	95.99%	Figure 3.10C	---	---	SRR7000941
RAD5-QD-FLAG (60min HU)	ANY38	ChIP	DG96	Single-end (50 bp)	15754883	64.64	98.11%	Figure 3.10C	---	---	SRR7000940
RAD5-FLAG (60min HU)	DGY19	Input	DG131	Single-end (75 bp)	32836623	156.81	97.45%	Figure 3.11C	---	---	SRR7000943
RAD5-FLAG (60min HU)	DGY19	ChIP	DG132	Single-end (75 bp)	78303370	364.51	98.67%	Figure 3.11C	---	---	SRR7000942
RAD5-FLAG rev1Δ (60min HU)	DGY200	Input	DG133	Single-end (75 bp)	20332093	98.66	98.68%	Figure 3.11C	---	---	SRR7000945
RAD5-FLAG rev1Δ (60min HU)	DGY200	ChIP	DG134	Single-end (75 bp)	16135727	77.71	98.72%	Figure 3.11C	---	---	SRR7000944
REV1-FLAG (60min HU)	DGY199	Input	DG253	Single-end (75 bp)	20270027	83.06	94.74%	Figure 3.11D	---	---	SRR7000947
REV1-FLAG (60min HU)	DGY199	ChIP	DG254	Single-end (75 bp)	20932016	82.00	92.21%	Figure 3.11D	---	---	SRR7000946
REV1-FLAG rad5Δ (60min HU)	DGY216	Input	DG257	Single-end (75 bp)	26317154	109.10	95.10%	Figure 3.11D	---	---	SRR7000939
REV1-FLAG rad5Δ (60min HU)	DGY216	ChIP	DG258	Single-end (75 bp)	18086076	54.19	68.15%	Figure 3.11D	---	---	SRR7000908
REV7-FLAG (60min HU)	DGY183	Input	DG143	Single-end (75 bp)	19704811	95.76	98.67%	Figure 3.13	---	---	---
REV7-FLAG (60min HU)	DGY183	ChIP	DG144	Single-end (75 bp)	19276731	90.57	95.45%	Figure 3.13	---	---	---
REV7-FLAG rad5Δ (60min HU)	DGY190	Input	DG145	Single-end (75 bp)	18073023	87.90	98.75%	Figure 3.13	---	---	---
REV7-FLAG rad5Δ (60min HU)	DGY190	ChIP	DG146	Single-end (75 bp)	18435236	85.69	94.43%	Figure 3.13	---	---	---
RAD5-YYAA-FLAG (60min HU)	ANY37	Input	DG93	Single-end (75 bp)	20863741	84.46	97.16%	Figure 3.14A	---	---	---
RAD5-YYAA-FLAG (60min HU)	ANY37	ChIP	DG94	Single-end (75 bp)	15753507	63.69	97.37%	Figure 3.14A	---	---	---
RAD5-FLAG (60min HU)	DGY19	Input	DG273	Single-end (75 bp)	21677190	89.44	95.25%	Figure 3.16A	---	---	---
RAD5-FLAG (60min HU)	DGY19	ChIP	DG274	Single-end (75 bp)	17875268	73.36	94.74%	Figure 3.16A	---	---	---
RAD5-FNAA-FLAG (60min HU)	DGY354	Input	DG275	Single-end (75 bp)	27202053	90.01	78.39%	Figure 3.16A	---	---	---
RAD5-FNAA-FLAG (60min HU)	DGY354	ChIP	DG276	Single-end (75 bp)	23340924	93.15	94.68%	Figure 3.16A	---	---	---
REV1-FLAG rad5-FNAA (60min HU)	DGY349	Input	DG269	Single-end (75 bp)	21139479	84.04	91.75%	Figure 3.16B	---	---	---
REV1-FLAG rad5-FNAA (60min HU)	DGY349	ChIP	DG270	Single-end (75 bp)	16705108	67.27	91.90%	Figure 3.16B	---	---	---
REV1-FLAG (120min HU)	DGY199	Input	DG255	Single-end (75 bp)	22681775	92.37	95.10%	Figure 3.16C	---	---	---
REV1-FLAG (120min HU)	DGY199	ChIP	DG256	Single-end (75 bp)	24058786	93.21	88.92%	Figure 3.16C	---	---	---
REV1-FLAG rad5Δ (120min HU)	DGY216	Input	DG259	Single-end (75 bp)	19617698	80.31	95.30%	Figure 3.16C	---	---	---
REV1-FLAG rad5Δ (120min HU)	DGY216	ChIP	DG260	Single-end (75 bp)	15751284	59.83	86.21%	Figure 3.16C	---	---	---
REV1-FLAG rad5-FNAA (120min HU)	DGY349	Input	DG271	Single-end (75 bp)	15564054	61.80	90.95%	Figure 3.16C	---	---	---
REV1-FLAG rad5-FNAA (120min HU)	DGY349	ChIP	DG272	Single-end (75 bp)	17695986	69.72	90.00%	Figure 3.16C	---	---	---

References

Achar, Y.J., Balogh, D., and Haracska, L. (2011). Coordinated protein and DNA remodeling by human HLTF on stalled replication fork. Proc. Natl. Acad. Sci. *2011*.

Acharya, N., Haracska, L., Johnson, R.E., Unk, I., Prakash, S., and Prakash, L. (2005). Complex Formation of Yeast Rev1 and Rev7 Proteins: a Novel Role for the Polymerase-Associated Domain. Mol. Cell. Biol. *25*, 9734–9740.

Aggarwal, P., Lessie, M.D., Lin, D.I., Pontano, L., Gladden, B., Nuskey, B., Goradia, A., Wasik, M.A., Klein-, A.J.P., Rustgi, A.K., et al. (2009). Nuclear accumulation of cyclin D1 during S phase inhibits Cul4- dependent Cdt1 proteolysis and triggers p53-dependent DNA rereplication. Genes Dev. *21*, 1–14.

Aguilera, A., and García-Muse, T. (2013). Causes of Genome Instability. Annu. Rev. Genet. *47*, 1–32.

Ait Saada, A., Teixeira-Silva, A., Iraqui, I., Costes, A., Hardy, J., Paoletti, G., Fréon, K., and Lambert, S.A.E. (2017). Unprotected Replication Forks Are Converted into Mitotic Sister Chromatid Bridges. Mol. Cell *66*, 398–410.e4.

Álamo, M.M. del, Sánchez-Gorostiaga, A., Serrano, A.M., Prieto, A., Cuéllar, J., Martín-Benito, J., Valpuesta, J.M., and Giraldo, R. (2010). Structural analysis of the interactions between Hsp70 chaperones and the yeast DNA replication protein Orc4p. J. Mol. Biol. *403*, 24–39.

Alfanos, C., and Mcmacken, R. (1989). Heat Shock Protein-mediated Disassembly of Nucleoprotein Structures Is Required for the Initiation of Bacteriophage X DNA Replication. J. Biol. Chem. *264*, 10709–10718.

Allen, J.B., Zhou, Z., Siede, W., Friedberg, E.C., and Elledge, S.J. (1994). The SAD1 / RAD53 protein kinase controls multiple checkpoints and DNA damage- induced transcription in yeast. Genes Dev. 2416–2428.

Alzu, A., Bermejo, R., Begnis, M., Lucca, C., Piccini, D., Carotenuto, W., Saponaro, M., Brambati, A., Cocito, A., Foiani, M., et al. (2012). Senataxin associates with replication forks to

protect fork integrity across RNA-polymerase-II-transcribed genes. Cell *151*, 835–846.

Amaral, N., Vendrell, A., Funaya, C., Idrissi, F.Z., Maier, M., Kumar, A., Neurohr, G., Colomina, N., Torres-Rosell, J., Geli, M.I., et al. (2016). The Aurora-B-dependent NoCut checkpoint prevents damage of anaphase bridges after DNA replication stress. Nat. Cell Biol. *18*, 516–526.

Askwith, C., Eide, D., Van Ho, A., Bernard, P.S., Li, L., Davis-Kaplan, S., Sipe, D.M., and Kaplan, J. (1994). The FET3 gene of S. cerevisiae encodes a multicopper oxidase required for ferrous iron uptake. Cell *76*, 403–410.

Azvolinsky, A., Giresi, P.G., Lieb, J.D., and Zakian, V.A. (2009). Highly Transcribed RNA Polymerase II Genes Are Impediments to Replication Fork Progression in Saccharomyces cerevisiae. Mol. Cell *34*, 722–734.

Bailly, V., Lauder, S., Prakash, S., and Prakash, L. (1997). Yeast DNA repair proteins Rad6 and Rad18 form a heterodimer that has ubiquitin conjugating, DNA binding, and ATP hydrolytic activities. J. Biol. Chem. *272*, 23360–23365.

Balint, A., Kim, T., Gallo, D., Cussiol, J.R., Bastos De Oliveira, F.M., Yimit, A., Ou, J., Nakato, R., Gurevich, A., Shirahige, K., et al. (2015). Assembly of Slx4 signaling complexes behind DNA replication forks. EMBO J. *34*, 2182–2197.

Ball, L.G., Zhang, K., Cobb, J.A., Boone, C., and Xiao, W. (2009). The yeast Shu complex couples error-free post-replication repair to homologous recombination. Mol. Microbiol. *73*, 89–102.

Ball, L.G., Xu, X., Blackwell, S., Hanna, M.D., Lambrecht, A.D., and Xiao, W. (2014). The Rad5 helicase activity is dispensable for error-free DNA post-replication repair. DNA Repair (Amst). *16*, 74–83.

Barkley, L.R., Palle, K., Durando, M., Day, T.A., Gurkar, A., Kakusho, N., Li, J., Masai, H., and Vaziri, C. (2012). c-Jun N-terminal kinase – mediated Rad18 phosphorylation facilitates Pol η recruitment to stalled replication forks. Mol. Biol. Cell *23*, 1943–1954.

Bartkova, J., Hořejší, Z., Koed, K., Krämer, A., Tort, F., Zleger, K., Guldberg, P., Sehested, M.,

Nesland, J.M., Lukas, C., et al. (2005). DNA damage response as a candidate anti-cancer barrier in early human tumorigenesis. Nature *434*, 864–870.

Bashkirov, V.I., Bashkirova, E. V, Haghnazari, E., and Heyer, W. (2003). Direct kinase-to-kinase signaling mediated by the FHA phosphoprotein recognition domain of the Dun1 DNA damage checkpoint kinase. Mol. Cell. Biol. *23*, 1441–1452.

BastosdeOliveira, F.M., Kim, D., Cussiol, J.R., Das, J., Jeong, M.C., Doerfler, L., Schmidt, K.H., Yu, H., and Smolka, M.B. (2015). Phosphoproteomics Reveals Distinct Modes of Mec1/ATR Signaling during DNA Replication. Mol. Cell *57*, 1124–1132.

Bavoux, C., Leopoldino, A.M., Bergoglio, V., O-Wang, J., Ogi, T., Bieth, A., Judde, J.G., Pena, S.D., Poupon, M.F., Helleday, T., et al. (2005). Up-regulation of the error prone DNA polymerase {kappa} promotes pleiotropic genetic alterations and tumorigenesis. Cancer Res *65*, 325–330.

Beck, H., Nahse-Kumpf, V., Larsen, M.S.Y., O'Hanlon, K.A., Patzke, S., Holmberg, C., Mejlvang, J., Groth, A., Nielsen, O., Syljuasen, R.G., et al. (2012). Cyclin-Dependent Kinase Suppression by WEE1 Kinase Protects the Genome through Control of Replication Initiation and Nucleotide Consumption. Mol. Cell. Biol. *32*, 4226–4236.

Becker, J.R., Nguyen, H.D., Wang, X., and Bielinsky, A.K. (2014). Mcm10 deficiency causes defective-replisome-induced mutagenesis and a dependency on error-free postreplicative repair. Cell Cycle *13*, 1737–1748.

Becker, J.R., Pons, C., Nguyen, H.D., Costanzo, M., Boone, C., Myers, C.L., and Bielinsky, A.K. (2015). Genetic Interactions Implicating Postreplicative Repair in Okazaki Fragment Processing. PLoS Genet. *11*, 1–24.

Bélanger, F., Angers, J.P., Fortier, É., Hammond-Martel, I., Costantino, S., Drobetsky, E., and Wurtele, H. (2016). Mutations in replicative stress response pathways are associated with S phase-specific defects in nucleotide excision repair. J. Biol. Chem. *291*, 522–537.

Bell, S.P., and Dutta, A. (2002). DNA Replication in Eukaryotic Cells. Annu. Rev. Biochem. *71*, 333–374.

Bergoglio, V., Boyer, A., Walsh, E., Naim, V., Legube, G., Lee, M.Y.W.T., Rey, L., Rosselli, F., Cazaux, C., Eckert, K.A., et al. (2013). DNA synthesis by Pol eta promotes fragile site stability by preventing under-replicated DNA in mitosis. J. Cell Biol. *201*, 395–408.

Bermejo, R., Capra, T., Gonzalez-Huici, V., Fachinetti, D., Cocito, A., Natoli, G., Katou, Y., Mori, H., Kurokawa, K., Shirahige, K., et al. (2009). Genome-Organizing Factors Top2 and Hmo1 Prevent Chromosome Fragility at Sites of S phase Transcription. Cell *138*, 870–884.

Bermejo, R., Capra, T., Jossen, R., Colosio, A., Frattini, C., Carotenuto, W., Cocito, A., Doksani, Y., Klein, H., Gómez-González, B., et al. (2011). The replication checkpoint protects fork stability by releasing transcribed genes from nuclear pores. Cell *146*, 233–246.

Bermejo, R., Lai, M.S., and Foiani, M. (2012). Preventing Replication Stress to Maintain Genome Stability: Resolving Conflicts between Replication and Transcription. Mol. Cell *45*, 710–718.

Bester, A.C., Roniger, M., Oren, Y.S., Im, M.M., Sarni, D., Chaoat, M., Bensimon, A., Zamir, G., Shewach, D.S., and Kerem, B. (2011). Nucleotide deficiency promotes genomic instability in early stages of cancer development. Cell *145*, 435–446.

Betous, R., Rey, L., Wang, G., Pillaire, M.J., Puget, N., Selves, J., Biard, D.S.F., Shin-Ya, K., Vasquez, K.M., Cazaux, C., et al. (2009). Role of TLS DNA polymerases eta and kappa in processing naturally occurring structured DNA in human cells. Mol. Carcinog. *48*, 369–378.

Bhat, A., Andersen, P.L., Qin, Z., and Xiao, W. (2013). Rev3, the catalytic subunit of Polζ, is required for maintaining fragile site stability in human cells. Nucleic Acids Res. *41*, 2328–2339.

Bhatia, V., Barroso, S.I., García-Rubio, M.L., Tumini, E., Herrera-Moyano, E., and Aguilera, A. (2014). BRCA2 prevents R-loop accumulation and associates with TREX-2 mRNA export factor PCID2. Nature *511*, 362–365.

Bi, X., Barkley, L.R., Slater, D.M., Tateishi, S., Yamaizumi, M., Ohmori, H., and Vaziri, C. (2006). Rad18 Regulates DNA Polymerase K and Is Required for Recovery from S-Phase Checkpoint-Mediated Arrest. Mol. Cell. Biol. *26*, 3527–3540.

Bienko, M., Green, C.M., Crosetto, N., Rudolf, F., Zapart, G., Coull, B., Kannouche, P., Wider,

G., Peter, M., Lehmann, A.R., et al. (2005). Ubiquitin-binding domains in translesion synthesis polymerases. Science (80-.). *310*, 1821–1824.

Bjergbaek, L., Cobb, J.A., Tsai-Pflugfelder, M., and Gasser, S.M. (2005). Mechanistically distinct roles for Sgs1p in checkpoint activation and replication fork maintenance. EMBO J. *24*, 405–417.

Blastyák, A., Pintér, L., Unk, I., Prakash, L., Prakash, S., and Haracska, L. (2007). Yeast Rad5 Protein Required for Postreplication Repair Has a DNA Helicase Activity Specific for Replication Fork Regression. Mol. Cell *28*, 167–175.

Blastyák, A., Hajdu, I., Unk, I., and Haracska, L. (2010). Role of Double-Stranded DNA Translocase Activity of Human HLTF in Replication of Damaged DNA. Mol. Cell. Biol. *30*, 684–693.

Bochman, M.L., Paeschke, K., and Zakian, V.A. (2012). DNA secondary structures: Stability and function of G-quadruplex structures. Nat. Rev. Genet. *13*, 770–780.

Boehm, E.M., Spies, M., and Washington, M.T. (2016). PCNA tool belts and polymerase bridges form during translesion synthesis. Nucleic Acids Res. *44*, 8250–8260.

Bournique, E., Dall'Osto, M., Hoffmann, J.S., and Bergoglio, V. (2017). Role of specialized DNA polymerases in the limitation of replicative stress and DNA damage transmission. Mutat. Res. - Fundam. Mol. Mech. Mutagen. *808*, 62–73.

Brachmann, C., Davies, A., Cost, G.J., Caputo, E., Li, J., Hieter, P., and Boeke, J.D. (1998). Designer deletion strains derived fromSaccharomyces cerevisiae S288C: A useful set of strains and plasmids for PCR-mediated gene disruption and other applications. Yeast *14*, 115–132.

Branzei, D., and Foiani, M. (2009). The checkpoint response to replication stress. DNA Repair (Amst). *8*, 1038–1046.

Branzei, D., and Szakal, B. (2016). DNA damage tolerance by recombination : Molecular pathways and DNA structures. DNA Repair (Amst). *44*, 68–75.

Branzei, D., Sollier, J., Liberi, G., Zhao, X., Maeda, D., Seki, M., Enomoto, T., Ohta, K., and

Foiani, M. (2006). Ubc9- and Mms21-Mediated Sumoylation Counteracts Recombinogenic Events at Damaged Replication Forks. Cell *127*, 509–522.

Branzei, D., Vanoli, F., and Foiani, M. (2008). SUMOylation regulates Rad18-mediated template switch. Nature *456*, 915–920.

Brendel, M., Marisco, G., Ganda, I., Wolter, R., and Pungartnik, C. (2010). DNA repair mutant pso2 of Saccharomyces cerevisiae is sensitive to intracellular acetaldehyde accumulated by disulfiram-mediated inhibition of acetaldehyde dehydrogenase. Genet. Mol. Res. *9*, 48–57.

Brewer, B.J., Lockshon, D., and Fangman, W.L. (1992). The arrest of replication forks in the rDNA of yeast occurs independently of transcription. Cell *71*, 267–276.

Brill, S.J., and Stillman, B. (1991). Replication Factor-A from Saccharomyces-Cerevisiae Is Encoded by Three Essential Genes Coordinately Expressed at S-Phase. Genes Dev. *5*, 1589–1600.

Brooks, P.J., and Theruvathu, J.A. (2005). DNA adducts from acetaldehyde: Implications for alcohol-related carcinogenesis. Alcohol *35*, 187–193.

De Bruin, R.A.M., and Wittenberg, C. (2009). All eukaryotes: Before turning off G1-S transcription, please check your DNA. Cell Cycle *8*, 214–217.

Buisson, R., Niraj, J., Pauty, J., Maity, R., Zhao, W., Coulombe, Y., Sung, P., and Masson, J.Y. (2014). Breast cancer proteins PALB2 and BRCA2 stimulate polymerase η in recombination-associated DNA Synthesis At Blocked Replication Forks. Cell Rep. *6*, 553–564.

Burgers, P.M.J., and Kunkel, T.A. (2017). Eukaryotic DNA Replication Fork. Annu. Rev. Biochem. *86*, 417–438.

Burkovics, P., Sebesta, M., Balogh, D., Haracska, L., and Krejci, L. (2014). Strand invasion by HLTF as a mechanism for template switch in fork rescue. Nucleic Acids Res. *42*, 1711–1720.

Burkovics, P., Dome, L., Juhasz, S., Altmannova, V., Sebesta, M., Pacesa, M., Fugger, K., Sorensen, C.S., Lee, Y.W.T., Haracska, L., et al. (2016). The PCNA-associated protein PARI negatively regulates homologous recombination via the inhibition of DNA repair synthesis.

Nucleic Acids Res. *44*, 3176–3189.

Burrell, R.A., McClelland, S.E., Endesfelder, D., Groth, P., Weller, M.C., Shaikh, N., Domingo, E., Kanu, N., Dewhurst, S.M., Gronroos, E., et al. (2013). Replication stress links structural and numerical cancer chromosomal instability. Nature *494*, 492–496.

Byun, T.S., Pacek, M., Yee, M., Walter, J.C., and Cimprich, K.A. (2005). Functional uncoupling of MCM helicase and DNA polymerase activities activates the ATR-dependent checkpoint. Genes Dev. 1040–1052.

Calzada, A., Hodgson, B., Kanemaki, M., Bueno, A., and Labib, K. (2005). Molecular anatomy and regulation of a stable replisome eukaryotic DNA at a paused replication fork. Genes Dev. *19*, 1905–1919.

Capouillez, A., Decaestecker, C., Filleul, O., Chevalier, D., Coppée, F., Leroy, X., Belayew, A., and Saussez, S. (2008). Helicase-like transcription factor exhibits increased expression and altered intracellular distribution during tumor progression in hypopharyngeal and laryngeal squamous cell carcinomas. Virchows Arch 491–499.

Capouillez, A., Debauve, G., Decaestecker, C., Filleul, O., Leroy, X., Chevalier, D., Mortuaire, G., Coppe, F., Belayew, A., and Saussez, S. (2009). The helicase-like transcription factor is a strong predictor of recurrence in hypopharyngeal but not in laryngeal squamous cell carcinomas. Histopathology 77–90.

Centore, R.C., Yazinski, S.A., Tse, A., and Zou, L. (2012). Spartan / C1orf124, a Reader of PCNA Ubiquitylation and a Regulator of UV-Induced DNA Damage Response. Mol. Cell *46*, 625–635.

Chabes, A., Domkin, V., Larsson, G., Liu, A., Graslund, A., Wijmenga, S., and Thelander, L. (2000). Yeast ribonucleotide reductase has a heterodimeric iron-radical-containing subunit. Proc. Natl. Acad. Sci. *97*, 2474–2479.

Chabes, A., Georgieva, B., Domkin, V., Zhao, X., Rothstein, R., and Thelander, L. (2003). Survival of DNA damage in yeast directly depends on increased dNTP levels allowed by relaxed feedback inhibition of ribonucleotide reductase. Cell *112*, 391–401.

Chang, D.J., Lupardus, P.J., and Cimprich, K.A. (2006). Monoubiquitination of Proliferating Cell Nuclear Antigen Induced by Stalled Replication Requires Uncoupling of DNA Polymerase and Mini-chromosome Maintenance Helicase Activities * □. J. Biol. Chem. *281*, 32081–32088.

Chen, S.H., and Zhou, H. (2009). Reconstitution of Rad53 activation by Mec1 through adaptor protein Mrc1. J. Biol. Chem. *284*, 18593–18604.

Chen, S.H., Smolka, M.B., and Zhou, H. (2007). Mechanism of Dun1 activation by Rad53 phosphorylation in Saccharomyces cerevisiae. J. Biol. Chem. *282*, 986–995.

Chen, S.H., Albuquerque, C.P., Liang, J., Suhandynata, R.T., and Zhou, H. (2010). A proteome-wide analysis of kinase-substrate network in the DNA damage response. J. Biol. Chem. *285*, 12803–12812.

Cherry, J.M., Hong, E.L., Amundsen, C., Balakrishnan, R., Binkley, G., Chan, E.T., Christie, K.R., Costanzo, M.C., Dwight, S.S., Engel, S.R., et al. (2012). Saccharomyces Genome Database: The genomics resource of budding yeast. Nucleic Acids Res. *40*, 700–705.

Choi, K., Batke, S., Szakal, B., Lowther, J., Hao, F., Sarangi, P., Branzei, D., Ulrich, H.D., and Zhao, X. (2015). Concerted and differential actions of two enzymatic domains underlie Rad5 contributions to DNA damage tolerance. Nucleic Acids Res. *43*, 2666–2677.

Chong, Y.T., Koh, J.L.Y., Friesen, H., Duffy, K., Cox, M.J., Moses, A., Moffat, J., Boone, C., and Andrews, B.J. (2015). Yeast proteome dynamics from single cell imaging and automated analysis. Cell *161*, 1413–1424.

Ciccia, A., and Elledge, S.J. (2010). The DNA Damage Response: Making It Safe to Play with Knives. Mol. Cell *40*, 179–204.

Ciccia, A., Nimonkar, A. V, Hu, Y., Hajdu, I., Achar, Y.J., Izhar, L., Petit, S.A., Adamson, B., Yoon, J.C., Kowalczykowski, S.C., et al. (2012). Polyubiquitinated PCNA Recruits the ZRANB3 Translocase to Maintain Genomic Integrity after Replication Stress. Mol. Cell.

Clarke, D.J., Segal, M., Jensen, S., and Reed, S.I. (2001). Mec1p regulates Pds1p levels in S phase: Complex coordination of DNA replication and mitosis. Nat. Cell Biol. *3*, 619–627.

Cobb, J.A., Bjergbaek, L., Shimada, K., Frei, C., and Gasser, S.M. (2003). DNA polymerase stabilization at stalled replication forks requires Mec1 and the RecQ helicase Sgs1. EMBO J. *22*, 4325–4336.

Cobb, J.A., Schleker, T., Rojas, V., Bjergbaek, L., Tercero, J.A., and Gasser, S.M. (2005). Replisome instability, fork collapse, and gross chromosomal rearrangements arise synergistically from Mec1 kinase and RecQ helicase mutations. Genes Dev. *19*, 3055–3069.

Costanzo, M., VanderSluis, B., Koch, E.N., Baryshnikova, A., Pons, C., Tan, G., Wang, W., Usaj, M., Hanchard, J., Lee, S.D., et al. (2016). A global genetic interaction network maps a wiring diagram of cellular function. Science (80-.). *353*.

Cotta-Ramusino, C., Fachinetti, D., Lucca, C., Doksani, Y., Lopes, M., Sogo, J., and Foiani, M. (2005). Exo1 processes stalled replication forks and counteracts fork reversal in checkpoint-defective cells. Mol. Cell *17*, 153–159.

Cyr, D.M., and Douglas, M.G. (1994). Differential regulation of Hsp70 subfamilies by the eukaryotic DnaJ homologue Ydj1. J. Biol. Chem. *269*, 9798–9804.

Daee, D.L., Ferrari, E., Longerich, S., Zheng, X.F., Xue, X., Branzei, D., Sung, P., and Myung, K. (2012). Rad5-dependent DNA repair functions of the Saccharomyces cerevisiae FANCM protein homolog Mph1. J. Biol. Chem. *287*, 26563–26575.

Daigaku, Y., Davies, A.A., and Ulrich, H.D. (2010). Ubiquitin-dependent DNA damage bypass is separable from genome replication. Nature *465*, 951–955.

Daigaku, Y., Etheridge, T.J., Nakazawa, Y., Nakayama, M., Watson, A.T., Miyabe, I., Ogi, T., Osborne, M.A., and Carr, A.M. (2017). PCNA ubiquitylation ensures timely completion of unperturbed DNA replication in fission yeast. PLoS Genet. *13*.

Dalgaard, J.Z. (2012). Causes and consequences of ribonucleotide incorporation into nuclear DNA. Trends Genet. *28*, 592–597.

DasGupta, S., Mukhopadhyay, G., Papp, P.P., Lewis, M.S., and Chattoraj, D.K. (1993). Activation of DNA Binding by the Monomeric Form of the P1 Replication Initiator RepA by Heat Shock Proteins DnaJ and DnaK. J. Mol. Biol. *232*, 23–34.

Davidson, M.B., Katou, Y., Keszthelyi, A., Sing, T.L., Xia, T., Ou, J., Vaisica, J.A., Thevakumaran, N., Marjavaara, L., Myers, C.L., et al. (2012). Endogenous DNA replication stress results in expansion of dNTP pools and a mutator phenotype. EMBO J. *31*, 895–907.

Davies, A.A., Huttner, D., Daigaku, Y., Chen, S., and Ulrich, H.D. (2008). Activation of Ubiquitin-Dependent DNA Damage Bypass Is Mediated by Replication Protein A. Mol. Cell *29*, 625–636.

Davis, E.J., Lachaud, C., Appleton, P., Macartney, T.J., Näthke, I., and Rouse, J. (2012). DVC1 (C1orf124) recruits the p97 protein segregase to sites of DNA damage. Nat. Struct. Mol. Biol. *19*, 1093–1100.

Desany, B.A., Alcasabas, A.A., Bachant, J.B., and Elledge, S.J. (1998). Recovery from DNA replicational stress is the essential function of the S-phase checkpoint pathway. Genes Dev. *12*, 2956–2970.

Despras, E., Sittewelle, M., Pouvelle, C., Delrieu, N., Cordonnier, A., and Kannouche, P. (2016). Rad18-dependent SUMOylation of human specialized DNA polymerase eta is required to prevent under-replicated DNA. Nat. Commun.

Ding, L., and Forsburg, S.L. (2014). Essential Domains of Schizosaccharomyces pombe Rad8 Required for DNA Damage Response. G3 Genes, Genomes, Genet. *4*, 1373–1384.

Doles, J., Oliver, T.G., Cameron, E.R., Hsu, G., Jacks, T., Walker, G.C., and Hemann, M.T. (2010). Suppression of Rev3, the catalytic subunit of Pol , sensitizes drug-resistant lung tumors to chemotherapy. Proc. Natl. Acad. Sci. *107*, 20786–20791.

Dominguez-Sola, D., Ying, C.Y., Grandori, C., Ruggiero, L., Chen, B., Li, M., Galloway, D.A., Gu, W., Gautier, J., and Dalla-Favera, R. (2007). Non-transcriptional control of DNA replication by c-Myc. Nature *448*, 445–451.

Duan, X.L., Liu, N.N., Yang, Y.T., Li, H.H., Li, M., Dou, S.X., and Xi, X.G. (2015). G-quadruplexes significantly stimulate Pif1 helicase-catalyzed duplex DNA unwinding. J. Biol. Chem. *290*, 7722–7735.

Dubacq, C., Chevalier, A., Courbeyrette, R., Petat, C., Gidrol, X., and Mann, C. (2006). Role of

the iron mobilization and oxidative stress regulons in the genomic response of yeast to hydroxyurea. Mol. Genet. Genomics *275*, 114–124.

Dumstorf, C.A., Mukhopadhyay, S., Krishnan, E., Haribabu, B., and Mcgregor, W.G. (2009). REV1 Is Implicated in the Development of Carcinogen-Induced Lung Cancer. Mol. Cancer Res. *7*, 247–255.

Eddins, M.J., Carlile, C.M., Gomez, K.M., Pickart, C.M., and Wolberger, C. (2006). Mms2-Ubc13 covalently bound to ubiquitin reveals the structural basis of linkage-specific polyubiquitin chain formation. Nat. Struct. Mol. Biol. *13*, 915–920.

Eddy, S., Ketkar, A., Zafar, M.K., Maddukuri, L., Choi, J., and Eoff, R.L. (2014). Human Rev1 polymerase disrupts G-quadruple DNA. Nucleic Acids Res. *42*, 3272–3285.

Ekholm-Reed, S., Méndez, J., Tedesco, D., Zetterberg, A., Stillman, B., and Reed, S.I. (2004). Deregulation of cyclin E in human cells interferes with prereplication complex assembly. J. Cell Biol. *165*, 789–800.

Elledge, S.J., Zhou, Z., Allen, J.B., and Navas, T.A. (1993). DNA damage and cell cycle regulation of ribonucleotide reductase. Bioessays *15*, 333–339.

Engel, S.R., Dietrich, F.S., Fisk, D.G., Binkley, G., Balakrishnan, R., Costanzo, M.C., Dwight, S.S., Hitz, B.C., Karra, K., Nash, R.S., et al. (2014). The Reference Genome Sequence of Saccharomyces cerevisiae: Then and Now. G3 Genes, Genomes, Genet. *4*, 389–398.

Esser, C., Alberti, S., and Höhfeld, J. (2004). Cooperation of molecular chaperones with the ubiquitin/proteasome system. Biochim. Biophys. Acta - Mol. Cell Res. *1695*, 171–188.

Fallet, E., Jolivet, P., Soudet, J., Lisby, M., Gilson, E., Teixeira, M.T., Lyon, D., and Cedex, L. (2014). Length-dependent processing of telomeres in the absence of telomerase. Nucleic Acids Res. *42*, 3648–3665.

Fan, Q., Xu, X., Zhao, X., Wang, Q., Xiao, W., Guo, Y., and Fu, Y. V. (2018). Rad5 coordinates translesion DNA synthesis pathway by recognizing specific DNA structures in saccharomyces cerevisiae. Curr. Genet.

Fowler, D.M., Stephany, J.J., and Fields, S. (2014). Measuring the activity of protein variants on a large scale using deep mutational scanning. Nat. Protoc. *9*, 2267–2284.

Frum, R.A., Singh, S., Vaughan, C., Mukhopadhyay, N.D., Grossman, S.R., Windle, B., Deb, S., and Deb, S.P. (2014). The human oncoprotein MDM2 induces replication stress eliciting early intra-S-phase checkpoint response and inhibition of DNA replication origin firing. Nucleic Acids Res. *42*, 926–940.

Fumasoni, M., Zwicky, K., Vanoli, F., Lopes, M., and Branzei, D. (2015). Error-Free DNA Damage Tolerance and Sister Chromatid Proximity during DNA Replication Rely on the Polα/Primase/Ctf4 Complex. Mol. Cell *57*, 812–823.

Fuss, J.O., Tsai, C.L., Ishida, J.P., and Tainer, J.A. (2015). Emerging critical roles of Fe-S clusters in DNA replication and repair. Biochim. Biophys. Acta - Mol. Cell Res. *1853*, 1253–1271.

Le Gac, N.T., and Boehmer, P.E. (2002). Activation of the herpes simplex virus type-1 origin-binding protein (UL9) by heat shock proteins. J. Biol. Chem. *277*, 5660–5666.

Gaillard, H., García-Muse, T., and Aguilera, A. (2015). Replication stress and cancer. Nat. Rev. Cancer *15*, 276–280.

Gali, H., Juhasz, S., Morocz, M., Hajdu, I., Fatyol, K., Szukacsov, V., Burkovics, P., and Haracska, L. (2018). Role of SUMO modification of human PCNA at stalled replication fork. Nucleic Acids Res. *40*, 6049–6059.

Gallo, D., Wang, G., Yip, C.M., and Brown, G.W. (2016). Analysis of Replicating Yeast Chromosomes by DNA Combing. Cold Spring Harb. Protoc 138–149.

Gao, Y., Mutter-Rottmayer, E., Greenwalt, A.M., Goldfarb, D., Yan, F., Yang, Y., Martinez-Chacin, R.C., Pearce, K.H., Tateishi, S., Major, M.B., et al. (2016). A neomorphic cancer cell-specific role of MAGE-A4 in trans-lesion synthesis. Nat. Commun. *7*.

Garaycoechea, J.I., Crossan, G.P., Langevin, F., Mulderrig, L., Louzada, S., Yang, F., Guilbaud, G., Park, N., Roerink, S., Nik-Zainal, S., et al. (2018). Alcohol and endogenous aldehydes damage chromosomes and mutate stem cells. Nature *553*, 171–177.

García-Luis, J., and Machín, F. (2014). Mus81-mms4 and yen1 resolve a novel anaphase bridge formed by noncanonical holliday junctions. Nat. Commun. *5*.

García-Muse, T., and Aguilera, A. (2016). Transcription-replication conflicts: How they occur and how they are resolved. Nat. Rev. Mol. Cell Biol. *17*, 553–563.

Garcia-Rodriguez, N., Wong, R.P., and Ulrich, H.D. (2016). Functions of ubiquitin and SUMO in DNA replication and replication stress. Front. Genet. *7*.

García-Rodríguez, N., Morawska, M., Wong, R.P., Daigaku, Y., and Ulrich, H.D. (2018). Spatial separation between replisome- and template-induced replication stress signaling. EMBO J. e98369.

Gasch, A.P., Huang, M., Metzner, S., Botstein, D., Elledge, S.J., and Brown, P.O. (2001). Genomic Expression Responses to DNA-damaging Agents and the Regulatory Role of the Yeast ATR Homolog Mec1p. Mol. Biol. Cell *12*, 2987–3003.

Germann, S.M., Schramke, V., Pedersen, R.T., Gallina, I., Eckert-Boulet, N., Oestergaard, V.H., and Lisby, M. (2014). TopBP1/Dpb11 binds DNA anaphase bridges to prevent genome instability. J. Cell Biol. *204*, 45–59.

Giaever, G., Chu, A.M., Ni, L., Connelly, C., Riles, L., Véronneau, S., Dow, S., Lucau-Danila, A., Anderson, K., André, B., et al. (2002). Functional profiling of the Saccharomyces cerevisiae genome. Nature *418*, 387–391.

Giannattasio, M., Zwicky, K., Follonier, C., Foiani, M., Lopes, M., and Branzei, D. (2014). Visualization of recombination-mediated damage bypass by template switching. Nat. Struct. Mol. Biol. *21*, 884–892.

Gilbert, C.S., van den Bosch, M., Green, C.M., Vialard, J.E., Grenon, M., Erdjument-Bromage, H., Tempst, P., and Lowndes, N.F. (2003). The budding yeast Rad9 checkpoint complex: Chaperone proteins are required for its function. EMBO Rep. *4*, 953–958.

Godin, S., Wier, A., Kabbinavar, F., Bratton-palmer, D.S., Ghodke, H., Houten, B. Van, Vandemark, A.P., and Bernstein, K.A. (2018). The Shu complex interacts with Rad51 through the Rad51 paralogues Rad55 – Rad57 to mediate error-free recombination. Nucleic Acids Res.

41, 4525–4534.

Gong, Y., Kakihara, Y., Krogan, N., Greenblatt, J., Emili, A., Zhang, Z., and Houry, W.A. (2009). An atlas of chaperone-protein interactions in Saccharomyces cerevisiae: Implications to protein folding pathways in the cell. Mol. Syst. Biol. *5*, 1–14.

Gonzalez-Huici, V., Szakal, B., Urulangodi, M., Psakhye, I., Castellucci, F., Menolfi, D., Rajakumara, E., Fumasoni, M., Bermejo, R., Jentsch, S., et al. (2014). DNA bending facilitates the error-free DNA damage tolerance pathway and upholds genome integrity. EMBO J. *33*, 327–340.

Greenfeder, S. a, and Newlon, C.S. (1992). Replication forks pause at yeast centromeres. Mol. Cell. Biol. *12*, 4056–4066.

Gritenaite, D., Princz, L.N., Szakal, B., Bantele, S.C.S., Wendeler, L., Schilbach, S., Habermann, B.H., Matos, J., Lisby, M., Branzei, D., et al. (2014). A cell cycle-regulated Slx4-Dpb11 complex promotes the resolution of DNA repair intermediates linked to stalled replication. Genes Dev. *28*, 1604–1619.

Groth, A., Corpet, A., Cook, A., Roche, D., Baratek, J., Lukas, J., and Almouzni, G. (2007). Regulation of Replication Fork Through Histone Supply and Demand. Science (80-.). *1928*, 1928–1932.

Hammond, C.M., Strømme, C.B., Huang, H., Patel, D.J., and Groth, A. (2017). Histone chaperone networks shaping chromatin function. Nature *18*, 141–158.

Hamperl, S., Bocek, M.J., Saldivar, J.C., Swigut, T., and Cimprich, K.A. (2017). Transcription-Replication Conflict Orientation Modulates R-Loop Levels and Activates Distinct DNA Damage Responses. Cell *170*, 774–786.e19.

Han, J., Liu, T., Huen, M.S.Y., Hu, L., Chen, Z., and Huang, J. (2014). SIVA1 directs the E3 ubiquitin ligase RAD18 for PCNA monoubiquitination. J. Cell Biol. *205*, 811–827.

Haracska, L., Unk, I., Johnson, E., Johansson, E., Burgers, P.M.J., Prakash, S., and Prakash, L. (2001). Roles of yeast DNA polymerases delta and zeta and of Rev1 in the bypass of abasic sites. Genes Dev. *15*, 945–954.

Hart, T., Chandrashekhar, M., Aregger, M., Steinhart, Z., Brown, K.R., MacLeod, G., Mis, M., Zimmermann, M., Fradet-Turcotte, A., Sun, S., et al. (2015). High-Resolution CRISPR Screens Reveal Fitness Genes and Genotype-Specific Cancer Liabilities. Cell *163*, 1515–1526.

Hedglin, M., and Benkovic, S.J. (2015). Regulation of Rad6 / Rad18 Activity During DNA Damage Tolerance. Annu. Rev. Biophys.

Helmrich, A., Ballarino, M., Nudler, E., and Tora, L. (2013). Transcription-replication encounters, consequences and genomic instability. Nat. Struct. Mol. Biol. *20*, 412–418.

Herrera-Moyano, E., Nia Mergui, X., García-Rubio, M.L., Barroso, S., and Aguilera, A.S. (2014). The yeast and human FACT chromatin- reorganizing complexes solve R-loop- mediated transcription–replication conflicts. Genes Dev. *28*, 735–748.

Herrero, A.B., and Moreno, S. (2011). Lsm1 promotes genomic stability by controlling histone mRNA decay. EMBO J. *30*, 2008–2018.

Hills, S.A., and Diffley, J.F.X. (2014). DNA replication and oncogene-induced replicative stress. Curr. Biol. *24*, R435–R444.

Hishiki, A., Hashimoto, H., Hanafusa, T., Kamei, K., Ohashi, E., Shimizu, T., Ohmori, H., and Sato, M. (2009). Structural Basis for Novel Interactions between Human Translesion Synthesis Polymerases and Proliferating Cell Nuclear Antigen * □. J. Biochem. *284*, 10552–10560.

Hishiki, A., Hara, K., Ikegaya, Y., Yokoyama, H., Shimizu, T., Sato, M., and Hashimoto, H. (2015). Structure of a Novel DNA-binding Domain of Helicase-like Transcription Factor (HLTF) and Its Functional Implication in DNA Damage Tolerance. J. Biol. Chem. *290*, 13215–13223.

Hoege, C., Pfander, B., Moldovan, G.L., Pyrowolakis, G., and Jentsch, S. (2002). RAD6-dependent DNA repair is linked to modification of PCNA by ubiquitin and SUMO. Nature *419*, 135–141.

Hoffmann, J., and Cazaux, C. (2010). Seminars in Cancer Biology Aberrant expression of alternative DNA polymerases : A source of mutator phenotype as well as replicative stress in cancer. Semin. Cancer Biol. J. *20*, 312–319.

Hu, F., Wang, Y., Liu, D., Li, Y., Qin, J., and Elledge, S.J. (2001). Regulation of the Bub2/Bfa1 GAP complex by Cdc5 and cell cycle checkpoints. Cell *107*, 655–665.

Hu, J., Sun, L., Shen, F., Chen, Y., Hua, Y., Liu, Y., Zhang, M., Hu, Y., Wang, Q., Xu, W., et al. (2012). The intra-S phase checkpoint targets Dna2 to prevent stalled replication forks from reversing. Cell *149*, 1221–1232.

Huang, D., Piening, B.D., and Paulovich, A.G. (2013). The Preference for Error-Free or Error-Prone Postreplication Repair in Saccharomyces cerevisiae Exposed to Low-Dose Methyl Methanesulfonate Is Cell Cycle Dependent. Mol. Cell. Biol. *33*, 1515–1527.

Huang, M., Zhou, Z., and Elledge, S.J. (1998). The DNA replication and damage checkpoint pathways induce transcription by inhibition of the Crt1 repressor. Cell *94*, 595–605.

Huang, M., Rio, A.-G., Nicolas, A., and Kolodner, R.D. (2003a). A genomewide screen in Saccharomyces cerevisiae for genes that suppress the accumulation of mutations. Proc. Natl. Acad. Sci. *100*, 11529–11534.

Huang, X., Kolbanovskiy, A., Wu, X., Zhang, Y., Wang, Z., Zhuang, P., Amin, S., and Geacintov, N.E. (2003b). Effects of Base Sequence Context on Translesion Synthesis Past a Bulky (+) - trans - anti -B [a] P- N 2 -dG Lesion Catalyzed by the Y-family Polymerase pol κ †. Biochemistry 2456–2466.

Huertas, P., and Aguilera, A. (2003). Cotranscriptionally formed DNA:RNA hybrids mediate transcription elongation impairment and transcription-associated recombination. Mol. Cell *12*, 711–721.

Huh, W.-K.K., Falvo, J. V, Gerke, L.C., Carroll, A.S., Howson, R.W., Weissman, J.S., and K, O'Shea, E. (2003). Global analysis of protein localization in budding yeast. Nature *425*, 686–691.

Iguchi, M., Osanai, M., Hayashi, Y., Koentgen, F., and Lee, G. (2014). The error-prone DNA polymerase i provides quantitative resistance to lung tumorigenesis and mutagenesis in mice. Oncogene *33*, 3612–3617.

Inagaki, A., Sleddens-Linkels, E., van Cappellen, W.A., Hibbert, R.G., Sixma, T.K.,

Hoeijmakers, J.H.J., Grootegoed, J.A., and Baarends, W.M. (2011). Human RAD18 interacts with ubiquitylated chromatin components and facilitates RAD9 recruitment to DNA double strand breaks. PLoS One *6*.

Ivessa, A.S., Zhou, J.Q., Schulz, V.P., Monson, E.K., and Zakian, V.A. (2002). Saccharomyces Rrm3p, a 5′ to 3′ DNA helicase that promotes replication fork progression through telomeric and subtelomeric DNA. Genes Dev. *16*, 1383–1396.

Ivessa, A.S., Lenzmeier, B.A., Bessler, J.B., Goudsouzian, L.K., Schnakenberg, S.L., and Zakian, V.A. (2003). The Saccharomyces cerevisiae Helicase Rrm3p Facilitates Replication Past Nonhistone Protein-DNA Complexes. Mol. Cell *12*, 1525–1536.

Izhar, L., Ziv, O., Cohen, I.S., Geacintov, N.E., and Livneh, Z. (2013). Genomic assay reveals tolerance of DNA damage by both translesion DNA synthesis and homology-dependent repair in mammalian cells. Proc. Natl. Acad. Sci. *110*.

Jackson, S.P., and Durocher, D. (2013). Regulation of DNA Damage Responses by Ubiquitin and SUMO. Mol. Cell *49*, 795–807.

Jiang, Y., Lucas, I., Young, D.J., Davis, E.M., Karrison, T., Rest, J.S., and Le Beau, M.M. (2009). Common fragile sites are characterized by histone hypoacetylation. Hum. Mol. Genet. *18*, 4501–4512.

Johnson, R.E., Henderson, S.T., Petes, T.D., Prakash, S., Bankmann, M., and Prakash, L. (1992). Saccharomyces cerevisiae RAD5-encoded DNA repair protein contains DNA helicase and zinc-binding sequence motifs and affects the stability of simple repetitive sequences in the genome. Mol. Cell. Biol. *12*, 3807–3818.

Johnson, R.E., Prakash, L., and Prakash, S. (2012). Pol31 and Pol32 subunits of yeast DNA polymerase δ are also essential subunits of DNA polymerase ζ. Proc. Natl. Acad. Sci. *109*, 12455–12460.

Johnsons, R.E., Prakashq, S., and Prakashsqn, L. (1994). Yeast DNA Repair Protein RAD5 That Promotes Instability of Simple Repetitive Sequences is a DNA-dependent ATPase *. J. Biochem. *269*, 28259–28262.

Johnstone, T.C., Suntharalingam, K., and Lippard, S.J. (2016). The Next Generation of Platinum Drugs: Targeted Pt(II) Agents, Nanoparticle Delivery, and Pt(IV) Prodrugs. Chem. Rev. *116*, 3436–3486.

Jones, R.M., Mortusewicz, O., Afzal, I., Lorvellec, M., García, P., Helleday, T., and Petermann, E. (2013). Increased replication initiation and conflicts with transcription underlie Cyclin E-induced replication stress. Oncogene *32*, 3744–3753.

Ju, D., Wang, X., Xu, H., and Xie, Y. (2008). Genome-wide analysis identifies MYND-domain protein Mub1 as an essential factor for Rpn4 ubiquitylation. Mol. Cell. Biol. *28*, 1404–1412.

Juhasz, S., Balogh, D., Hajdu, I., Burkovics, P., Villamil, M.A., Zhuang, Z., and Haracska, L. (2018). Characterization of human Spartan / C1orf124, an ubiquitin-PCNA interacting regulator of DNA damage tolerance. Nucleic Acids Res. *40*, 10795–10808.

Kamentsky, L., Jones, T.R., Fraser, A., Bray, M.A., Logan, D.J., Madden, K.L., Ljosa, V., Rueden, C., Eliceiri, K.W., and Carpenter, A.E. (2011). Improved structure, function and compatibility for cellprofiler: Modular high-throughput image analysis software. Bioinformatics *27*, 1179–1180.

Karras, G.I., and Jentsch, S. (2010). The RAD6 DNA damage tolerance pathway operates uncoupled from the replication fork and is functional beyond S phase. Cell *141*, 255–267.

Karras, G.I., Fumasoni, M., Sienski, G., Vanoli, F., Branzei, D., and Jentsch, S. (2013). Noncanonical Role of the 9-1-1 Clamp in the Error-Free DNA Damage Tolerance Pathway. Mol. Cell *49*, 536–546.

Katou, Y., Kanoh, Y., Bando, M., Noguchi, H., Tanaka, H., Ashikari, T., Sugimoto, K., and Shirahige, K. (2003). S-phase checkpoint proteins Tof1 and Mrc1 form a stable replication-pausing complex. Nature *424*, 1078–1083.

Kats, E.S., Enserink, J.M., Martinez, S., and Kolodner, R.D. (2009). The Saccharomyces cerevisiae Rad6 Postreplication Repair and Siz1/Srs2 Homologous Recombination-Inhibiting Pathways Process DNA Damage That Arises in asf1 Mutants. Mol. Cell. Biol. *29*, 5226–5237.

Khare, V., and Eckert, K.A. (2002). The proofreading 3 → 5 exonuclease activity of DNA

polymerases : a kinetic barrier to translesion DNA synthesis. Mutat. Res. *510*, 45–54.

Kikuchi, S., Hara, K., Shimizu, T., Sato, M., and Hashimoto, H. (2012). Structural basis of recruitment of DNA polymerase ζ by interaction between REV1 and REV7 proteins. J. Biol. Chem. *287*, 33847–33852.

Kile, A.C., Chavez, D.A., Bacal, J., Bezsonova, I., Eichman, B.F., Cimprich, K.A., Kile, A.C., Chavez, D.A., Bacal, J., Eldirany, S., et al. (2015). HLTF's Ancient HIRAN Domain Binds 3' DNA Ends to Drive Replication Fork Reversal. Mol. Cell *58*, 1090–1100.

Kim, J.C., and Mirkin, S.M. (2013). The balancing act of DNA repeat expansions. Curr. Opin. Genet. Dev. *23*, 280–288.

Kim, H., Dejsuphong, D., Adelmant, G., Ceccaldi, R., Yang, K., Marto, J.A., and Andrea, A.D.D. (2014). Promotes Chromatin Remodeling and Translesion DNA Synthesis. Mol. Cell *54*, 107–118.

Kim, N., Huang, S., and Jinks-Roberston, S. (2011). Mutagenic Processing of Ribonucleotides in DNA by Yeast Topoisomerase I. Science (80-.). *332*, 1561–1564.

Kobbe, D., Kahles, A., Walter, M., Klemm, T., Mannuss, A., Knoll, A., Focke, M., and Puchta, H. (2016). AtRAD5A is a DNA translocase harboring a HIRAN domain which confers binding to branched DNA structures and is required for DNA repair in vivo. Plant J. *88*, 521–530.

Korzhnev, D.M., and Hadden, M.K. (2016). Targeting the Translesion Synthesis Pathway for the Development of Anti-Cancer Chemotherapeutics. J. Med. Chem. *59*, 9321–9336.

Korzhnev, D.M., Neculai, D., Dhe-Paganon, S., Arrowsmith, C.H., and Bezsonova, I. (2016). Solution NMR structure of the HLTF HIRAN domain : a conserved module in SWI2 / SNF2 DNA damage tolerance proteins. J. Biomol. NMR *66*, 209–219.

Kota, P., Summers, D.W., Ren, H.-Y., Cyr, D.M., and Dokholyan, N. V. (2009). Identification of a consensus motif in substrates bound by a Type I Hsp40. Proc. Natl. Acad. Sci. *106*, 11073–11078.

Kotsantis, P., Silva, L.M., Irmscher, S., Jones, R.M., Folkes, L., Gromak, N., and Petermann, E.

(2016). Increased global transcription activity as a mechanism of replication stress in cancer. Nat. Commun. *7*, 1–13.

Kottemann, M.C., and Smogorzewska, A. (2013). Fanconi anaemia and the repair of Watson and Crick DNA crosslinks. Nature *493*, 356–363.

Krejci, L., Van Komen, S., Li, Y., Villemain, J., Reddy, M.S., Klein, H., Ellenberger, T., and Sung, P. (2003). DNA helicase Srs2 disrupts the Rad51 presynaptic filament. Nature *423*, 305–309.

Kuang, L., Kou, H., Xie, Z., Zhou, Y., Feng, X., Wang, L., and Wang, Z. (2013). A non-catalytic function of Rev1 in translesion DNA synthesis and mutagenesis is mediated by its stable interaction with Rad5. DNA Repair (Amst). *12*, 27–37.

Kuhlbusch, T.A., Lobert, J.M., Crutzen, P.J., and Peter Warneck (1991). Function of DnaJ and DnaK as chaperones in origin-specific DNA binding by RepA. Nature *350*, 135–137.

Kumar, S., and Burgers, P.M. (2013). Lagging strand maturation factor Dna2 is a component of the replication checkpoint initiation machinery. Genes Dev. *27*, 313–321.

Lang, G.I., and Murray, A.W. (2008). Estimating the per-base-pair mutation rate in the yeast Saccharomyces cerevisiae. Genetics *178*, 67–82.

Lang, G.I., and Murray, A.W. (2011). Mutation rates across budding yeast chromosome VI Are correlated with replication timing. Genome Biol. Evol. *3*, 799–811.

Lange, S.S., Wittschieben, J.P., and Wood, R.D. (2012). DNA polymerase zeta is required for proliferation of normal mammalian cells. Nucleic Acids Res. *40*, 4473–4482.

Langmead, B., and Salzberg, S.L. (2012). Fast gapped-read alignment with Bowtie 2. Nat. Methods *9*, 357–359.

Larsen, N.B., Sass, E., Suski, C., Mankouri, H.W., and Hickson, I.D. (2014). The Escherichia coli Tus-Ter replication fork barrier causes site-specific DNA replication perturbation in yeast. Nat. Commun. *5*.

Lawrence, C.W., and Christensen, R.B. (1979). Metabolic Suppressors of Trimethoprim and Ultraviolet Light Sensitivities of Saccharomyces cerevisiae rad6 Mutantst. J. Bacteriol. *8765*.

Lazzaro, F., Novarina, D., Amara, F., Watt, D.L., Stone, J.E., Costanzo, V., Burgers, P.M., Kunkel, T.A., Plevani, P., and Muzi-Falconi, M. (2012). RNase H and postreplication repair protect cells from ribonucleotides incorporated in DNA. Mol. Cell *45*, 99–110.

Leach, C.A., and Michael, W.M. (2005). Ubiquitin/SUMO modification of PCNA promotes replication fork progression in Xenopus laevis egg extracts. J. Cell Biol. *171*, 947–954.

Lee, H., Yuan, C., Hammet, A., Mahajan, A., Chen, E.S.W., Wu, M.R., Su, M.I., Heierhorst, J., and Tsai, M.D. (2008a). Diphosphothreonine-Specific Interaction between an SQ/TQ Cluster and an FHA Domain in the Rad53-Dun1 Kinase Cascade. Mol. Cell *30*, 767–778.

Lee, Y., Gregory, M.T., and Yang, W. (2014). Human Pol ζ purified with accessory subunits is active in translesion DNA synthesis and complements Pol η in cisplatin bypass. Proc. Natl. Acad. Sci. *111*, 2954–2959.

Lee, Y.D., Wang, J., Stubbe, J.A., and Elledge, S.J. (2008b). Dif1 Is a DNA-Damage-Regulated Facilitator of Nuclear Import for Ribonucleotide Reductase. Mol. Cell *32*, 70–80.

Lemontt, J.F. (1971). MUTANTS OF YEAST DEFECTIVE I N MUTATION INDUCED BY ULTRAVIOLET LIGHT. Genetics 21–33.

Leung, W.K., Yu, J., Bai, A.H.C., Chan, M.W.Y., Chan, K., To, K., Chan, F.K.L., Ng, E.K.W., Chung, S.C.S., and Sung, J.J.Y. (2003). Inactivation of Helicase-Like Transcription Factor by Promoter Hypermethylation in Human Gastric Cancer. Mol. Carcinog. *97*, 91–97.

Li, X., and Manley, J.L. (2005). Inactivation of the SR protein splicing factor ASF/SF2 results in genomic instability. Cell *122*, 365–378.

Liberi, G., Maffioletti, G., Lucca, C., Chiolo, I., Baryshnikova, A., Cotta-ramusino, C., Lopes, M., Pellicioli, A., Haber, J.E., and Foiani, M. (2005). Rad51-dependent DNA structures accumulate at damaged replication forks in. Genes Dev. 339–350.

Liefshitz, B., Steinlauf, R., Friedl, A., Eckardt-schupp, F., and Kupiec, M. (1998). Genetic

interactions between mutants of the “ error-prone ” repair group of Saccharomyces cere Õ isiae and their effect on recombination and mutagenesis. Mutat. Res. 135–145.

Lin, B.Y., Makhov, A.M., Griffith, J.D., Broker, T.R., and Chow, L.T. (2002). Chaperone proteins abrogate inhibition of the human papillomavirus (HPV) E1 replicative helicase by the HPV E2 protein. Mol. Cell. Biol. *22*, 6592–6604.

Lin, J.R., Zeman, M.K., Chen, J.Y., Yee, M.C., and Cimprich, K.A. (2011). SHPRH and HLTF Act in a Damage-Specific Manner to Coordinate Different Forms of Postreplication Repair and Prevent Mutagenesis. Mol. Cell *42*, 237–249.

Lisby, M., Barlow, J.H., Burgess, R.C., and Rothstein, R. (2004). Choreography of the DNA damage response: Spatiotemporal relationships among checkpoint and repair proteins. Cell *118*, 699–713.

Loll-Krippleber, R., and Brown, G.W. (2017). P-body proteins regulate transcriptional rewiring to promote DNA replication stress resistance. Nat. Commun. *8*.

Lopes, M., Cotta-Ramusino, C., Pellicioli, A., Liberi, G., Plevani, P., Muzi-Falconi, M., Newlon, C.S., and Foiani, M. (2001). The DNA replication checkpoint response stabilizes stalled replication forks. Nature *412*, 557–561.

Lopez-Mosqueda, J., Maas, N.L., Jonsson, Z.O., Defazio-Eli, L.G., Wohlschlegel, J., and Toczyski, D.P. (2010). Damage-induced phosphorylation of Sld3 is important to block late origin firing. Nature *467*, 479–483.

López-Otín, C., Blasco, M.A., Partridge, L., Serrano, M., and Kroemer, G. (2013). The hallmarks of aging. Cell *153*.

Lorenti Garcia, C., Mechilli, M., Proietti De Santis, L., Schinoppi, A., Katarzyna, K., and Palitti, F. (2009). Relationship between DNA lesions, DNA repair and chromosomal damage induced by acetaldehyde. Mutat. Res. - Fundam. Mol. Mech. Mutagen. *662*, 3–9.

Lyakhovich, A., and Shekhar, M.P. V (2004). RAD6B overexpression confers chemoresistance : RAD6 expression during cell cycle and its redistribution to chromatin during DNA damage-induced response. Oncogene 3097–3106.

Macheret, M., and Halazonetis, T.D. (2015). DNA Replication Stress as a Hallmark of Cancer. Annu. Rev. Pathol. Mech. Dis. *10*, 425–448.

Mackay, C., Toth, R., and Rouse, J. (2009). Biochemical characterisation of the SWI / SNF family member HLTF. Biochem. Biophys. Res. Commun. *390*, 187–191.

Madura, K., Prakash, S., and Prakashl, L. (1990). Expression of the Saccharomyces cerevisiae DNA repair gene RAD6 that encodes a ubiquitin conjugating enzyme, increases in response to DNA damage and in meiosis but remains constant during the mitotic cell cycle. Nucleic Acids Res. *18*, 771–778.

Majka, J., and Burgers, P.M.J. (2003). Yeast Rad17/Mec3/Ddc1: a sliding clamp for the DNA damage checkpoint. Proc. Natl. Acad. Sci. *100*, 2249–2254.

Majka, J., Binz, S.K., Wold, M.S., and Burgers, P.M.J. (2006a). Replication protein a directs loading of the DNA damage checkpoint clamp to 5'-DNA junctions. J. Biol. Chem. *281*, 27855–27861.

Majka, J., Niedziela-Majka, A., and Burgers, P.M.J. (2006b). The Checkpoint Clamp Activates Mec1 Kinase during Initiation of the DNA Damage Checkpoint. Mol. Cell *24*, 891–901.

Makarova, A. V., Stodola, J.L., and Burgers, P.M. (2012). A four-subunit DNA polymerase ζ complex containing Pol δ accessory subunits is essential for PCNA-mediated mutagenesis. Nucleic Acids Res. *40*, 11618–11626.

Masai, H., and Vaziri, C. (2010). Phosphorylated Rad18 directs DNA Polymerase to sites of stalled replication. J. Cell Biol. *191*, 953–966.

Masuda, Y., Kanao, R., Kaji, K., Ohmori, H., Hanaoka, F., and Masutani, C. (2015). Different types of interaction between PCNA and PIP boxes contribute to distinct cellular functions of Y-family DNA polymerases. Nucleic Acids Res. *43*, 7898–7910.

Masutani, C., Araki, M., Yamada, A., Kusumoto, R., Nogimori, T., Maekawa, T., Iwai, S., and Hanaoka, F. (1999a). Xeroderma pigmentosum variant (XP-V) correcting protein from HeLa cells has a thymine dimer bypass DNA polymerase activity. EMBO J. *18*, 3491–3501.

Masutani, C., Kusumoto, R., Yamada, A., and Hanaoka, F. (1999b). The XPV (xeroderma pigmentosum variant) gene encodes human DNA polymerase eta. Nature *399*, 700–704.

Masuyama, S., Tateishi, S., Yomogida, K., and Nishimune, Y. (2005). Regulated expression and dynamic changes in subnuclear localization of mammalian Rad18 under normal and genotoxic conditions. Genes to Cells *10*, 753–762.

McElhinny, S.A.N., Kumar, D., Clark, A.B., Watt, D.L., Watts, B.E., Lundström, E.B., Johansson, E., Chabes, A., and Kunkel, T.A. (2010). Genome instability due to ribonucleotide incorporation into DNA. Nat. Chem. Biol. *6*, 774–781.

Mcintyre, J., and Woodgate, R. (2015). Regulation of translesion DNA synthesis : Posttranslational modification of lysine residues in key proteins. DNA Repair (Amst). *29*, 166–179.

McMurray, C.T. (2010). Mechanisms of trinucleotide repeat instability during human development. Nat. Rev. Genet. *11*, 786–799.

Mejlvang, J., Feng, Y., Alabert, C., Neelsen, K.J., Jasencakova, Z., Zhao, X., Lees, M., Sandelin, A., Pasero, P., Lopes, M., et al. (2014). New histone supply regulates replication fork speed and PCNA unloading. J. Cell Biol. *204*, 29–43.

Menolfi, D., Delamarre, A., Lengronne, A., Pasero, P., Menolfi, D., Delamarre, A., Lengronne, A., Pasero, P., and Branzei, D. (2015). Essential Roles of the Smc5 / 6 Complex in Replication through Natural Pausing Sites and Endogenous DNA Damage Tolerance. Mol. Cell *60*, 835–846.

Merrikh, H., MacHón, C., Grainger, W.H., Grossman, A.D., and Soultanas, P. (2011). Co-directional replication-transcription conflicts lead to replication restart. Nature *470*, 554–558.

Minca, E.C., and Kowalski, D. (2010). Multiple Rad5 Activities Mediate Sister Chromatid Recombination to Bypass DNA Damage at Stalled Replication Forks. Mol. Cell *38*, 649–661.

Mirkin, E. V., and Mirkin, S.M. (2007). Replication Fork Stalling at Natural Impediments. Microbiol. Mol. Biol. Rev. *71*, 13–35.

Mizuno, K., Lambert, S., Baldacci, G., Murray, J.M., and Carr, A.M. (2009). Nearby inverted

repeats fuse to generate acentric and dicentric palindromic chromosomes by a replication template exchange mechanism. Genes Dev. *23*, 2876–2886.

Mizuno, K., Miyabe, I., Schalbetter, S.A., Carr, A.M., and Murray, J.M. (2013). Recombination-restarted replication makes inverted chromosome fusions at inverted repeats. Nature *493*, 246–249.

Mohebi, S., Mizuno, K., Watson, A., Carr, A.M., and Murray, J.M. (2015). Checkpoints are blind to replication restart and recombination intermediates that result in gross chromosomal rearrangements. Nat. Commun. *6*.

Moinova, H.R., Chen, W., Shen, L., Smiraglia, D., Olechnowicz, J., Ravi, L., Kasturi, L., Myeroff, L., Plass, C., Parsons, R., et al. (2002). HLTF gene silencing in human colon cancer. Proc. Natl. Acad. Sci. *99*.

Moldovan, G., Dejsuphong, D., Petalcorin, M.I.R., Hofmann, K., Takeda, S., Boulton, S.J., and Andrea, A.D.D. (2012). Inhibition of Homologous Recombination by the PCNA-Interacting Protein PARI. Mol. Cell *45*, 75–86.

Moraes, T.F., Edwards, R. a, Mckenna, S., Pastushok, L., Xiao, W., Glover, J.N.M., and Ellison, M.J. (2001). Crystal structure of the human ubiquitin complex , hMms2 – hUbc13. Nature *8*, 715–719.

Morafraile, E.C., Diffley, J.F.X., Tercero, J.A., and Segurado, M. (2015). Checkpoint-dependent RNR induction promotes fork restart after replicative stress. Sci. Rep. *5*, 1–9.

Moriel-Carretero, M., Tous, C., and Aguilera, A. (2011). Control of the function of the transcription and repair factor TFIIH by the action of the cochaperone Ydj1. Proc. Natl. Acad. Sci. *108*, 15300–15305.

Morin, I., Ngo, H.P., Greenall, A., Zubko, M.K., Morrice, N., and Lydall, D. (2008). Checkpoint-dependent phosphorylation of Exo1 modulates the DNA damage response. EMBO J. *27*, 2400–2410.

Mosbech, A., Gibbs-seymour, I., Kagias, K., Thorslund, T., Beli, P., Povlsen, L., Nielsen, S.V., Smedegaard, S., Sedgwick, G., Lukas, C., et al. (2012). DVC1 (C1orf124) is a DNA damage –

targeting p97 adaptor that promotes ubiquitin-dependent responses to replication blocks. Nat. Struct. Mol. Biol. *19*, 1084–1092.

Motegi, A., Kuntz, K., Majeed, A., Smith, S., and Myung, K. (2006). Regulation of gross chromosomal rearrangements by ubiquitin and SUMO ligases in Saccharomyces cerevisiae. Mol. Cell. Biol. *26*, 1424–1433.

Mourón, S., Rodriguez-Acebes, S., Martínez-Jiménez, M.I., García-Gómez, S., Chocrón, S., Blanco, L., and Méndez, J. (2013). Repriming of DNA synthesis at stalled replication forks by human PrimPol. Nat. Struct. Mol. Biol. *20*, 1383–1389.

Muñoz, S., and Méndez, J. (2017). DNA replication stress: from molecular mechanisms to human disease. Chromosoma *126*, 1–15.

Murakumo, Y., Ogura, Y., Ishii, H., Numata, S., Ichihara, M., Croce, C.M., Fishel, R., and Takahashi, M. (2001). Interactions in the Error-prone Postreplication Repair Proteins hREV1 , hREV3 , and hREV7 *. J. Biochem. *276*, 35644–35651.

Murakumo, Y., Mizutani, S., Yamaguchi, M., and Ichihara, M. (2006). Analyses of ultraviolet-induced focus formation of hREV1 protein. Genes to Cells 193–205.

Nano, N., and Houry, W.A. (2013). Chaperone-like activity of the AAA+ proteins Rvb1 and Rvb2 in the assembly of various complexes. Philos. Trans. R. Soc. *368*, 20110399–20110399.

Navadgi-Patil, V.M., and Burgers, P.M. (2009). The Unstructured C-Terminal Tail of the 9-1-1 Clamp Subunit Ddc1 Activates Mec1/ATR via Two Distinct Mechanisms. Mol. Cell *36*, 743–753.

Niimi, A., Brown, S., Sabbioneda, S., Kannouche, P.L., Scott, A., Yasui, A., Green, C.M., and Lehmann, A.R. (2008). Regulation of proliferating cell nuclear antigen ubiquitination in mammalian cells. Proc. Natl. Acad. Sci. 1–6.

Northam, M.R., Garg, P., Baitin, D.M., Burgers, P.M.J., and Shcherbakova, P. V (2006). A novel function of DNA polymerase ζ regulated by PCNA. EMBO J. *25*, 4316–4325.

Northam, M.R., Robinson, H.A., Kochenova, O. V., and Shcherbakova, P. V. (2010).

Participation of DNA polymerase ζ in replication of undamaged DNA in Saccharomyces cerevisiae. Genetics *184*, 27–42.

Northam, M.R., Moore, E.A., Mertz, T.M., Binz, S.K., Stith, C.M., Stepchenkova, E.I., Wendt, K.L., Burgers, P.M.J., and Shcherbakova, P. V. (2014). DNA polymerases ζ and Rev1 mediate error-prone bypass of non-B DNA structures. Nucleic Acids Res. *42*, 290–306.

Nyholm, S., Thelander, L., and Gräslund, A. (1993). Reduction and Loss of the Iron Center in the Reaction of the Small Subunit of Mouse Ribonucleotide Reductase with Hydroxyurea. Biochemistry *32*, 11569–11574.

Ogi, T., Shinkai, Y., Tanaka, K., and Ohmori, H. (2002). Pol K protects mammalian cells against the lethal and mutagenic effects of benzo [a] pyrene. Proc. Natl. Acad. Sci. *99*.

De Oliveira, F.M.B., Harris, M.R., Brazauskas, P., De Bruin, R.A.M., and Smolka, M.B. (2012). Linking DNA replication checkpoint to MBF cell-cycle transcription reveals a distinct class of G1/S genes. EMBO J. *31*, 1798–1810.

Onge, R.P.S., Mani, R., Oh, J., Proctor, M., Fung, E., Davis, R.W., Nislow, C., Roth, F.P., and Giaever, G. (2007). Systematic pathway analysis using high-resolution fitness profiling of combinatorial gene deletions. Nat. Genet. *39*, 199–206.

Ortiz-Bazán, M.Á., Gallo-Fernández, M., Saugar, I., Jiménez-Martín, A., Vázquez, M.V., and Tercero, J.A. (2014). Rad5 plays a major role in the cellular response to DNA damage during chromosome replication. Cell Rep. *9*, 460–468.

Osborn, A.J., and Elledge, S.J. (2003). Mrc1 is a replication fork component whose phosphorylation in response to DNA replication stress activates Rad53. Genes Dev. 1755–1767.

Paeschke, K., Bochman, M.L., Daniela Garcia, P., Cejka, P., Friedman, K.L., Kowalczykowski, S.C., and Zakian, V.A. (2013). Pif1 family helicases suppress genome instability at G-quadruplex motifs. Nature *497*, 458–462.

Pages, V., Santa Maria, S.R., Prakash, L., and Prakash, S. (2009). Role of DNA damage-induced replication checkpoint in promoting lesion bypass by translesion synthesis in yeast. Genes Dev. *3*, 1438–1449.

Pagès, V., Bresson, A., Acharya, N., Prakash, S., Fuchs, R.P., and Prakash, L. (2008). Requirement of Rad5 for DNA polymerase ζ-dependent translesion synthesis in Saccharomyces cerevisiae. Genetics *180*, 73–82.

Papouli, E., Chen, S., Davies, A.A., Huttner, D., Krejci, L., Sung, P., and Ulrich, H.D. (2005). Crosstalk between SUMO and ubiquitin on PCNA is mediated by recruitment of the helicase Srs2p. Mol. Cell *19*, 123–133.

Parker, J.L., and Ulrich, H.D. (2009). Mechanistic analysis of PCNA poly-ubiquitylation by the ubiquitin protein ligases Rad18 and Rad5. EMBO J. *28*, 3657–3666.

Parker, J.L., Bucceri, A., Davies, A.A., Heidrich, K., Windecker, H., and Ulrich, H.D. (2008). SUMO modification of PCNA is controlled by DNA. EMBO J. *27*, 2422–2431.

Parnas, O., Zipin-roitman, A., Pfander, B., Liefshitz, B., Mazor, Y., Ben-aroya, S., Jentsch, S., and Kupiec, M. (2010). Elg1, an alternative subunit of the RFC clamp loader, preferentially interacts with SUMOylated PCNA. EMBO J. *29*, 2611–2622.

Paulsen, R.D., Soni, D. V., Wollman, R., Hahn, A.T., Yee, M.C., Guan, A., Hesley, J.A., Miller, S.C., Cromwell, E.F., Solow-Cordero, D.E., et al. (2009). A Genome-wide siRNA Screen Reveals Diverse Cellular Processes and Pathways that Mediate Genome Stability. Mol. Cell *35*, 228–239.

Pellicioli, A., Lucca, C., Liberi, G., Marini, F., Lopes, M., Plevani, P., Romano, A., Di Fiore, P.P., and Foiani, M. (1999). Activation of Rad53 kinase in response to DNA damage and its effect in modulating phosphorylation of the lagging strand DNA polymerase. EMBO J. *18*, 6561–6572.

Pfander, B., Moldovan, G.L., Sacher, M., Hoege, C., and Jentsch, S. (2005). SUMO-modified PCNA recruits Srs2 to prevent recombination during S phase. Nature *436*, 428–433.

De Piccoli, G., Katou, Y., Itoh, T., Nakato, R., Shirahige, K., and Labib, K. (2012). Replisome Stability at Defective DNA Replication Forks Is Independent of S Phase Checkpoint Kinases. Mol. Cell *45*, 696–704.

Poli, J., Tsaponina, O., Crabbé, L., Keszthelyi, A., Pantesco, V., Chabes, A., Lengronne, A., and

Pasero, P. (2012). dNTP pools determine fork progression and origin usage under replication stress. EMBO J. *31*, 883–894.

Prado, F., and Aguilera, A. (2005). Impairment of replication fork progression mediates RNA polII transcription-associated recombination. EMBO J. *24*, 1267–1276.

Prakash, L. (1981). Characterization of postreplication repair in Saccharomyces cerevisiae and effects of rad6, rad18, rev3 and rad52 mutations. MGG Mol. Gen. Genet. *184*, 471–478.

Puddu, F., Granata, M., Di Nola, L., Balestrini, A., Piergiovanni, G., Lazzaro, F., Giannattasio, M., Plevani, P., and Muzi-Falconi, M. (2008). Phosphorylation of the Budding Yeast 9-1-1 Complex Is Required for Dpb11 Function in the Full Activation of the UV-Induced DNA Damage Checkpoint. Mol. Cell. Biol. *28*, 4782–4793.

Puig, S., Ramos-Alonso, L., Romero, A.M., and Martínez-Pastor, M.T. (2017). The elemental role of iron in DNA synthesis and repair. Metallomics 1483–1500.

Putnam, C.D., Hayes, T.K., and Kolodner, R.D. (2009). Specific pathways prevent duplication-mediated genome rearrangements. Nature *460*, 984–989.

Putnam, C.D., Hayes, T.K., and Kolodner, R.D. (2010). Post-replication repair suppresses duplication-mediated genome instability. PLoS Genet. *6*, e1000933.

Qiu, X.B., Shao, Y.M., Miao, S., and Wang, L. (2006). The diversity of the DnaJ/Hsp40 family, the crucial partners for Hsp70 chaperones. Cell. Mol. Life Sci. *63*, 2560–2570.

Raghuraman, M.K., Winzeler, E. a, Collingwood, D., Hunt, S., Wodicka, L., Conway, A., Lockhart, D.J., Davis, R.W., Brewer, B.J., and Fangman, W.L. (2001). Replication Dynaics of the Yeast Genome. Science (80-.). *294*, 115–121.

Rey, L., Sidorova, J.M., Puget, N., Biard, D.S.F., Monnat, R.J., Cazaux, C., U, C.I., and Lwoff-cnrs, I.A. (2009). Human DNA Polymerase eta Is Required for Common Fragile Site Stability during Unperturbed DNA Replication. Mol. Cell. Biol. *29*, 3344–3354.

Rocha, E.P.C. (2004). The replication-related organization of bacterial genomes. Microbiology *150*, 1609–1627.

Röhl, A., Wengler, D., Madl, T., Lagleder, S., Tippel, F., Herrmann, M., Hendrix, J., Richter, K., Hack, G., Schmid, A.B., et al. (2015). Hsp90 regulates the dynamics of its cochaperone Sti1 and the transfer of Hsp70 between modules. Nat. Commun. *6*.

Rossi, S.E., Ajazi, A., Carotenuto, W., Foiani, M., and Giannattasio, M. (2015). Rad53-Mediated Regulation of Rrm3 and Pif1 DNA Helicases Contributes to Prevention of Aberrant Fork Transitions under Replication Stress. Cell Rep. *13*, 80–92.

Rouse, J., and Jackson, S.P. (2002). Lcd1p recruits Mec1p to DNA lesions in vitro and in vivo. Mol. Cell *9*, 857–869.

Roux, K.J., Kim, D.I., Raida, M., and Burke, B. (2012). A promiscuous biotin ligase fusion protein identifies proximal and interacting proteins in mammalian cells. J. Cell Biol. *196*, 801–810.

Roy, S., Luzwick, J.W., and Schlacher, K. (2018). SIRF: Quantitative in situ analysis of protein interactions at DNA replication forks. J. Cell Biol. *217*, jcb.201709121.

Rozenzhak, S., Mejía-Ramírez, E., Williams, J.S., Schaffer, L., Hammond, J.A., Head, S.R., and Russell, P. (2010). Rad3-ATR decorates critical chromosomal domains with γH2A to protect genome integrity during S-phase in fission yeast. PLoS Genet. *6*, 1–17.

Rydberg, B., and Lindahl, T. (1982). Nonenzymatic methylation of DNA by the intracellular methyl group donor S-adenosyl-L-methionine is a potentially mutagenic reaction. EMBO J. *1*, 211–216.

Saayman, X., Ramos-Perez, C., and Brown, G.W. (2018). DNA Replication Profiling Using Deep Sequencing. Genome Instab. Methods Protoc. *1672*, 195–207.

Sabatinos, S.A., Ranatunga, N.S., Yuan, J.-P., Green, M.D., and Forsburg, S.L. (2015). Replication stress in early S phase generates apparent micronuclei and chromosome rearrangement in fission yeast. Mol. Biol. Cell *26*, 3439–3450.

Sabbioneda, S., Bortolomai, I., Giannattasio, M., Plevani, P., and Muzi-falconi, M. (2006). Yeast Rev1 is cell cycle regulated , phosphorylated in response to DNA damage and its binding to chromosomes is dependent upon MEC1. DNA Repair (Amst). *6*, 121–127.

Saldivar, J.C., Miuma, S., Bene, J., Hosseini, S.A., Shibata, H., Sun, J., Wheeler, L.J., Mathews, C.K., and Huebner, K. (2012). Initiation of Genome Instability and Preneoplastic Processes through Loss of Fhit Expression. PLoS Genet. *8*.

Sanchez, Y., Bachant, J., Wang, H., Hu, F., Liu, D., Tetzlaff, M., and Elledge, S.J. (1999). Control of the DNA Damage Checkpoint by Chk1 and Rad53 Protein Kinases Through Distinct Mechanisms. Science (80-.). *286*, 1166–1171.

Sandhu, S., Wu, X., Nabi, Z., Rastegar, M., Kung, S., Mai, S., and Ding, H. (2012). Loss of HLTF function promotes intestinal carcinogenesis. Mol. Cancer 1–16.

Saner, N., Karschau, J., Natsume, T., Gierliński, M., Retkute, R., Hawkins, M., Nieduszynski, C.A., Blow, J.J., de Moura, A.P.S., and Tanaka, T.U. (2013). Stochastic association of neighboring replicons creates replication factories in budding yeast. J. Cell Biol. *202*, 1001–1012.

Santocanale, C., and Diffley, J.F.X. (1998). A Mec1-and Rad53-dependent checkpoint controls late-firing origins of DNA replication. Nature *395*, 615–618.

Santos-Pereira, J.M., and Aguilera, A. (2015). R loops: New modulators of genome dynamics and function. Nat. Rev. Genet. *16*, 583–597.

Schiestl, R.H., Prakash, S., and Prakasht, L. (1990). The SRS2 Supressor of rad6 Mutations of Saccharomyceses cerevisiae Acts by channeling DNA Lesions Into RAD52 DNA Repair Pathway. Genetics *831*.

Schmidt, G.W., Frey, O., and Rudolf, F. (2018). The CellClamper: A convenient microfluidic device for time-lapse imaging of yeast. In Methods in Molecular Biology, pp. 537–555.

Segurado, M., and Diffley, J. (2008). Separate roles for the DNA damage checkpoint protein kinases in stabilizing DNA replication forks. Genes Dev. 1816–1827.

Sekimoto, T., Oda, T., Kurashima, K., Hanaoka, F., and Yamashita, T. (2015). Both High-Fidelity Replicative and Low-Fidelity Y-Family Polymerases Are Involved in DNA Rereplication. Mol. Cell. Biol. *35*, 699–715.

Sertic, S., Evolvi, C., Tumini, E., Plevani, P., Muzi-falconi, M., and Rotondo, G. (2013). Non-Canonical CRL4A / 4B CDT2 Interacts with RAD18 to Modulate Post Replication Repair and Cell Survival. PLoS One *8*.

Shah, K.A., Shishkin, A.A., Voineagu, I., Pavlov, Y.I., Shcherbakova, P. V, and Mirkin, S.M. (2012). Role of DNA Polymerases in Repeat-Mediated Genome Instability. Cell Rep. *2*, 1088–1095.

Shimizu, T., Tateishi, S., Tanoue, Y., Azuma, T., and Ohmori, H. (2017). Somatic hypermutation of immunoglobulin genes in Rad18 knockout mice. DNA Repair (Amst). *50*, 54–60.

Shirahige, K., Hori, Y., Shiraishi, K., Yamashita, M., Takahashi, K., Obuse, C., Tsurimoto, T., and Yoshikawa, H. (1998). Regulation of DNA-replication origins during cell-cycle progression. Nature *395*, 618–621.

Simpson, A.J.G., Caballero, O.L., Jungbluth, A., Chen, Y.T., and Old, L.J. (2005). Cancer/testis antigens, gametogenesis and cancer. Nat. Rev. Cancer *5*, 615–625.

Simpson, L.J., Ross, A., and Sale, J.E. (2006). RAD18-independant ubiquitination of proliferating-cell nuclear antigen in the avian cell line DT40. EMBO Rep. *7*.

Singh, A., and Xu, Y.-J. (2016). The Cell Killing Mechanisms of Hydroxyurea. Genes (Basel).

Smith, S., Hwang, J.-Y., Banerjee, S., Majeed, A., Gupta, A., and Myung, K. (2004). Mutator genes for suppression of gross chromosomal rearrangements identified by a genome-wide screening in Saccharomyces cerevisiae. Proc. Natl. Acad. Sci. *101*, 9039–9044.

Smolka, M.B., Chen, S.H., Maddox, P.S., Enserink, J.M., Albuquerque, C.P., Wei, X.X., Desai, A., Kolodner, R.D., and Zhou, H. (2006). An FHA domain-mediated protein interaction network of Rad53 reveals its role in polarized cell growth. J. Cell Biol. *175*, 743–753.

Smolka, M.B., Albuquerque, C.P., Chen, S., and Zhou, H. (2007). Proteome-wide identification of in vivo targets of DNA damage checkpoint kinases. Proc. Natl. Acad. Sci. *104*, 10364–10369.

Sofueva, S., Osman, F., Lorenz, A., Steinacher, R., Castagnetti, S., Ledesma, J., and Whitby, M.C. (2011). Ultrafine anaphase bridges, broken DNA and illegitimate recombination induced

by a replication fork barrier. Nucleic Acids Res. *39*, 6568–6584.

Sogo, J.M., Lopes, M., and Foiani, M. (2002). Fork reversal and ssDNA accumulation at stalled replication forks owing to checkpoint defects. Science (80-.). *297*, 599–602.

Sollier, J., and Branzei, D. (2009). The Saccharomyces cerevisiae Esc2 and Smc5-6 Proteins Promote Sister Chromatid Junction-mediated Intra-S Repair. Mol. Biol. Cell *20*, 327–331.

Sollier, J., Stork, C.T., García-Rubio, M.L., Paulsen, R.D., Aguilera, A., and Cimprich, K.A. (2014). Transcription-Coupled Nucleotide Excision Repair Factors Promote R-Loop-Induced Genome Instability. Mol. Cell *56*, 777–785.

Sood, R., Makalowska, I., Galdzicki, M., Hu, P., Eddings, E., Robbins, C.M., Moses, T., Namkoong, J., Chen, S., and Trent, J.M. (2003). Cloning and characterization of a novel gene , SHPRH , encoding a conserved putative protein with SNF2 / helicase and PHD-finger domains from the 6q24 region. Genomic *82*, 153–161.

Sparks, J.L., Chon, H., Cerritelli, S.M., Kunkel, T.A., Johansson, E., Crouch, R.J., and Burgers, P.M. (2012). RNase H2-Initiated Ribonucleotide Excision Repair. Mol. Cell *47*, 980–986.

Srinivasan, S. V., Dominguez-Sola, D., Wang, L.C., Hyrien, O., and Gautier, J. (2013). Cdc45 Is a Critical Effector of Myc-Dependent DNA Replication Stress. Cell Rep. *3*, 1629–1639.

Srivatsan, A., Tehranchi, A., MacAlpine, D.M., and Wang, J.D. (2010). Co-orientation of replication and transcription preserves genome integrity. PLoS Genet. *6*.

Srivatsan, A., Putnam, C.D., and Kolodner, R.D. (2018). Analyzing Genome Rearrangements in Saccharomyces cerevisiae. In Genome Instability: Methods and Protocols, M. Muzi-Falconi, and G.W. Brown, eds. (New York, NY: Springer New York), pp. 43–61.

Stamatoyannopoulos, J.A., Adzhubei, I., Thurman, R.E., Kryukov, G. V., Mirkin, S.M., and Sunyaev, S.R. (2009). Human mutation rate associated with DNA replication timing. Nat. Genet. *41*, 393–395.

Stearman, R., Yuan, D.S., Yamaguchi-Iwai, Y., Klausner, R.D., and Dancis, A. (1996). A Permease-Oxidase Complex Involved in High-Affinity Iron Uptake in Yeast. Science (80-.).

271, 1552–1557.

Stirling, P.C., Chan, Y.A., Minaker, S.W., Aristizabal, M.J., Barrett, I., Sipahimalani, P., Kobor, M.S., and Hieter, P. (2012). R-loop-mediated genome instability in mRNA cleavage and polyadenylation mutants. Genes Dev. *26*, 163–175.

Sun, H., Zou, S., Zhang, S., Liu, B., Meng, X., Li, X., Yu, J., and Wu, J. (2015). Elevated DNA polymerase iota (Poli) is involved in the acquisition of aggressive phenotypes of human esophageal squamous cell cancer. Int J Clin Exp Pathol 2015;8(4)3591-3601 *8*, 3591–3601.

Szakal, B., and Branzei, D. (2013). Premature Cdk1/Cdc5/Mus81 pathway activation induces aberrant replication and deleterious crossover. EMBO J. *32*, 1155–1167.

Szilard, R.K., Jacques, P.T., Laramée, L., Cheng, B., Galicia, S., Bataille, A.R., Yeung, M., Mendez, M., Bergeron, M., Robert, F., et al. (2010). Systematic identification of fragile sites via genome-wide location analysis of γ-H2AX. Nat. Struct. Mol. Biol. *17*, 299–305.

Takeuchi, Y., Horiuchi, T., and Kobayashi, T. (2003). Transcription-dependent recombination and the role of fork collision in yeast rDNA. Genes Dev. *17*, 1497–1506.

Tanaka, K., and Russell, P. (2004). Cds1 phosphorylation by Rad3-Rad26 kinase is mediated by forkhead-associated domain interaction with Mrc1. J. Biol. Chem. *279*, 32079–32086.

Tercero, J.A., and Diffley, J.F.X. (2001). Regulation of DNA replication fork progression through damaged DNA by the Mec1/Rad53 checkpoint. Nature *412*, 553–557.

Tercero, J.A., Longhese, M.P., and Diffley, J.F. (2003). A central role for DNA replication forks in checkpoint activation and response. Mol. Cell *11*, 1323–1336.

Thomas, G., Munoz, I.M., Rouse, J., and Blow, J.J. (2008). PTIP / Swift is required for efficient PCNA ubiquitination in response to DNA damage. DNA Repair (Amst). *7*, 775–787.

Tkach, J.M., Yimit, A., Lee, A.Y., Riffle, M., Costanzo, M., Jaschob, D., Hendry, J.A., Ou, J., Moffat, J., Boone, C., et al. (2012). Dissecting DNA damage response pathways by analysing protein localization and abundance changes during DNA replication stress. Nat. Cell Biol. *14*, 966–976.

Tong, A.H.Y., and Boone, C. (2006). Synthetic genetic array analysis in Saccharomyces cerevisiae. Methods Mol. Biol. *313*, 171–192.

Torres, N.P., and Brown, G.W. (2015). A High-Throughput Confocal Fluorescence Microscopy Platform to Study DNA Replication Stress in Yeast Cells. Methods Mol. Biol.

Travesa, A., Kuo, D., De Bruin, R.A.M., Kalashnikova, T.I., Guaderrama, M., Thai, K., Aslanian, A., Smolka, M.B., Yates, J.R., Ideker, T., et al. (2012). DNA replication stress differentially regulates G1/S genes via Rad53-dependent inactivation of Nrm1. EMBO J. *31*, 1811–1822.

Truman, A.W., Kristjansdottir, K., Wolfgeher, D., Ricco, N., Mayampurath, A., Volchenboum, S.L., Clotet, J., and Kron, S.J. (2015). Quantitative proteomics of the yeast Hsp70/Hsp90 interactomes during DNA damage reveal chaperone-dependent regulation of ribonucleotide reductase. J. Proteomics *112*, 285–300.

Tsuji, Y., Watanabe, K., Araki, K., Shinohara, M., Yamagata, Y., Tsurimoto, T., Hanaoka, F., Yamamura, K. ichi, Yamaizumi, M., and Tateishi, S. (2008). Recognition of forked and single-stranded DNA structures by human RAD18 complexed with RAD6B protein triggers its recruitment to stalled replication forks. Genes to Cells *13*, 343–354.

Tuduri, S., Crabbé, L., Conti, C., Tourrière, H., Holtgreve-Grez, H., Jauch, A., Pantesco, V., De Vos, J., Thomas, A., Theillet, C., et al. (2009). Topoisomerase I suppresses genomic instability by preventing interference between replication and transcription. Nat. Cell Biol. *11*, 1315–1324.

Tyler, J.K., Adams, C.R., Chen, S.R., Kobayashi, R., Kamakaka, R.T., and Kadonaga, J.T. (1999). The RCAF complex mediates chromatin assembly during DNA replication and repair. Nature *402*, 555–560.

Ulrich, H.D. (2000). Two RING finger proteins mediate cooperation between ubiquitin-conjugating enzymes in DNA repair. EMBO J. *19*, 3388–3397.

Ulrich, H.D. (2001). The srs2 suppressor of UV sensitivity acts specifically on the RAD5- and MMS2-dependent branch of the RAD6 pathway. Nucleic Acids Res. *29*, 3487–3494.

Ulrich, H.D. (2003). Protein-protein interactions within an E2-RING finger complex:

Implications for ubiquitin-dependent DNA damage repair. J. Biol. Chem. *278*, 7051–7058.

Unk, I., Hajdú, I., Blastyák, A., and Haracska, L. (2010). Role of yeast Rad5 and its human orthologs , HLTF and SHPRH in DNA damage tolerance. DNA Repair (Amst). *9*, 257–267.

Urulangodi, M., Sebesta, M., Menolfi, D., Szakal, B., Sollier, J., Sisakova, A., Krejci, L., and Branzei, D. (2015). Local regulation of the Srs2 helicase by the SUMO-like domain protein Esc2 promotes recombination at sites of stalled replication. Genes Dev. *29*, 2067–2080.

Vaisman, A., and Woodgate, R. (2017). Translesion DNA polymerases in eukaryotes : what makes them tick? Crit. Rev. Biochem. Mol. Biol. *52*, 274–303.

Vaisman, A., Masutani, C., Hanaoka, F., and Chaney, S.G. (2000). Efficient Translesion Replication Past Oxaliplatin and Cisplatin GpG Adducts by human DNA polymerase eta. Biochemistry 4575–4580.

Vaisman, A., Takasawa, K., Iwai, S., and Woodgate, R. (2006). DNA polymerase i-dependent translesion replication of uracil containing cyclobutane pyrimidine dimers. DNA Repair (Amst). *5*, 210–218.

VanDemark, A.P., Hofmann, R.M., Tsui, C., Pickart, C.M., and Wolberger, C. (2001). Molecular insights into polyubiquitin chain assembly: Crystal structure of the Mms2/Ubc13 heterodimer. Cell *105*, 711–720.

Vanoli, F., Fumasoni, M., Szakal, B., Maloisel, L., and Branzei, D. (2010). Replication and recombination factors contributing to recombination-dependent bypass of DNA lesions by template switch. PLoS Genet. *6*.

Veaute, X., Jeusset, J., Soustelle, C., Kowalczykowski, S.C., Le Cam, E., and Fabre, F. (2003). The Srs2 helicase prevents recombination by disrupting Rad51 nucleoprotein filaments. Nature *423*, 309–312.

Venkatesh, S., and Workman, J.L. (2015). Histone exchange ,chromatin structure and the regulation of transcription. Nature *16*, 178–189.

Verghese, J., Abrams, J., Wang, Y., and Morano, K.A. (2012). Biology of the Heat Shock

Response and Protein Chaperones: Budding Yeast (Saccharomyces cerevisiae) as a Model System. Microbiol. Mol. Biol. Rev. *76*, 115–158.

Vilette, D., Ehrlich, S.D., and Michel, B. (1996). Transcription-induced deletions in plasmid vectors: M13 DNA replication as a source of instability. Mol. Gen. Genet. *252*, 398–403.

Vincent, C.T., Fedorov, V.D., Patsialou, A., Cherrington, B.D., Wakshlag, J.J., Mohanan, S., Zee, M., Zhang, X., Garcia, B.A., Condeelis, J.S., et al. (2013). BRCA1 promotes the ubiquitination of PCNA and recruitment of translesion polymerases in response to replication blockade. Proc. Natl. Acad. Sci. *110*.

Vujanovic, M., Krietsch, J., Raso, M.C., Ciccia, A., Penengo, L., and Lopes, M. (2017). Replication Fork Slowing and Reversal upon DNA Damage Require PCNA Polyubiquitination and ZRANB3 DNA Translocase Activity. Mol. Cell *67*, 882–890.e5.

Waga, S., and Stillman, B. (1998). The DNA replication fork in eukaryotic cells. Annu. Rev. Biochem. *67*, 721–751.

Wahba, L., Amon, J.D., Koshland, D., and Vuica-Ross, M. (2011). RNase H and Multiple RNA Biogenesis Factors Cooperate to Prevent RNA:DNA Hybrids from Generating Genome Instability. Mol. Cell *44*, 978–988.

Wahl, M.C., and Sundaralingam, M. (2000). B-form to A-form conversion by a 3 ′ -terminal ribose : crystal structure of the chimera d (CCACTAGTG) r (G). Nucleic Acids Res. *28*, 4356–4363.

Wang, T., Birsoy, K., Hughes, N.W., Krupczak, K.M., Post, Y., Wei, J.J., Lander, E.S., and Sabatini, D.M. (2015). Identification and characterization of essential genes in the human genome. Science (80-.). *350*, 1096–1101.

Wang, Y., Vujcic, M., and Kowalski, D. (2001). DNA replication forks pause at silent origins near the HML locus in budding yeast. Mol. Cell. Biol. *21*, 4938–4948.

Wanrooij, P.H., Tannous, E., Kumar, S., Navadgi-Patil, V.M., and Burgers, P.M. (2016). Probing the Mec1 ATR Checkpoint Activation Mechanism with Small Peptides. J. Biol. Chem. *291*, 393–401.

Watanabe, K., Tateishi, S., Kawasuji, M., Tsurimoto, T., Inoue, H., and Yamaizumi, M. (2004). Rad18 guides pol eta to replication stalling sites through physical interaction and PCNA monoubiquitination. EMBO J. *23*, 3886–3896.

Waters, L.S., and Walker, G.C. (2006). The critical mutagenic translesion DNA polymerase Rev1 is highly expressed during G2/M phase rather than S phase. Proc. Natl. Acad. Sci. *103*, 8971–8976.

Watt, D.L., Buckland, R.J., Lujan, S.A., Kunkel, T.A., and Chabes, A. (2015). Genome-wide analysis of the specificity and mechanisms of replication infidelity driven by imbalanced dNTP pools. Nucleic Acids Res. *44*, 1669–1680.

Weile, J., Sun, S., Cote, A.G., Knapp, J., Verby, M., Mellor, J.C., Wu, Y., Pons, C., Wong, C., Lieshout, N. van, et al. (2017). Expanding the Atlas of Functional Missense Variation for Human Genes. bioRxiv *1*, 166595.

West, S.C., Blanco, M.G., Chan, Y.W., Matos, J., Sarbajna, S., and Wyatt, H.D.M. (2015). Resolution of Recombination Intermediates: Mechanisms and Regulation. Cold Spring Harb. Symp. Quant. Biol. *80*, 103–109.

Weston, R., Peeters, H., and Ahel, D. (2012). ZRANB3 is a structure-specific ATP-dependent endonuclease involved in replication stress response. Genes Dev. 1558–1572.

Wickner, S., Skowyra, D., Hoskins, J., and McKenney, K. (1992). DnaJ, DnaK, and GrpE heat shock proteins are required in oriP1 DNA replication solely at the RepA monomerization step. Proc. Natl. Acad. Sci. *89*, 10345–10349.

Williams, J.S., Smith, D.J., Marjavaara, L., Lujan, S.A., Chabes, A., and Kunkel, T.A. (2013). Topoisomerase 1-Mediated Removal of Ribonucleotides from Nascent Leading-Strand DNA. Mol. Cell *49*, 1010–1015.

Willis, N.A., Chandramouly, G., Huang, B., Kwok, A., Follonier, C., Deng, C., and Scully, R. (2014). BRCA1 controls homologous recombination at Tus/Ter-stalled mammalian replication forks. Nature *510*, 556–559.

Wittschieben, J.P., Patil, V., Glushets, V., Robinson, L.J., Kusewitt, D.F., and Wood, R.D.

(2010). Loss of DNA Polymerase ζ Enhances Spontaneous Tumorigenesis. Mol. Cell. Pathobiol. Loss *70*, 2770–2779.

Wold, M.S. (1997). Replication protein A: a heterotrimeric, single-stranded DNA-binding protein required for eukaryotic DNA metabolism. Annu. Rev. Biochem. *66*, 61–92.

Wu, X., and Huang, M. (2008). Dif1 controls subcellular localization of ribonucleotide reductase by mediating nuclear import of the R2 subunit. Mol. Cell. Biol. *28*, 7156–7167.

Wu, F., Lin, X., Okuda, T., and Howell, S.B. (2004). DNA Polymerase ζ Regulates Cisplatin Cytotoxicity , Mutagenicity , and The Rate of Development of Cisplatin Resistance. Cancer Res. 8029–8035.

Xie, K., Doles, J., Hemann, M.T., and Walker, G.C. (2010). Error-prone translesion synthesis mediates acquired chemoresistance. Proc. Natl. Acad. Sci. *107*, 20792–20797.

Xie, M., Yen, Y., Owonikoko, T.K., Ramalingam, S.S., Khuri, F.R., Curran, W.J., Doetsch, P.W., and Deng, X. (2014). Bcl2 induces DNA replication stress by inhibiting ribonucleotide reductase. Cancer Res. *74*, 212–223.

Xu, X., Ball, L., Chen, W., Tian, X., Lambrecht, A., Hanna, M., and Xiao, W. (2013). The Yeast Shu Complex Utilizes Homologous Recombination Machinery for Error-free Lesion Bypass via Physical Interaction with a Rad51 Paralogue. PLoS One *8*, 1–9.

Xu, X., Lin, A., Zhou, C., Blackwell, S.R., Zhang, Y., Wang, Z., Feng, Q., Guan, R., Hanna, M.D., Chen, Z., et al. (2016). Involvement of budding yeast Rad5 in translesion DNA synthesis through physical interaction with Rev1. Nucleic Acids Res. *44*, 5231–5245.

Yabuki, N., Terashima, H., and Kitada, K. (2002). Mapping of early firing origins on a replication profile of budding yeast. Genes to Cells *7*, 781–789.

Yanagihara, H., Kobayashi, J., Tateishi, S., Kato, A., Matsuura, S., and Tauchi, H. (2011). Article NBS1 Recruits RAD18 via a RAD6-like Domain and Regulates Pol eta -Dependent Translesion DNA Synthesis. Mol. Cell *43*, 788–797.

Yang, S.S., Yeh, E., Salmon, E.D., and Bloom, K. (1997). Identification of a mid-anaphase

checkpoint in budding yeast. J. Cell Biol. *136*, 345–354.

Yang, X.H., Shiotani, B., Classon, M., and Zou, L. (2008). Chk1 and Claspin potentiate PCNA ubiquitination. Genes Dev. 1147–1152.

Yang, Y., Gao, Y., Mutter-Rottmayer, L., Zlatanou, A., Durando, M., Ding, W., Wyatt, D., Ramsden, D., Tanoue, Y., Tateishi, S., et al. (2017). DNA repair factor RAD18 and DNA polymerase Polκ confer tolerance of oncogenic DNA replication stress. J. Cell Biol. *216*, 3097–3115.

Yonekura, S.-I., Nakamura, N., Yonei, S., and Zhang-Akiyama, Q.-M. (2009). Generation, biological consequences and repair mechanisms of cytosine deamination in DNA. J. Radiat. Res. *50*, 19–26.

Yuan, F., Xu, Z., Yang, M., Wei, Q., Zhang, Y., Yu, J., Zhi, Y., and Liu, Y. (2013). Overexpressed DNA Polymerase Iota Regulated by JNK / c-Jun Contributes to Hypermutagenesis in Bladder Cancer. PLoS One *8*.

Yuan, J., Ghosal, G., and Chen, J. (2012). The HARP-like Domain-Containing Protein AH2 / ZRANB3 Binds to PCNA and Participates in Cellular Response to Replication Stress. Mol. Cell *47*, 410–421.

Yuce, O., and West, S.C. (2013). Senataxin, Defective in the Neurodegenerative Disorder Ataxia with Oculomotor Apraxia 2, Lies at the Interface of Transcription and the DNA Damage Response. Mol. Cell. Biol. *33*, 406–417.

Zegerman, P., and Diffley, J.F.X. (2010). Checkpoint-dependent inhibition of DNA replication initiation by Sld3 and Dbf4 phosphorylation. Nature *467*, 474–478.

Zeman, M.K., and Cimprich, K.A. (2014). Causes and consequences of replication stress. Nat. Cell Biol. *16*, 2–9.

Zhang, H., and Lawrence, C.W. (2005). The error-free component of the RAD6/RAD18 DNA damage tolerance pathway of budding yeast employs sister-strand recombination. PLoS Pathog. *102*, 1–6.

Zhang, Y., Yuan, F., Wu, X., Rechkoblit, O., Taylor, J., Geacintov, N.E., and Wang, Z. (2000). Error-prone lesion bypass by human DNA polymerase η. Nu *28*, 4717–4724.

Zhao, X., and Rothstein, R. (2002). The Dun1 checkpoint kinase phosphorylates and regulates the ribonucleotide reductase inhibitor Sml1. Proc. Natl. Acad. Sci. *99*, 3746–3751.

Zhao, R., Davey, M., Hsu, Y.C., Kaplanek, P., Tong, A., Parsons, A.B., Krogan, N., Cagney, G., Mai, D., Greenblatt, J., et al. (2005). Navigating the chaperone network: An integrative map of physical and genetic interactions mediated by the hsp90 chaperone. Cell *120*, 715–727.

Zhao, X., Muller, E.G.D., and Rothstein, R. (1998). A suppressor of two essential checkpoint genes identifies a novel protein that negatively affects dNTP pools. Mol. Cell *2*, 329–340.

Zhao, X., Chabes, A., Domkin, V., Thelander, L., and Rothstein, R. (2001). The ribonucleotide reductase inhibitor Sml1 is a new target of the Mec1/Rad53 kinase cascade during growth and in response to DNA damage. EMBO J. *20*, 3544–3553.

Zhong, X., Garg, P., Stith, C.M., Mcelhinny, S.A.N., Kissling, G.E., Burgers, P.M.J., and Kunkel, T.A. (2018). The fidelity of DNA synthesis by yeast DNA polymerase zeta alone and with accessory proteins. Nucleic Acids Res. *34*, 4731–4742.

Zhou, C., Elia, A.E.H., Naylor, M.L., Dephoure, N., Ballif, B.A., Goel, G., Xu, Q., Ng, A., Chou, D.M., Xavier, R.J., et al. (2016). Profiling DNA damage-induced phosphorylation in budding yeast reveals diverse signaling networks. Proc. Natl. Acad. Sci. *113*, E3667–E3675.

Zou, L., and Elledge, S.J. (2003). Sensing DNA Damage Through ATRIP Recognition of RPA-ssDNA. Science (80-.). *300*, 1542–1548.

Zylicz, M., Ang, D., Liberek, K., and Georgopoulos, C. (1989). Initiation of lambda DNA replication with purified host- and bacteriophage-encoded proteins: the role of the dnaK, dnaJ and grpE heat shock proteins. EMBO J. *8*, 1601–1608.

Appendices

Published work not included in this thesis:

Becker J.R., **Gallo D.**, Leung W., Thu, Y.M., Croissant, T., Nguyen H.D., Starr T.K., Brown G.W., Bielinsky A.J. (2018) Flap endonuclease overexpression is a potent driver of genome instability and mutation. Nucleic Acids Research, In Press

Gallo D., Wang G., Yip C.M., Brown G.W. (2016) Analysis of Replicating Yeast Chromosomes by DNA Combing. Cold Spring Harb Protoc. 2016 (2):pdb.prot085118

Gallo D., Wang G., Yip C.M., Brown G.W. (2016) Single-Molecule Analysis of Replicating Yeast Chromosomes. Cold Spring Harb Protoc. 2016 (2)):pdb.top077784

Tkac J., Xu G., Adhikary H., Young J.T.F., **Gallo D**., Escribano-Diaz C., Krietsch J., Orthwein A., Munro M., Sol W., Al-Hakim A., Lin Z.Y., Jonkers J., Borst P., Brown G.W., Gingras A.C., Rottenberg S., Masson J.Y., Durocher D. (2016) HELB is a Feedback Inhibitor of DNA End Resection. Mol Cell 61: 405-418.

Balint A., Kim T., **Gallo D**., Cussiol J.R., Basto de Oliveira F.M., Yimit A., Ou J., Nakato R., Gurevich A., Shirahige K., Smolka M.B., Zhang Z., Brown G.W. (2015) Assembly of Slx4 signaling complexes behind DNA replication forks. EMBO J. 34: 2182-2197

Larin M.E., **Gallo D**., Tamblyn L.,Yang J., Liao Y., Sabat N., Brown G.W., McPherson P.J. (2014) Fanconi Anemia signaling and Mus81 Cooperate to safeguard development and crosslink repair. Nucleic Acids Research 42: 9807-9820

Coshi C.H., Ishak C.A., **Gallo D**., Marshall A., Talluri S., Wang J., Cecchini M.J., Martens A.L., Percy V., Welch I., Boutros P.C., Brown G.W., Dick F.A. (2014) Haploinsufficiency of an RB-E2F1-Condensin II complex leads to aberrant replication and aneuploidy. Cancer Discov. 4: 840-853

Jagannathan M., Nguyen T, **Gallo D**., Luthra N., Brown G.W., Saridakis V., Frappier L. (2014) A role for USP7 in DNA Replication. Molecular and Cellular Biology 34: 132-145

Cheung-Ong, K., Song, K. T., Ma, Z., Shabtai, D., Lee, A. Y., **Gallo, D**., Heisler, L. E., Brown, G. W., Bierbach, U., Giaever, G., and Nislow, C. (2012) Comparative Chemogenomics to Examine the mechanism of Action of DNA-Targeted Platinum-Acridine Anticancer Agents. ACS Chemical Biology 7: 1892-1901.